UNIVERSIDADE DO ALGARVE

Faculdade de Ciências e Tecnologia

Evaluation of the binding of vanadium-based anticancer drugs to human serum proteins

BY IELYZAVETA CHORNA

Mestrado em Qualidade em Análises

(European Master in Quality in Analytical Laboratories)

2015

Evaluation of the binding of vanadium-based anticancer drugs

to human serum proteins

Thesis for the degree of European Master in Quality in Analytical Laboratories

IELYZAVETA CHORNA

July, 2015

Supervised by:

Prof. João da Costa Pessoa, CQE I, IST, Lisbon

And

Prof. Isabel Cavaco, University of Algarve, Faro

Co-supervised by:

Dr. Isabel Correia

UNIVERSIDADE DO ALGARVE
Faculdade de Ciências e Tecnologia
Faro, Portugal

AKNOWLEDGEMENT

This research was funded by the European Commision under the Master's Program "European Master in Quality in Analytical Laboratories" and conducted at Centro de Química Estrutural Complexo I (CQE I), Instituto Superior Técnico, Lisboa under supervision of Prof. João da Costa Pessoa and Prof. Isabel Cavaco.

I would like to thank Prof. João da Costa Pessoa for kind sharing of his knowledge, guidance and help during all my RMT period. I'm also very grateful to Prof. João for translating my abstract to Portuguese.

I would like to thank Prof. Isabel Cavaco for her kind assistance and help, constant accessibility and support, knowledge and advices.

I would like to thank Isabel Correia, researcher at CQE, for her guidance, teaching me all the new techniques and helping me to better understand the field of my study.

I would like to thank Prof. Miquel Esteban Cortada and Prof. Angels Sahuquillo Estrugo from the University of Barcelona for their hospitality, kind assistance and help in solving all the problems during the whole Master Program period.

I would like to thank Pedro Adão, Cristina Matos, Catarina Quintanova and Carlos Teixeira from Group I for their kind help and teaching me in the laboratory of CQE.

I would like to thank Enoch Cobbina, Somnath Roy and Ashis Kumar Patra for kind sharing of their knowlenge in my field of study and encouragement.

I would like to thank my wonderful fiancé Igor Kozlenko for his help, great moral support and believing in me during this Master thesis research.

I would like to thank my mother Olena Skrypnik and grandmother Ludmila Branets for their encouragement and moral support.

I would like to thank my colleagues at CQE Magdalena Domarus, Hesham Alsoghier, Anna Irto and Nihel Bekhti for your collaboration, friendship and support during this Master thesis.

I would like to thank CQE for providing work facilities and technical support.
I would like to thank all the workers of International & Mobility Office of University of Algarve for their accessibility, help and guidance during my entire stay in Portugal.
Lisbon, July, 2015.

TABLE OF CONTENT

LIST OF TABLES

LIST OF FIGURES

ABSTRACT

Oxidovanadium(IV) complexes, namely those containing organic polydentate ligands, often designated by $VO(carrier)_n$ compounds, have attracted a great interest due to their prospective therapeutic effects, particularly in the treatment of diabetes, cancer and diseases caused by parasites. Partly due to their more adequate lipophilicity characteristics, they are better absorbed in the gastrointestinal tract which, in turn, allows the use of smaller doses of vanadium-based drug to achieve the same therapeutic effect when compared with vanadium inorganic salts.

Transport in blood is an essential step for any drug to reach the target tissues. Since serum proteins play a significant role in the pharmacokinetics of the drugs in human body, it is of primary importance to know if the drug binds under physiological conditions to human serum proteins, namely human serum Transferrin (hTF) and human serum albumin (HSA), and if so, to know the nature of binding and in which form it is bound and delivered to the cells.

In this work the binding of $V^{IV}O(oda)(H_2O)_2$, $V^{IV}O(oda)(bipy)$, $V^{IV}O(oda)(phen)$ (H_2oda = oxodiacetic acid) and $V^{IV}O(acac)_2$ (acac = acetylacetone) to hTF and HSA are studied. The three oda-containing complexes are synthesized, characterized and described in the work as well. Aqueous solutions of $V^{IV}O(oda)(H_2O)_2$ at pH ~7.4 are reasonably stable at least for ~60 minutes, but after this period of time some hydrolysis of the complex occurs, as well as oxidation of V^{IV} to V^{V}. $V^{IV}O(oda)(bipy)$ and $V^{IV}O(oda)(phen)$ are significantly more stable in the same conditions.

The interaction of the complexes with hTF and HSA is studied by means of UV-Vis absorption, circular dichroism (CD), Electron Paramagnetic Resonance (EPR) and fluorescence spectroscopy. The results of CD and EPR analyses prove that all $V^{IV}O$-complexes studied bind to hTF maintaining at least one organic ligand in the coordination sphere. The comparative EPR analysis of the hTF-$V^{IV}O(oda)(phen)$ system and related systems suggest that $V^{IV}O(oda)(phen)$ may lose the oda ligand when binding to hTF, but the CD spectra do not confirm this and suggest that $V^{IV}O$-oda-containing species are also present.

The CD study of hTF-$V^{IV}O(acac)_2$ system proved that $V^{IV}O$-acac species bind to hTF, contradicting previous findings which stated that $V^{IV}O(acac)_2$ does not bind to hTF. The CD analysis of HSA-$V^{IV}O(acac)_2$ system suggest and somewhat confirm also some previous findings that $V^{IV}O(acac)_2$ does not bind to HSA. However, EPR and fluorescence data suggest that $V^{IV}O(acac)_2$ binds to HSA, possibly with at least one ligand, but it is not confirmed that this binding involves coordination of V^{IV} to donor atoms of HSA.

The results of the studies of the interaction of $V^{IV}O(oda)(bipy)$ and $V^{IV}O(acac)_2$ complexes with hTF, after passing the samples through size-exclusion gel-filtration chromatographic columns, and analysis of vanadium in the eluates by ICP, further show that V^{IV} binds to hTF. The more V^{IV} is added, the higher is the amount bound to hTF, but the total V:hTF ratio did not exceed 3 (for $V^{IV}O(acac)_2$) or 4 (for $V^{IV}O(oda)(bipy)$). $V^{IV}O(oda)(bipy)$ and $V^{IV}O(acac)_2$ bind close to tyrosine residues, but tryptophan residues are not much affected.

All complexes studied are able to partly quench the fluorescence of both hTF and HSA at both excitement wavelength, 280 and 295 nm, but this quenching is not very effective. Thus, the binding when therapeutically relevant amounts of complexes are added possibly does not take place close to Trp residues of both proteins. The main trend of quenching for most of the complex-protein systems supports the existence of more than one binding site on hTF and HSA.

The extent of HSA fluorescence quenching by $V^{IV}O(oda)(bipy)$ is significant. In the HSA-$V^{IV}O(oda)(bipy)$ system a remarkable red shift of the emission spectra towards longer wavelength is observed meaning that tryptophan and/or tyrosine residues partly go out of the HSA hydrophobic cavity and become surrounded with slightly more hydrophilic media during the binding process, which may be associated to a more open HSA conformation.

Key words. *Vanadium, oxidovanadium (IV) complexes, human serum Transferrin, human serum albumin, circular dichroism, electron paramagnetic resonance, fluorescence spectroscopy, anticancer activity.*

RESUMO

Complexos de oxidovanádio(IV), em particular os que contêm ligandos orgânicos polidentados, frequentemente designados por compostos VO(carrier)$_n$, têm atraído muito interesse devido ao seu potencial como agentes terapêuticos, nomeadamente no tratamento de diabetes, cancro e doenças causadas por parasitas. Em parte devido a melhores características de lipofilicidade, os VO(carrier)$_n$ são melhor absorvidos no tracto gastro-intestinal o que, quando comparados com os sais inorgânicos de vanádio, permite a utilização de menores quantidades para atingir o mesmo efeito terapêutico.

O transporte de um agente terapêutico no sangue é um passo fundamental para atingir os tecidos alvo. As proteínas do soro desempenham frequentemente um papel determinante na farmacocinética de drogas no corpo humano, pelo que é importante determinar como é que, em condições fisiológicas, o agente terapêutico se liga às proteínas do soro, nomeadamente à transferrina (hTF) e albumina (HSA) humanas, bem como se essa ligação será relevante na entrega da droga aos tecidos alvo.

Neste trabalho estuda-se a ligação dos complexos $V^{IV}O(oda)(H_2O)_2$, $V^{IV}O(oda)(bipy)$, $V^{IV}O(oda)(phen)$ (H_2oda = ácido oxodiacético) e $V^{IV}O(acac)_2$ (acac = acetilacetona) à hTF e HSA. Os três complexos contendo oda são também sintetizados e caracterizados. Verificou-se que soluções aquosas tamponizadas de $V^{IV}O(oda)(H_2O)_2$ a pH ~7.4 são razoavelmente estáveis durante pelo menos ~60 minutos. Começa entãoa ser detectada alguma hidrólise, bem como alguma oxidação de V^{IV} to V^{V}. Os compostos $V^{IV}O(oda)(bipy)$ e $V^{IV}O(oda)(phen)$ são bastante mais estáveis nas mesmas condições do que o $V^{IV}O(oda)(H_2O)_2$, bem como o $V^{IV}O(acac)_2$.

A interacção dos complexos com hTF e HSA é estudada por espectroscopia de absorção de UV-Vis, dicroísmo circular (CD), Espectroscopia de Ressonância Paramagnética Electrónica (EPR) e de Fluorescência. Os resultados de CD e EPR comprovam que todos os complexos de $V^{IV}O^{2+}$ se ligam à hTF mantendo pelo menos um dos seus ligandos orgânicos na esfera de coordenação. A comparação dos espectros de EPR nos sistemas hTF-$V^{IV}O(oda)(phen)$ e hTF-$V^{IV}O(oda)(bipy)$ dá alguma indicação de que estes podem perder o ligando oda na sua ligação à hTF, no entanto os espectros CD não confirmam isso, pelo contrário, sugerem que espécies contendo $V^{IV}O$-oda também estão presentes.

Os estudos por CD do sistema hTF-$V^{IV}O(acac)_2$ comprovam que complexos de $V^{IV}O^{2+}$ contendo $acac^-$ se ligam à hTF, contradizendo trabalhos publicados anteriormente, que afirmavam o contrário. Estudos com o sistema HSA-$V^{IV}O(acac)_2$ de certa forma confirmam resultados publicados anteriormente, afirmando que o $V^{IV}O(acac)_2$ não se liga à albumina. Os resultados aqui obtidos não confirmam uma ligação envolvendo coordenação do V^{IV} a átomos doadores da HSA, mas dão indicações que há interacções do complexo com a albumina.

Os resultados de estudos de interacção do $V^{IV}O(oda)(bipy)$ e $V^{IV}O(acac)_2$ com hTF, depois de fazer passar as soluções através de colunas de exclusão molecular que retêm as moléculas pequenas, após análise do vanádio nos eluatos por ICP, comprovaram a ligação destes complexos à hTF. Quanto mais V^{IV} é adicionado na solução, maior quantidade se liga à proteína, mas a relação V:hTF não excedeu 3 (no sistema $V^{IV}O(acac)_2$) ou 4 (no sistema $V^{IV}O(oda)(bipy)$). $V^{IV}O(oda)(bipy)$ e $V^{IV}O(acac)_2$ ligam-se provavelmente a resíduos tirosina. Os resultados de fluorescência sugerem que os resíduos triptofano não são muito afectados.

Todos os complexos estudados provocam algum quench da fluorescência da hTF e da HSA, quando se faz a excitação a 280 ou 295 nm, mas este quenching não é muito pronunciado. Portanto, se estes compostos forem introduzidos no sangue em doses relevantes para efeitos terapêuticos, a ligação não se irá dar perto dos resíduos Trp de ambas as proteínas, excepto no caso abaixo mencionado. Por outro lado, as características de quenching observadas para a maior parte dos sistemas aqui estudados é compatível com a existência de mais do que um mecanismo e/ou local de ligação em ambas as proteínas.

O efeito de quenching observado na ligação do $V^{IV}O(oda)(bipy)$ à HSA é significativo. No sistema HSA-$V^{IV}O(oda)(bipy)$ observa-se também um desvio para o vermelho no máximo das bandas de emissão, isto provavelmente significando que os resíduos tirosina e/ou triptofano se deslocam da cavidade hidrofóbica para zonas mais hidrofílicas durante o processo de ligação ao complexo; a isso poderá também estar associada uma conformação mais aberta da albumina.

Palavras chave. *Vanádio, complexos de oxidovanádio(IV), transferrina do soro humano, albumina do soro humano, dicroísmo circular, Ressonância paramagnética electrónica, espectroscopia de fluorescência, actividade anticancerígena.*

LIST OF ABBREVIATIONS

hTF	human serum Transferrin
HSA	human serum albumin
oda	oxidiacetate
bipy	2,2'-bipyridine
phen	1,10-phenanthroline
MBS	metal binding site
ACTUN-motif	N-terminal copper and nickel binding site
VBS1	Vanadium binding site 1
VBS2	Vanadium binding site 2
CD	Circular dichroism
EPR	Electron paramagnetic resonance
Ref	Reference
Tris	(tris(hydroxymethyl)aminomethane
PBS	Phosphate buffered saline
ROS	Reactive oxygen species
DMEM	Dulbeccos modified Eagles medium
ADME	**A**bsorption, **D**istribution, **M**etabolism, **E**xcretion
$NADH^+$	Reduced form of nicotinamide adenine dinucleotide
ERK	extracellular-signal-regulated kinase
DNA	Deoxyribonucleic acid
MEK	MAPK/ERK kinase
GSH	Glutathione
MMP	Mitochondria membrane potencial
pDNA	DNA plasmid model
MOPS	3-(N-morpholino)propansulfonic acid buffer
(Sc) DNA	supercoiled DNA
(Nck) DNA	nicked DNA
DMSO	Dimethyl sulfoxide
MeOH	Methanol
EtOH	Ethanol
LCFA	Long-chain fatty acids

Introduction

1.0. INTRODUCTION

1.1.0. Vanadium in the Earth.

Vanadium, named after the Nordic goddess Vanadis, is a transition metal which has two naturally occurring isotopic forms: ^{51}V (99.75%) and ^{50}V (0.25%). In the Earth's crust, its abundance is 0.013% w/w (22ndplace). In sea water vanadium is mostly present as NaH_2VO_4 in concentration of ca. 30 nM.[1] In drinking water vanadium concentration is within 10 nM range. In vulcanic groundwater the concentration may reach 2.5 μM.[1] Interesting is the fact that in human blood plasma it is quite high - about 200 nM and in tissue about 6 μM which emphasizes vanadium biological role. In living organisms vanadium is mostly accumulated in bones, liver and kidneys.[1]

1.2.0. Pharmacological properties and application of Vanadium and its complexes in medicine.

In the literature vanadium has been reported to have positive medicinal effects in the treatment of HIV[1,2-5,6], diabetes mellitus (insulin-mimetic effect), herpes, amoebiasis[1], tuberculosis[1,7-9], influenza, parainfluenza, Dengue fever, Severe Acute Respiratory Syndrome (SARS)[10-11] and cancer.[1] It was also discovered that vanadium compounds possess anti-parasitic[12], antibacterial[13] and spermicidal[14-16,17-18]activities.

Since vanadium has demonstrated interesting biological and pharmacological properties, it deserves a precise attention for its application in medicine and biomedical sciences. Some vanadium complexes were reported to be much more efficient in this field than the simple vanadium (V^{IV} and V^{V}) salts both in vitro and in vivo.[33] Therefore, the development of new anticancer drugs containing vanadium derivatives with organic ligands is of great importance as it may improve their bioavailability and diminish side effects.[33-36] Moreover, some vanadium compounds are poorly absorbed in the gastrointestinal tract; normally organic ligands increase the gastrointestinal absorption. Consequently, smaller dose of vanadium will be needed for the patient to intake to reach the same therapeutic effect.[19-22]

Vanadium has potential to both prevent and treat the cancer. Vanadium was found to be effective against at least the following types of cancer: osteosarcoma[23-27], leukaemia, carcinomas of the breast, liver, testes, prostate, gastrointestinal tract, lung, ovaria, Ehrlich ascites tumours, nasopharyngeal carcinoma and malignant myeloma cells.[1]

The chemo-preventive effect, or "carcinogen interception mechanism"[28,29] of vanadium may be realized through activation of signal transduction pathways which lead to activation of tumour suppressor genes or to tumour cells apoptosis. It can be reached by inhibition of tyrosine phosphatase, so the phosphorylation of tyrosine residues in proteins increases and activates the mentioned pathways. Additionally, vanadium compounds may generate or interfere with reactive oxygen species (ROS), and detoxify the DNA alkylating agents.[1] Both oxovanadium(IV) and (V) exhibit an action of scavengers as well as generators of ROS (peroxide, superoxide, hydroxylradicals, singlet oxygen). The reaction products are very dependent on the booster ligands which temporarily bind to vanadium and shift the redox potentials, and also on pH.[30]

Some studies report that vanadate can regulate cell differentiation, and that vanadium derivatives behave like growth factors, as it was shown on osteoblast-like cells. Hence, they are potential tools for the cell growth control.[31]

Vanadate (V), oxidovanadium (VO^{2+}), bis(maltolato)oxidovanadium (IV), (BMOV), and bis(maltolato)dioxidovanadium (V), (BMV), were reported to be able to stimulate cell growth in a small range of concentrations in MC3T3EI osteoblast-like cells and to inhibit their growth at high concentrations. All these compounds induce the phosphorylation of tyrosine residues in several proteins and inhibit phosphotyrosine phosphatases.[32]

Complex formed by oxidovanadium (IV) and flavonoid ligand hesperidin showed higher antiproliferative action than the one of free ligands and caused morphological alterations towards apoptosis in the cell lines in culture (human colon adenocarcinoma Caco-2 and rat osteosarcoma UMR106). Vanadium complexes with such ligands as, for example, naturally occurred flavonoids are also good scavengers and antioxidants which play a role of protectors of biomolecules from the attack of free radicals which may appear in regular inter- and intracellular metabolic processes and interact with the molecules, thus, causing pathologic changes in cells, and, consequently, tumoral processes.[33]

Other complexes of oxidovanadium (IV) with glucose (GluVO) and with naproxen (NapVO) have shown antineoplastic activity in osteosarcoma cell lines (cultured in Dulbeccos modified Eagles medium (DMEM)).[37]

Same cell lines as in study[37] (but in culture and in zebrafish model) were tested by the treatment with oxidovanadium (V) complexes with hydroxyl-amino ligand and amino acids:

valine(val) and methionine(met). Both complexes, $[VO(NH_2O)_2(val)]$ and $[VO(NH_2O)_2(met)]$ are reported to inhibit both cell lines proliferation, and also the viability of zebrafish eggs.[38]

$V^{IV}OSO_4$ is reported to cause molecular oxygen dependent 2'-deoxyguanosine (dG, nucleoside, one of DNA constituents) hydroxylation which results in formation of 8-hydroxyl-2'-deoxyguanosine (8-OHdG) and also molecular oxygen-dependent DNA strand breaks.[39] Another study[40] reports nicks in pUC18 DNA in the absence or in the presence of H_2O_2 and also lipid peroxidation in isolated rat hepatocytes caused by oxidovanadiumn (IV) complexes.

1.2.1. Vanadium drug uptake, distribution, metabolism and elimination.

Absorption and distribution of any drug comprises a set of such physico-chemical processes as diffusion, penetration through cell membranes, binding to blood proteins, transport to target cells and partition between different tissues of organism. All these processes depend on the particular way of drug administration. In pharmacology the disposition of the drug is divided into four stages which for convenience are designated by the acronym 'ADME'. ADME stands for:

- **A**bsorption – passage of the drug from the site of administration to the plasma;
- **D**istribution between main body fluid compartments;
- **M**etabolism (anabolism and catabolism) – the build-up and breakdown of compounds mediated by enzymes within the whole body;
- **E**xcretion – elimination of the drug metabolites or the rest of drug which remained chemically unchanged.[41]

The biological effect of vanadium is dependent on its oxidation state and the stability of its compounds under physiological conditions.[42] Vanadium has three oxidation states relevant for biological systems: +3, +4 and +5. In aerobic conditions V^V is stable while in anaerobic, like in the cytoplasm, it can be easily reduced from to $V^{IV}O^{2+}$ by such reducing agents as ascorbate, glutathione and $NADH^+$. The reduction of $V^{IV}O^{2+}$ to V^{3+} does not occur easily under common conditions. For this reason V^{III} is normally considered to be less important in physiological action of vanadium compounds. V^{III} and $V^{IV}$are not very stable at physiological pH and in aerobic conditions, and V^{IV} can be easily oxidized to V^V.[1] However, the stability of V^{IV} complexes is dependent on the type of ligand coordinated. For example, the $V^{IV}O$-transferrin complexes are quite stable.[43]

V^{V} can form a wide variety of complexes ranging from tetrahedral and octahedral to trigonal- and pentagonal-bipyramidal; V^{IV} often forms square pyramidal structures or, in case the 6th site is occupied, the distorted octahedral structure is formed.[44-47]

The schematic ADME model of vanadium compounds in the body is presented in the Figure 1.

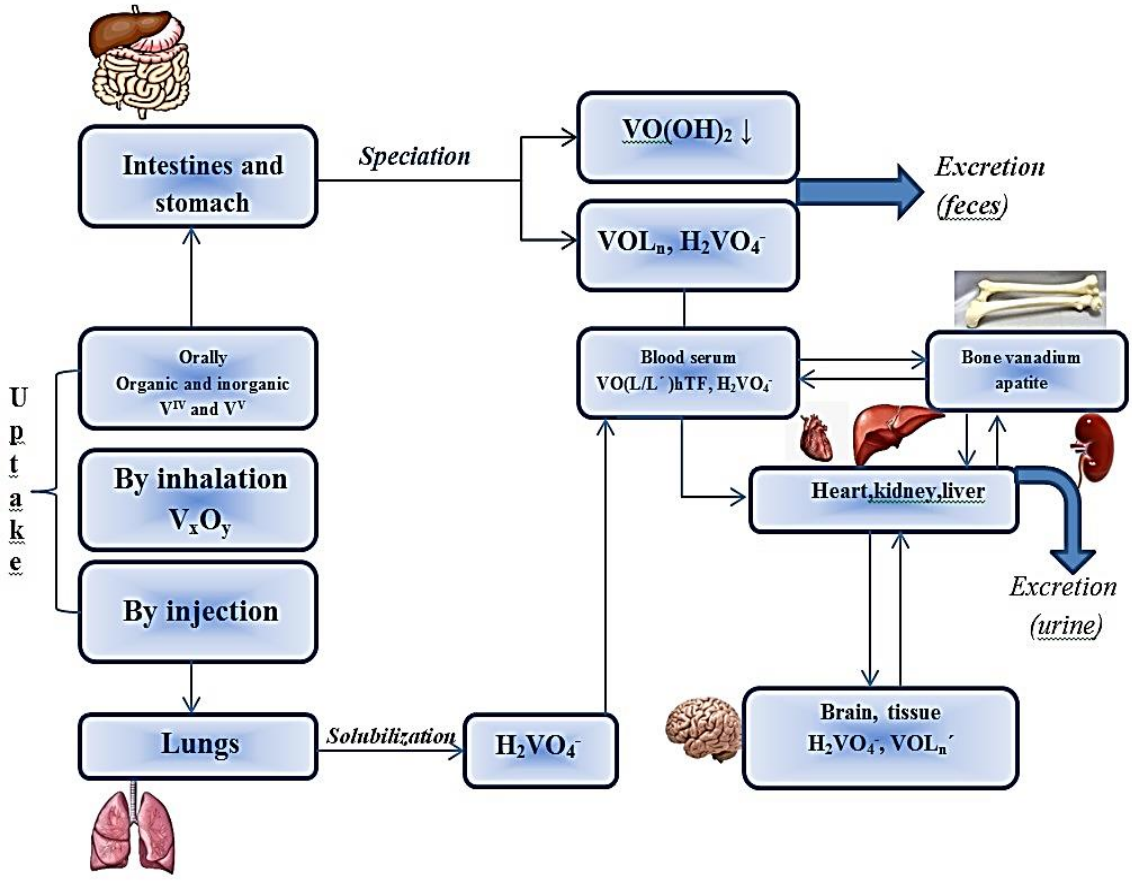

Figure 1. Schematic ADME model of vanadium compounds in the human body. The uptake and the transport routes of vanadium are indicated by arrows. Excretion ways are indicated by the large arrows."L" indicates a ligand in vanadium complex, "L´" indicates a ligand from body system, hTF – human transferrin. Adapted from ref. [48]

After oral administration vanadium-containing drug meets saliva's and small intestine's weak alkaline media, and then strong acidic (pH ≈ 2) media of the stomach. Drug encapsulation can help to avoid the immediate destruction of the drug in the stomach. Thus, the original drug undergoes the speciation due to pH changes and interaction with available bio-ligands. Besides, the redox interaction of the drug takes place in the oral cavity (oxidation) and in the gastrointestinal tract (reduction). Different ligands of low and high molecular mass are present in the food and in body fluids. Hence, original vanadium compound is distributed between these ligands. $V^{IV}O^{2+}$ may be converted to $VO(OH)_2$ (precipitate, secreted with the feces);

vanadates to $H_2VO_4^-$ (pH = 7 ± 0,7) and $V^{IV}O^{2+}$ (pH = 2–3). Then, $H_2VO_4^-$ is easily resorbed in the small intestine and is distributed within the body. Inhalation of vanadium oxides from dust particles is an another way of vanadium uptake. The major part of vanadium oxides solubilizes in the lungs (is converted to vanadate) and thus enters the blood stream.[48]

Complexes of general formula VOL_n, where L is an organic ligand, are subjected to speciation by pH too. Body ligands L´ may cause coordination sphere reorganization and form VOL'_n or mixed L/L´ species and thus change the level of resorption. Once vanadium comes into the blood stream, the blood serum components define the formation of vanadium species (which includes ligand exchange and/or redox reactions between V^{IV} and V^V and, possibly, V^{III}), the pathways to target cells and the final uptake of vanadium by the cells.[48] Some authors[49] reported that vanadium level in blood plasma is regulated homeostatically. Ligands which take part in the exchange are the low molecular mass and high molecular mass ligands. Lactate and citrate belong to the first group, and transferrin (hTF), albumin and immunoglobulin G are the most important ligands in the second group, where hTF plays a predominant role.[48]

Around 95% of the vanadium which is transported in the blood has the form of oxidovanadium ($V^{IV}O^{2+}$) bound to hTF.[50] Ascorbate, glutathione and NADH can cause the reduction of V^V to V^{IV}, while NAD^+, O_2, O_2^{2-} and O_2^- can cause the reverse process of oxidation of V^{IV} to V^V.[48]

Once vanadium compounds are uptaken, they enter the blood stream and, apart from speciation, they are subjected to redox interconversion between V^V and V^{IV} species. hTF is the main transporter of anionic vanadate(V), $V^{IV}O^{2+}$ and $V^{IV}OL$ (neutral or charged) species in blood.[6]

V^V exists mainly in form of $H_2VO_4^-$and HVO_4^{2-} (often referred as VO_3^-) or as mono-vanadate when present at very low concentrations, like in blood plasma.,and several potential ligands being present, it is not expected that Divanadates (V_2) or tetravanadates (c-V_4) usualy do not form in blood plasma at pH 7.4 and low concentration of V^V. In cells vanadate concentrations also do not allow for the formation of oligovanadates. However, if concentration enhancement or template-directed nucleation occurs locally, the oligovanadate(s) formed can interact with pro-teins and DNA. [6]

$V^{IV}O^{2+}$ is probably totally bound to high and low molecular mass bio-ligands in blood serum. Inside the cells many of bio-ligands form complexes with $V^{IV}O^{2+}$ with quite high binding constants so most of the $V^{IV}O^{2+}$ is also bound. However, it cannot be ruled out that very small amounts of $V^{IV}O(OH)_3$−(free or bound?) are present; and it has some relevance in physiological media.[6]

Vanadium may accumulate in liver, kidney, thyroid, heart, brain, muscle, blood, spleen, lungs, adipose, hair and bone at relatively high levels [51-53] and in cardiac fat and lungs at relatively low levels.[51] The highest concentrations were found in liver, kidney and bone. [51-53] Most human tissues contain less than 10 ng/gm of vanadium, and the total adult body pool size is less than 1 mg.[54] In the bone vanadium partially substitutes the phosphate, and its half-life there is about 1 month.[55] Bone is considered to be a long-term storage place for vanadium.[56]

1.2.2. The toxicity of Vanadium.

Some studies[1,54,48,57,6] report the toxicity of vanadium compounds in the environment and nutrition, but this thesis mainly considers the vanadium-based anticancer drugs effect on human body, and particularly, on nontransformed (normal) cells so general toxicity will be described briefly. The cytotoxicity, genotoxicity and apoptotic features of oxidovanadium (IV) complexes studied will be considered in *Sections 1.4.0 - 1.4.8.*

In human body vanadium possesses a broad range of toxic effects on the respiratory, circulatory and central nervous systems, digestive organs, kidneys, and skin. In certain tissues vanadium may be involved in pathogenesis of some neurological disorders and cardiovascular diseases. Vanadium has spasmogenic activity in some smooth, cardiac and skeletal muscles. For instance, exposure to V_2O_5 may cause hand tremor, hypertension, wheeze, rale, rhonchi, hepatomegaly, eye irritation, injected pharynx, green tongue. Vanadate, when administered intravenously in cumulative doses, significantly increases arterial blood pressure. As vanadate inhibits Ca-ATPase and reduces calcium efflux, it may act as vasoconstrictor. The distinct effect of vanadate is to mobilize the intracellular calcium in many of smooth muscles. Dimercaprol and ascorbic acid have been used in the treatment of vanadium poisoning in humans.[57]

It was reported that vanadium toxicity is the highest in intravenous administration, and is lower in the oral one.[58] The maximum allowable concentration of vanadium is 0.05 $mg \cdot m^{-3}$. At one-time exposure the immediate danger to average human's health is caused by limit of 7

mg of vanadium(intravenously), and by 35 $mg \cdot m^{-3}$ of V in the air being inhaled. In food, the oral intake of maximum of 1 $mg\ kg^{-1}\ day^{-1}$ will cause no effect.[48]

1.3.0. Oxidovanadium (IV) - complexes.

The complexes investigated in this study are $V^{IV}O$(oda), $V^{IV}O$(oda)(bipy), $V^{IV}O$(oda)(phen) and $V^{IV}O(acac)_2$. As it was mentioned before, organic ligands are of particular interest in the new anticancer drug development as they may increase its absorption in gastrointestinal tract which, in turn, allows the smaller doses of vanadium drug to reach the same therapeutic effect. Good examples of such ligand are oxodiacetate (oda), $O(CH_2COO^-)_2$ where the donor group is OOO, and acetylacetone (acac) with the donor binding set is OOO.[26] The formulae of these ligands are presented in Figures 2-3. The other 2 ligands, complexed with $V^{IV}O^{2+}$ in studied complexes, are 2,2'-bipyridine (bipy) and 1,10-phenantroline (phen), whose coordination properties are similar. They are bidentate ligands with two nitrogen donor atoms. Their formulae are presented in Figure 4.

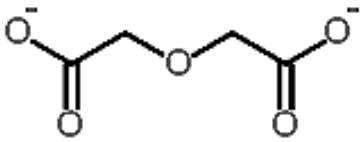

Figure 2. Ctructural formula of the oxodiacetate (oda) ligand. From ref. [59]

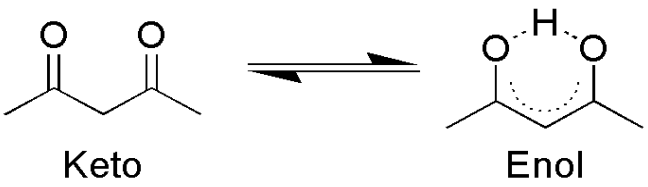

Figure 3. Ctructural formula of acetylacetone (acac) ligand (keto- and enol forms). From ref. [60]

Acetylacetone in solution exists in two tautomeric forms: keto and enol. In enol form hydrogen atom equally belongs to both oxygen atoms, so this form has C_{2v} symmetry.[61] These two forms can be easily distinguished by NMR spectroscopy, IR spectroscopy, and some other methods.[62,63]

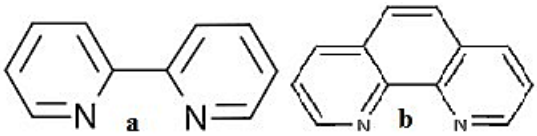

Figure 4. Structural formula of (a) 2,2'-bipyridine (bipy) ligand[64] and (b) 1,10-phenanthroline (phen) ligand. [65]

1.3.1. Complex $V^{IV}O(oda)(H_2O)_2$.

The structural formula of the complex is presented in Figure 5.

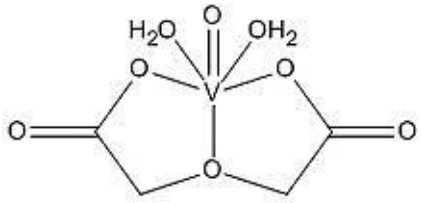

Figure 5. Structural formula of $V^{IV}O(oda)(H_2O)_2$. Drawn in computer program ChemDraw.[70]

The molecule has approximate C_{2v} symmetry. The complex has a distorted octahedral geometry. Two water ligands are in mutual trans-position (O-V-O angle is 174.2˚). The oxydiacetate ligand is distributed meridionally.[66]

1.3.2. Complex $V^{IV}O(oda)(bipy)$.

The structural formula is presented in Figure 6.

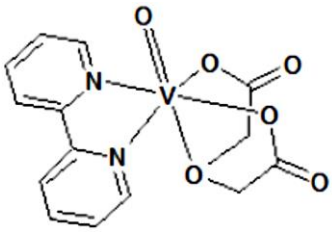

Figure 6. Structural formula of $V^{IV}O(oda)(bipy)$. From ref. [26]

The complex is yellow-brown and has a distorted octahedral geometry. The equatorial base is made up by two bipyridine N-atoms and two carboxylic O-atoms from the acetate groups. The central O-atom of oda and the oxygen of the V=O group make up the axis.[67]

1.3.3. Complex $V^{IV}O(oda)(phen)$.

The structural formula of the complex is presented in Figure 7.

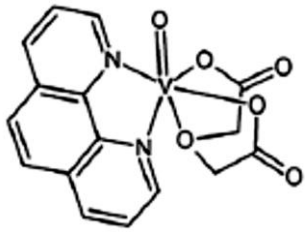

Figure 7. Structural formula of $V^{IV}O(oda)(phen)$. From ref. [26]

The complex is yellow-green and has a distorted octahedral geometry. The equatorial base is made up by two o-phenanthroline N-atoms and two carboxylic O-atoms from the acetate groups. The central O-atom of oda and the oxygen of the V=O group make up the axis.[68]

1.3.4. Complex $V^{IV}O(acac)_2$.

The structural formula of the complex is presented in Figure 8.

The complex is blue green and has a square-based pyramidal geometry; it is able to accommodate one more monodentate ligand.[69]

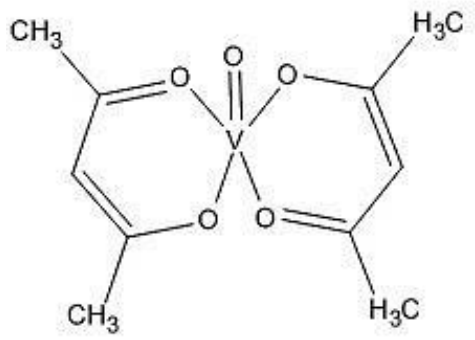

Figure 8. Structural formula of $V^{IV}O(acac)_2$. Drawn in computer program ChemDraw.[70]

1.3.5. UV-Vis of oxidovanadium (IV) - complexes.

The diagram of molecule orbitals of $[V^{IV}O(H_2O)_5]^{2+}$ is presented in Figure 9.

The energy of the orbitals increases in the following order: $d_{xy} < d_{xz}, d_{yz} < d_{x2-y2} << d_{z2}$. Three d-d transitions are observed in the visible absorption spectra. They are identified as bands:

Band I: $d_{xy} \rightarrow d_{xz}, d_{yz}$ ($b_2 \rightarrow e$), usually in the 900-625 nm range;

Band II: $d_{xy} \rightarrow d_{x2-y2}$ ($b_2 \rightarrow b_1$), in the 690-520 nm range;

Band III: $d_{xy} \rightarrow d_{z2}$ ($b_2 \rightarrow a_1$), usually in the 470-330 nm range.[71]

In $V^{IV}O$-complexes d-electron is often located in essentially non-bonding orbital d_{xy} so the ordering of the d levels is as depicted in Figure 10. In complexes with low symmetry four transitions are expected.[71]

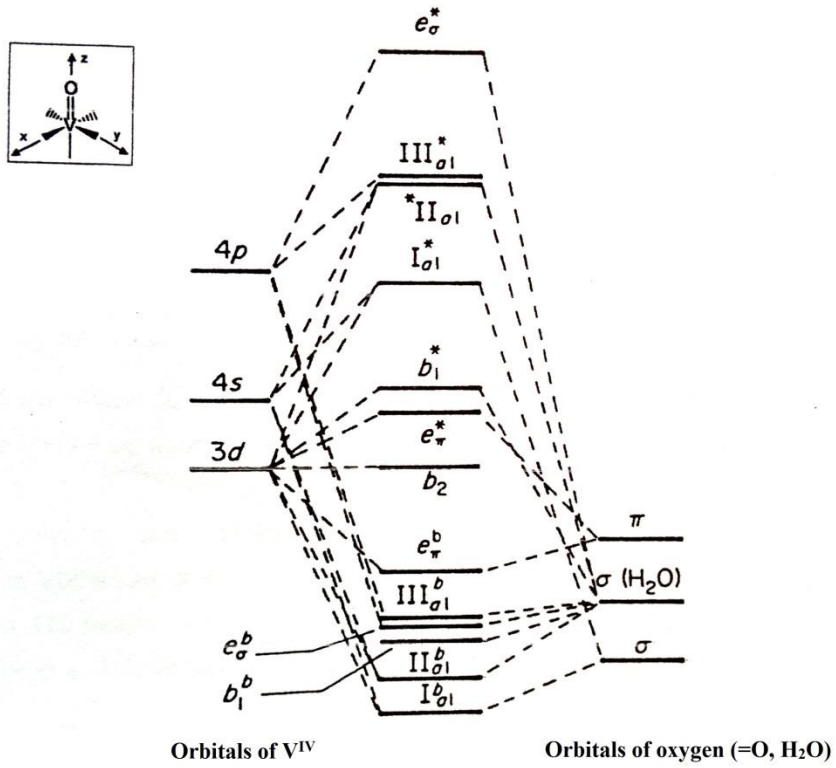

Figure 9. Diagram of molecular orbitals of the oxidovanadium aquacomplex $[V^{IV}O(H_2O)_5]^{2+}$ with C_{4v} symmetry. The molecular orbitals of the symmetry b_2, e_π^*, b_1^*, I_{a1}^* are fundamentally metal orbitals: $b_2 \equiv d_{xy}$, $e_\pi^* \equiv d_{xz}, d_{yz}$, $b_1^* \equiv d_{x2-y2}$ and $I_{a1}^* \equiv d_{z2}$. From ref. [71]

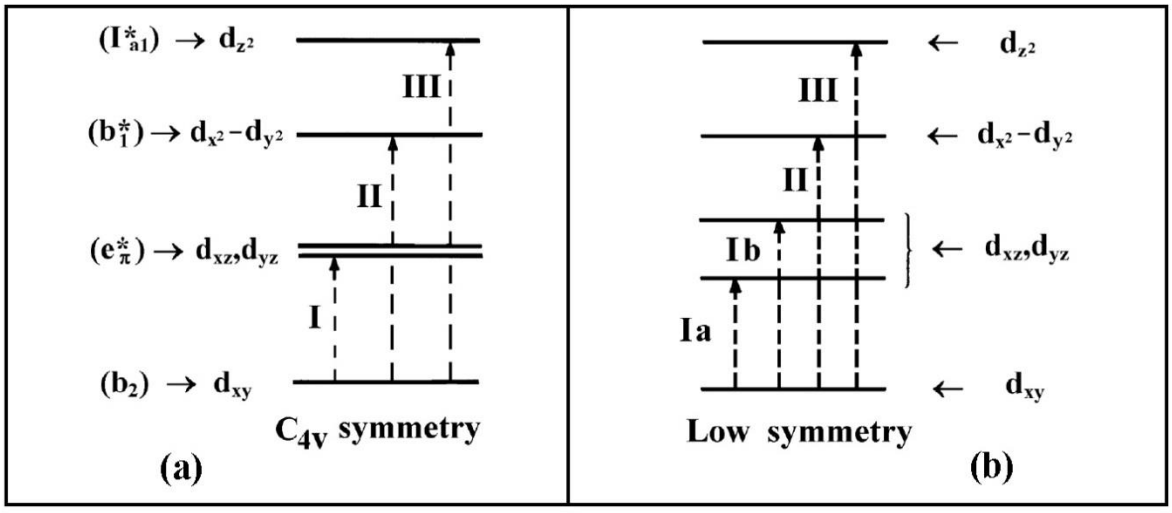

Figure 10. Ordering of d levels in $V^{IV}O$-complexes. (a) for complexes with C_{4v} symmetry (e.g. $[V^{IV}O(H_2O)_5]^{2+}$); (b) complexes with low symmetry (e.g. $V^{IV}O(lactato)_2$). From ref. [71]

1.4.0. Complexes $V^{IV}O(oda)(H_2O)_2$, $V^{IV}O(oda)(bipy)$, $V^{IV}O(oda)(phen)$ and $V^{IV}O(acac)_2$ as potential anticancer drugs.

Many studies [26,66-68,72-74] report the anticancer activity of these complexes. The results are quite interesting as the replacement of the two water molecules in the parent complex $V^{IV}O(oda)(H_2O)_2$ with heterocyclic bidentate ligand (bipy or phen) causes a significant change in biological activity. Moreover, slight difference in structure of bipy and phen ligands leads to quite different anticancer behavior.[74] In this study anticancer action is considered in terms of cytotoxicity, genotoxicity, lysosomal activity alterations, mitochondria activity alterations, morphological changes in the cells, role of oxidative stress, apoptotic action and nuclease activity (plasmid DNA cleavage).

1.4.1. Cytotoxicity and putative mechanisms of the complex cytotoxic action.

In cytotoxicity studies it is always important to evaluate the drug selectivity, i.e. how many times the particular drug is more toxic to tumoral cells than to nontransformed ones.

In human osteosarcoma MG-63 cell line $V^{IV}O(oda)(H_2O)_2$, $V^{IV}O(oda)(bipy)$ and $V^{IV}O(oda)(phen)$ were reported to cause concentration-dependent inhibition of cell viability.$V^{IV}O(oda)(phen)$ shows antiproliferative action at the lowest concentration of the complex, next is $V^{IV}O(oda)(bipy)$, and then, at higher concentrations, $V^{IV}O(oda)(H_2O)_2$ acts.[26]

$V^{IV}O(oda)(H_2O)_2$, $V^{IV}O(oda)(bipy)$ and $V^{IV}O(oda)(phen)$ have been tested on MC3T3E1 osteoblastic mouse calvaria-derived cells and UMR106 rat osteosarcoma-derived cells in culture. $V^{IV}O(oda)(phen)$ was reported to cause inhibition of cell proliferation in both cell lines, but the cytotoxicity was stronger in the normal (MC3T3E1) cell line than in the tumoral (UMR106) one.[68] $V^{IV}O(oda)(bipy)$ was reported to cause inhibition of cell proliferation in both cell lines, but the cytotoxicity was statistically stronger in the tumoral cells in the whole range of concentrations, especially in the high concentration range. At the highest tested concentration nontransformed cells showed a survival of 56%, while only 30% of the tumoral cells survived.[67] $V^{IV}O(oda)(H_2O)_2$ was more deleterious in the normal cell line than in the tumoral one.[73,74] In the UMR106 cell line $V^{IV}O(oda)(H_2O)_2$ significantly inhibits the marker of osteoblast differentiation - alkaline phosphatase activity.[73]

In the cytotoxicity mechanism studies of the same cell line $V^{IV}O(oda)(H_2O)_2$ was reported to induce dose-dependent extracellular-signal-regulated kinase (ERK) cascade activation

through ERK phosphorylation. ERK pathway plays role of transducer in the signal cascade mediating cell proliferation and differentiation, cell cycle arrest, antiproliferation, apoptotic and non-apoptotic death.The relative intensity of ERK cascade stimulation is higher in nontransformed osteoblasts than in tumoral ones. These results indicate that the ERK pathway may be involved in the $V^{IV}O(oda)(H_2O)_2$ cytotoxic effects.[74]

In human colon adenocarcinoma cell line Caco-2 $V^{IV}O(oda)(H_2O)_2$ was found to induce dose-dependent inhibition of Caco-2 cell proliferation. The inhibition is statistically significant starting from the complex concentration of 25 μM. The $V^{IV}O(oda)(H_2O)_2$ effect is partially diminished by such free radicals scavenger as a mixture of vitamins C and E. The free ligand does not show any effect on cell proliferation. The main cytotoxic mechanisms of $V^{IV}O(oda)(H_2O)_2$ are oxidative stress increase and GSH level decrease. Scavengers partially reverse the effect of free radicals. [72]

1.4.2. Genotoxicity.

Genotoxic effects must not be confused with cytotoxic ones as DNA degradation may happen because of necrosis or apoptosis which may show a false positive response. [72]

In human osteosarcoma MG-63 cell line $V^{IV}O(oda)(H_2O)_2$ causes no damage in tumour cells DNA at the whole range of studied concentrations while $V^{IV}O(oda)(phen)$ induces the damage in this whole range, and $V^{IV}O(oda)(bipy)$ only at the highest concentration studies.[26]

In human colon adenocarcinoma cell line Caco-2 $V^{IV}O(oda)(H_2O)_2$ causes statistically significant DNA damage in the low range of concentrations. [72]

1.4.3. Lysosomal activity alterations.

In human osteosarcoma MG-63 cell line the decrease in lysosomal activity, the result of lysosomal metabolism alteration, occurs at the whole range of the tested concentrations of $V^{IV}O(oda)(phen)$ and only at high concentrations of both $V^{IV}O(oda)(H_2O)_2$ and $V^{IV}O(oda)bipy$.[26]

In human colon adenocarcinoma cell line Caco-2 lysosomal activity alterations start at the $V^{IV}O(oda)(H_2O)_2$ concentration lower than the concentration at which inhibition of proliferation becomes statistically significant.[72]

1.4.4. Mitochondria activity alterations.

In human osteosarcoma MG-63 cell line all three complexes decrease mitochondria enzyme activity, which is stronger for $V^{IV}O(oda)(phen)$ in the whole range of concentrations, but for $V^{IV}O(oda)bipy$ and $V^{IV}O(oda)(H_2O)_2$ it is significant only at high concentrations.[26]

In both MC3T3E1 osteoblastic mouse calvaria-derived cells and UMR106 rat osteosarcoma-derived cells in culture $V^{IV}O(oda)(H_2O)_2$ shows dose-dependent Mitochondria Membrane Potencial (MMP) dissipation. Presence of GSH keeps the MMP under control in nontransformed cell line. Moreover, pre-incubation of the tumoral cells with GSH prevented the loss of MMP. [74]

In human colon adenocarcinoma cell line Caco-2 the presence of $V^{IV}O(oda)(H_2O)_2$ causes a significant decrease in the mitochondrial succinic dehydrogenase reduction activity starting from concentration of 10 μM and higher. At higher concentrations mitochondria enzyme activity decrease becomes stabilized at the value of 45%.[72]

1.4.5. Morphological changes in the cells.

In human osteosarcoma MG-63 cell line at low concentration $V^{IV}O(oda)(H_2O)_2$ causes a slight decrease in the cell number, at higher concentrations this decrease is observed with significant alterations in the cytoplasm and the nuclei. $V^{IV}O(oda)(bipy)$ shows similar effect, which is stronger at higher concentrations. Comparatively, $V^{IV}O(oda)(phen)$ affects much more the morphology of the tumour cells as it causes the nuclei fragmentation and dramatic decrease in cell number at higher concentrations.[26]

In MC3T3E1 osteoblastic mouse calvaria-derived cell line $V^{IV}O(oda)(H_2O)_2$ exhibits it's effect starting from concentration of 10 μM through gradual cytoplasm condensation and loss of the cytoplasmic connections between the cells. The effect increases with the increase of concentration. In UMR106 rat osteosarcoma-derived cells cytoplasm condensation occurs at the same complex concentration as for nontransformed cells. All morphological changes result from the modification of the cytoskeleton proteins. $V^{IV}O(oda)(H_2O)_2$ causes rearrangement of the actin and significant alterations in the cell shape. At the highest concentration of the complex actin gets accumulated in a form of patches in the cytoplasm. For the tumoral cells the first microfilaments changes are observed at 25 μM. At the highest concentration complete disorganization of the fibers around nucleus and alteration of the cell shape are observed. These changes are stronger in the nontransformed osteoblasts than in the tumoral ones. According to reversibility studies, these changes are irreversible. [74]

In human colon adenocarcinoma cell nucleus the $V^{IV}O(oda)(H_2O)_2$ causes chromatine condensation. In cytoplasm it causes numerous irregular vacuoles and loss of connections. The apoptosis of significant number of cells and their detachment from monolayers occurs. The complex causes concentration directly related rearrangement of the actin microfilaments with the total loss of the network the highest complex concentration. [72]

1.4.6. Role of oxidative stress.

Oxidative stress is an imbalance between the regular formation of reactive oxygen species and organism sability to either detoxify immediately these species or to repair damage caused by them. If normal redox state of the cell is altered, the peroxides and free radicals are produced. As they are toxic, they damage all the cell components, including DNA. Later on, some ROS may start acting as messengers in redox signaling.[75]

In human osteosarcoma MG-63 cell line $V^{IV}O(oda)(phen)$ is able to induce a concentration - dependent oxidative stress (fourfold increase of ROS level) in tumour cell line at the lowest concentration studied. However, $V^{IV}O(oda)(H_2O)_2$ and $V^{IV}O(oda)(bipy)$ increase the ROS level only at high concentrations. [26]

In osteoblastic mouse calvaria-derived cells and UMR106 rat osteosarcoma-derived cells in culture $V^{IV}O(oda)(H_2O)_2$ triggers a dose-dependent oxidative stress in both cell lines with a stronger effect in the nontransformed cells. The oxidative stress is a major component of the $V^{IV}O(oda)(H_2O)_2$ cytotoxicity. Reduced glutathione (GSH) completely reverses the deleterious action of $V^{IV}O(oda)(H_2O)_2$. The GSH level plays a crucial role in the osteoblast cells survival as the GSH depletion is one of the $V^{IV}O(oda)(H_2O)_2$ cytotoxicity mechanism. It was found that tumoral cells are more protected from the $V^{IV}O(oda)(H_2O)_2$ induced oxidative stress than the nontransformed ones. [74]

In human colon adenocarcinoma cell line $V^{IV}O(oda)(H_2O)_2$ causes a great rhodamine level increase. However, a mixture of vitamins C and E, decrease this oxidative stress. GSH levels decrease is dose-dependent. Glutathione oxidation to GSSG creates a kind of redox buffer protecting the cells from oxidative stress. [72]

1.4.7. Apoptotic action.

In human osteosarcoma MG-63 cell $V^{IV}O(oda)(bipy)$ and $V^{IV}O(oda)(phen)$ start causing the increase in cell apoptosis from 24 h of incubation. $V^{IV}O(oda)(H_2O)_2$ shows no significant effect comparing to basal conditions. $V^{IV}O(oda)(bipy)$ increases the percentage of apoptotic

cells from 4 to 23% and $V^{IV}O(oda)(phen)$ from 4% to 37% over initial conditions at the highest concentration studied.[26]

In MC3T3E1 osteoblastic mouse calvaria-derived cell line $V^{IV}O(oda)(H_2O)_2$ causes apoptosis of significant number of the cells only at high concentrations. In UMR106 rat osteosarcoma-derived cells cytoplasm condensation occurs at the same complex concentration as for nontransformed cells. [74]

In human colon adenocarcinoma cells $V^{IV}O(oda)(H_2O)_2$ causes the apoptosis of significant number of cells and their detachment from monolayers occurs only at high concentrations. [72]

1.4.8. Nuclease activity (plasmid DNA cleavage).

In human osteosarcoma MG-63 cell line the interaction of the $V^{IV}O(oda)(H_2O)_2$, $V^{IV}O(oda)(bipy)$ and $V^{IV}O(oda)(phen)$ complexes with in vitro DNA plasmid model (pDNA) was studied. [26] Nuclease activity of the complexes depend on the nature of the buffer media. In phosphate buffer $V^{IV}O(oda)(bipy)$ nuclease activity is similar to that of $V^{IV}O(oda)(H_2O)_2$. $V^{IV}O(oda)(phen)$ exhibited very efficient DNA cleavage together with linearization in the whole range of studied concentrations. The nuclease activity of the complexes increases in the following sequence: $V^{IV}O(oda)(bipy)<V^{IV}O(oda)(H_2O)_2<V^{IV}O(acac)_2$(positive control)$<V^{IV}O(oda)(phen)$ in phosphate buffer and $V^{IV}O(acac)_2$(positive control)$<V^{IV}O(oda)(bipy)<V^{IV}O(oda)(H_2O)_2<V^{IV}O(oda)(phen)$ in MOPS (3-(N-morpholino)propansulfonic acid) buffer. In MOPS buffer the cleavage of the supercoiled(Sc) DNA occurs along with the cleavage of nicked (Nck) DNA form into linear form (Lin).[26]

In the presence of scavengers of singlet oxygen (NaN_3) and of free radicals (sodium benzoate, NaBz and DMSO) in phosphate buffer at the highest concentration $V^{IV}O(oda)(bipy)$ effectively linearizes plasmid DNA. [26]

Oxodiacetate and bipyridyne do not cause DNA degradation. [26] It was found, that all the ROS formed are hydroxyl radicals, not the singlet oxygen. H_2O_2 significantly increases DNA cleavage and leads to its complete degradation to nicked and linear forms. The scavenger effect decreases in the following row: NaN_3> NaBz > DMSO. In addition, H_2O_2 together with the $V^{IV}O(oda)(phen)$ show dramatic increase in the nuclease activity so the linear DNA is degraded as a result. Oxodiacetate and phenanthroline do not cause DNA degradation. [26]

In human colon adenocarcinoma cell line Caco-2 $V^{IV}O(oda)(H_2O)_2$ cleaves DNA under relatively mild conditions. Even relatively low concentrations it induces extensive single-strand cleavage. Double-strand cleavage is also observed. Addition of mercaptopropionic acid (MPA) slightly increases nuclease activity of the complex. [72]

$V^{IV}O(acac)_2$, was reported to show a remarkable degrading of plasmid DNA amplified in *Escherichia coli* DH5α in the absence of activating agents, air and photoirradiation.[76]

1.5.0. Blood serum proteins and their binding to vanadium complexes.

The function of blood as one of the most important animal body fluids is to transport all the substances essential for cells life and their normal functioning and to take away from the cell the toxic products of their metabolism. The blood of vertebrates presents cells (erythrocytes, leukocytes, thrombocytes) suspended in blood plasma. Plasma containes 92% of water. Blood serum is a name for blood plasma which does not contain fibrinogens. Serum comprises such proteins as albumin (55%), globulins (38%), fibrinogen (7%), regulatory proteins (1%, i.e., hormones, enzymes and proenzymes). As both human serum albumin and transferrin affect the different metal transport and distribution they are always considered in the evaluation of the interaction and transformation of any metal-containing drugs administered. [75]

It was reported that *in vitro* apo-hTF binds VO^{2+} 10^6 times stronger than HSA. HSA is present in blood serum in higher concentration (630 μM) than hTF (37 μM) and HSA may possibly be a vanadium transporter in the blood for some V-complexes, hTF being the vanadium primary binder.[103]

1.5.1. Human serum albumin: structure and functions.

Human serum albumin (HSA) makes up the major part of serum proteins. The molecular mass is about 66.5 kDa. Its half-life in the blood serum is about 20 days. [75]

Primary structure. HSA is made up of 585 amino acids with 8 Cys-Cys sequences, and one sulfydryl at Cys-34 residue which is free. For full amino acid sequence of HSA see ref.[78]

Secondary structure. The disulfide bond pattern is one unique characteristic of albumins, which assures their stability in the blood stream. HSA has 3 domains I, II, III, named so according to start of count from N-terminus and linked to each other by helical structures. Each domain has 2 subdomains, A and B, which are densely packed helices and are linked to

each other by extended peptide strands; the subdomains are assigned as IA, IB, IIA, IIB, IIIA, and IIIB. The loops linear pattern and the inter-binding of the half of residual cysteines make HSA molecule both flexible and resistant to aggressive conditions, and HSA can take different conformations easily. The loops are also able to reversibly associate into globule, for instance, in acid or concentrated urea solutions. For the schematic image of HSA secondary structure with domains see ref. [78]

Tertiary structure. When dissolved HSA molecule has the shape of ellipse which plays an important role of prevention of blood plasma from becoming too viscous. Many of HSA residues are in the ionic form and its total charge at physiological pH is negative, increasing from domain III (close to zero) towards domain I (very negative).[78]

1.5.2. Ligand binding to human serum albumin.

Human serum albumin is well-known to bind a variety of small molecules. It is able to bind cationic, neutral and anionic ligands.[77]

ATCUN motif is well-described Cu^{II} and Ni^{II} primary binding site located at the N-terminus. The ATCUN motif amino acid sequence is Asp-1, Ala-2, His-3. [79]

Multi-metal binding site (MBS) is a primary binding site for Zn^{II} and the secondary binding site for Ni^{II} and Cu^{II} and other metal ions with this oxidation state (+2). It is located at the domains I and II interface. The donors of the site are His-67 (imidazole nitrogen) and Asn-99 (carboxyl oxygen) from domain I, His-247 (imidazole nitrogen) and Asp-249 (carboxylate oxygen) from domain II. [79]

Binding site B is a primary binding site for Cd^{II} and is suitable for Zn^{II} as well. Reduced thiol group of Cys-34 is a binding site for Au and Pt compounds. [79]

Site II is a binding site for fatty acids (FA2). It is located at the subdomains IA and IIA interface. Long chain fatty acids (LCFA) bind here so the domain I rotates relatively to domain II. It causes a separation of His-247 and Asp-249 from His-67 and Asn-99 by distance of 4–6 Å. Thus, MBS becomes disrupted and can no longer bind Zn^{II}. As a conclusion, only one of these bindings is possible at the same time. [78]

Most of the drugs are transported in blood plasma and reach their target cell by being bound to HSA. Hence, in the ADME cycle HSA controls the drug distribution. HSA is able to

solubilize hydrophobic drugs, promote homogeneous drug distribution and prevent them from untimely metabolism thus increasing their biological lifetime. [78]

Sudlow has proposed two main HSA drug-binding sites. Sudlow I, or warfarin site, preferably binds large heterocyclic and negatively charged ligands and is located in IIA subdomain. Sudlow II, or indole-benzodiazepine site, preferably binds small aromatic carboxylic acids and is located in IIIA subdomain. The HSA molecule with all domains and binding sites is schematically presented in Figure 11. A simple scheme of HSA binding sites including Sudlow I and II sites is presented in the Figure 12. [78]

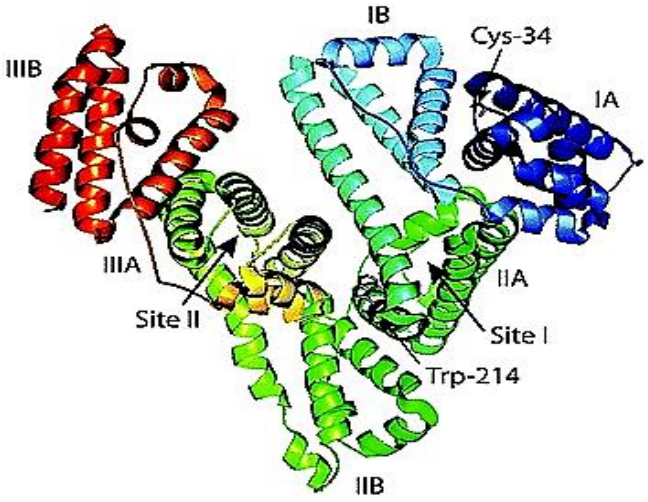

Figure 11. Domains and binding sites of HSA molecule. From ref. [80]

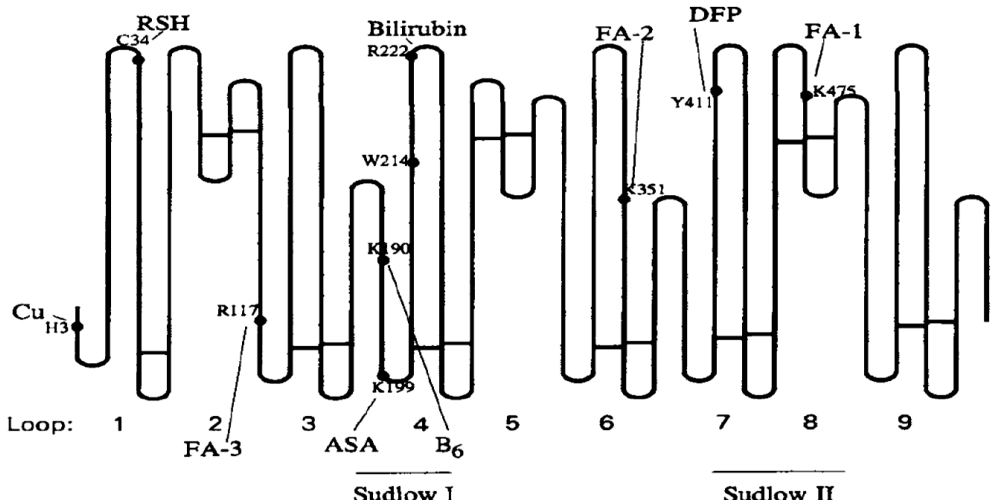

Figure 12. Scheme of HSA binding sites for different compounds.
FA - long-chain fatty acids; ASA - acetylsalicylate; B_6-pyridoxal 5'-phosphate; RSH - mixed disulfides; DFP- diisopropyl fluorophosphate. From ref. [77]

Free drug concentration in plasma is strongly affected by its binding to HSA and in most cases the HSA is far from saturation.[78]

1.5.3. $V^{IV}O^{2+}$ binding to human serum albumin.

Several studies[79,112-115] report that $V^{IV}O$ occupies two types of HSA binding sites: the strong vanadium binding site (VBS1) and the weak vanadium binding sites (VBS2).[112] VBS1 is considered to be the ATCUN motif, which was reported to bind 1 mol equivalent of $V^{IV}O^{2+}$. VBS2 are considered to be: a number of carboxylates and imidazoles in HSA side chains which are non-specific, and MBS. [79] VBS2 can bind several mol equivalents of $V^{IV}O^{2+}$.[112] The ACTUN and MBS binding sites structures with the metal center are presented in the Figure 13 (a,b). These two types of binding sites compete both with each other and with the metal ion hydrolysis. [79]

$V^{IV}O^{2+}$ binding to ATCUN motif amino acid side chains is different from Cu^{II} binding. $V^{IV}O^{2+}$ ions are not able to cause deprotonation of the amide groups. Cu^{II}, when binding to the ATCUN site, replaces $V^{IV}O^{2+}$. Replaced $V^{IV}O^{2+}$ can go to the bulk solution forming $[(V^{IV}O)_2(OH)_5]^-$, and oxidation of V^{IV} to V^{V} may occur. [79]

Two $V^{IV}O^{2+}$ centers are able to bind to MBS. [79] Zn^{II} replaces $V^{IV}O^{2+}$ when binding to MBS as it binds very strongly. However, it cannot replace $V^{IV}O^{2+}$ at other sites, e.g. at the ATCUN site. At the same time, $V^{IV}O^{2+}$ can replace Cu^{II} at the MBS. In the dinuclear form vanadium can coordinate Glu-252 located near Asp-249 at MBS. [79]

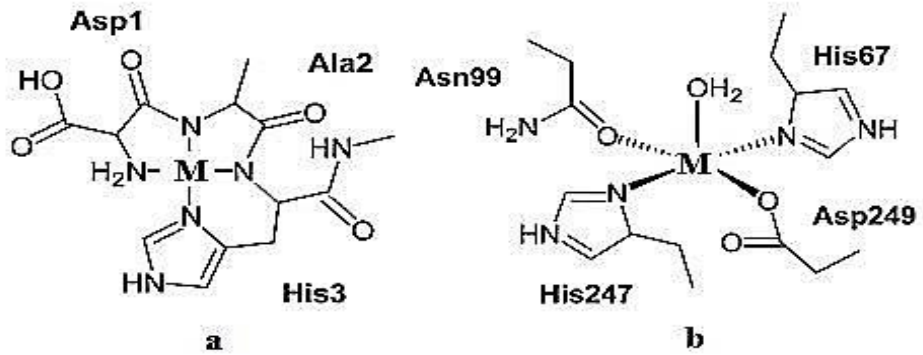

Figure 13. The structure of ACTUN (a) and MBS (b) binding sites of HSA, where M=Cu (a), Zn (b). Adapted from ref. [79]

Presence of carrier ligands may enhance $V^{IV}O^{2+}$ binding to HSA. The formation of ternary complexes HSA-$V^{IV}O^{2+}$-ligand was studied [79] by means of EPR and CD with maltol(mal), picolinic acid(pic), 2-hydroxypyridine-N-oxide(hpno) and 1,2-dimethyl-3-hydroxy-4(1H)-

pyridinone(dhp). $(V^{IV}OL_2)_n$(HSA) type complexes (and other types) are formed with ligands mal, pic, hpno, and dhp with maximum n=6 (for ligands mal and pic). Vanadium in these complexes is assumed to bind to HSA via His side chains. The binding strength of $V^{IV}OL_2$ to HSA is different and decreases in the row: hpno > pic ≥ mal > dhp. [79]

1.5.4. Human serum transferrin: structure and functions.

Transferrin is a non-haem monomeric iron-binding glycoprotein. Human serum transferrin has a molecular weight of about 79.550 kDa and in vivo half-life of 8-10 days.[81-83]

Primary structure. Human transferrin contains 678 amino acid residues and asparagine-linked glycans.[83] For the amino acid sequence of hTF see ref.[83] hTF does not have any free SH-groups, it contains 19 intrachain disulphide bridges.

6% of the hTF molecular weight corresponds to the carbohydrate moiety.[81] This moiety contains heterosaccharide chains called glycans. Transferrin derived from the same tissue of the same species may vary in glycan structures depending on the degree of sialylation (number of sialyl groups).[84-86]

There are many assumptions in the literature about the functions of carbohydrate moiety. It may enhance the protein solubility as it has many hydrophilic groups and high charges.[87] The other assumption is that this moiety may be responsible for the hTF binding during the iron exchange process to specific hTF receptors located in cell membrane.[88]

Secondary structure. Transferrin comprises two equally-sized lobes with clefts at their junction point. These two lobes correspond to the two domains, N-terminal (residues 1-336) and C-terminal (residues 337-678) halves of the polypeptide chain. The C-terminal domain has features distingushing it from N-terminal part. One is the glycan moieties attached; another one is the higher number of disulfide bonds (11 against 8).[83]

hTF functions include**:**

- transport of iron between the absorption, utilization, storage sites and sites of haemoglobin degradation (iron metabolism control); [81]
- inflammation decrease by iron withholding;
- transport of other metals.[89]

1.5.5. Metal binding by human serum transferrin.

Human serum transferrin (hTF) is capable to bind both anions and cations, but metal cation binding is of particular interest of this work. hTF has two similar metal binding sites located in its N-termal and C-terminal sites.[83]

In vivo Fe^{3+} ion binding occurs in the presence of so called 'synergistic' anions such as carbonate/bicarbonate. In the absence of these two anions, other anions may facilitate iron binding; examples are oxalate, thioglycolate, phenylalanine, pyruvate, glycine, nitrilotriacetate. However, the mentioned two anions, if present, will always replace other anions from the $(Fe^{3+})_2$ – transferrin anion complex as their binding to transferrin is stronger. One hTF binding site binds one Fe^{3+} ion and one bicarbonate or carbonate ion and the process is pH dependent. The favorable pH is 7.5-10. With the pH decrease partial dissociation happens, and complete dissociation occurs at pH = 4.5.[81] From the three protons released from Fe (III) binding, two of them are released from the two coordinated tyrosine residues, and the other ones are released from the metal ion own hydrolysis.[81]

hTF with bound iron is called holo-transferrin while apo-transferrin stands for iron-free transferrin. Holo-transferrin acquires the "closed" conformation when two domains move towards each other so it can be recognized by human transferrin receptor and then taken up by cell via receptor-mediated endocytosis of transferrin. Once iron is released the domains move apart again to form the "open" conformation of apo-transferrin.[90] A schematic view of these two conformations is presented in Figure 14.

The two Fe^{3+} and bicarbonate anion binding sites are located near the junction of two domains formed by Cys-117 to Cys-194 bond in the N-terminus. Tyr-185 and Tyr-188, and two of the three histidines - 119, 207, 249 are ligands binding to iron, and Arg-124 and/or the cluster made of Lys-ll5, Lys-116 and His-119 are electrostatically bound to the bicarbonate/carbonate anion binding site. In the C-terminus the amino acid arrangement and the coordination mode are similar.[91]

Binding sites behave differently depending on pH, i.e. N-terminus site does not bind iron at pH less than 5.7 whereas the C-terminus site binds till pH = 4.8. The binding constant of the C-terminus site is 5 times higher than the one of the N-terminus site at blood pH = 7.4. In fresh human serum the two sites are unequally occupied: there is a preferential occupation of the N-terminal site, and upon incubation at 37°C, the preference becomes even more marked.[92-95]

In serum hTF is normally saturated by iron only by 30% so it has the capacity to bind additional iron, and thus to control the toxic excess of iron. Moreover, it can bind many other metal ions, like Cu^{2+}, Al^{3+}, Zn^{2+}, Eu^{3+}, Th^{4+}, Nd^{3+},Pr^{3+}, Cr^{3+}, Bi^{3+}, Ga^{3+}, In^{3+}, Mn^{2+}, Ni^{2+}, Ru^{3+} and VO^{2+}, and even lanthanides and actinides, one ion at each binding site.[81]

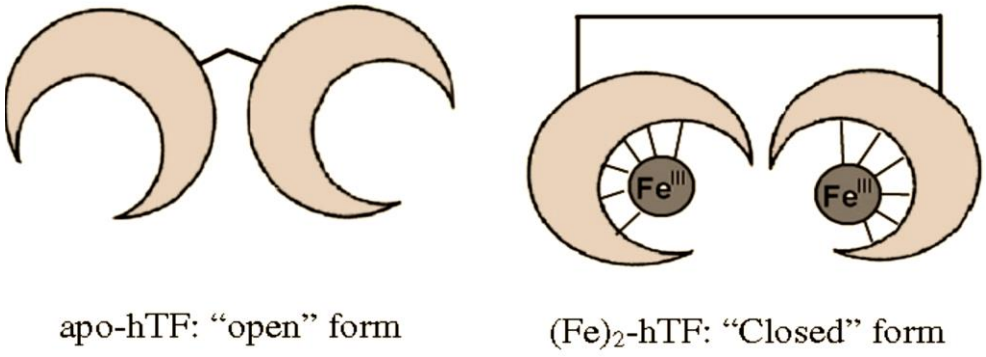

Figure14. Schematic view of "open" and "closed" conformations of apo- and holo-transferrin respectively. From ref.[96]

1.5.6. $V^{IV}O^{2+}$ binding by human serum transferrin.

Most of the blood serum vanadium is bound to hTF. hTF is capable to bind $V^{IV}O$ and $V^{IV}O(carrier)_n$ as well as V^{V} and V^{III} species.[97] $V^{IV}O$-hTF complexes are quite stable.[48] It is interesting that V^{III} binding to hTF is quite strong, almost as strong as binding of Fe^{III}.[97]

Some authors report that one oxidovanadium (IV) ion binds to one Fe-binding site of apo-hTF. However, other authors report that $V^{IV}O^{2+}$ - complexes with such lgands as maltolate, dhp (1,2-dimethyl-3-hydroxy-4-pyridinone) and picolinate bind at N-imidazole groups of surface histidines.[98-101] The study[102] reports that if >2 mol equivalents of $V^{IV}O(carrier)_n$ is added to apo-hTF, the binding of some molecules of $V^{IV}O(carrier)_n$ to the surface N-imidazole groups may occur, but it would be much weaker and is not relevant to the blood serum conditions. Later on, same authors[103] reported that $V^{IV}O(carrier)_2$ complexes are capable to interact with holo-hTF by binding to its assumed surface donors His-N, Asp-COO^- and Glu-COO^- with the most probable residues His-289, His-349, His-473 and His-606; and that when bound to holo-hTF vanadium can also be transported to the cells.[103]

There were proposed two $V^{IV}O^{2+}$binding types (both are presented in Figure 15).[97]
Binding type 1 implies the formation of $(V^{IV}O)$(hTF)(carrier ligand) structure where carrier ligand plays a role of synergistic anion or formation of cis-$(V^{IV}O)(carrier)_2$(hTF) with the

predominating complex form of octahedral cis-($V^{IV}O$)(carrier)$_2$(H_2O) at pH ≈ 7.4 where carrier ligand is not a synergistic anion. [98-103]

Binding type 2 implies that $V^{IV}O^{2+}$ binds to hTF at the Fe-binding sites with a $V^{IV}O$:ligand stoichiometry of 1:1. [98-103]

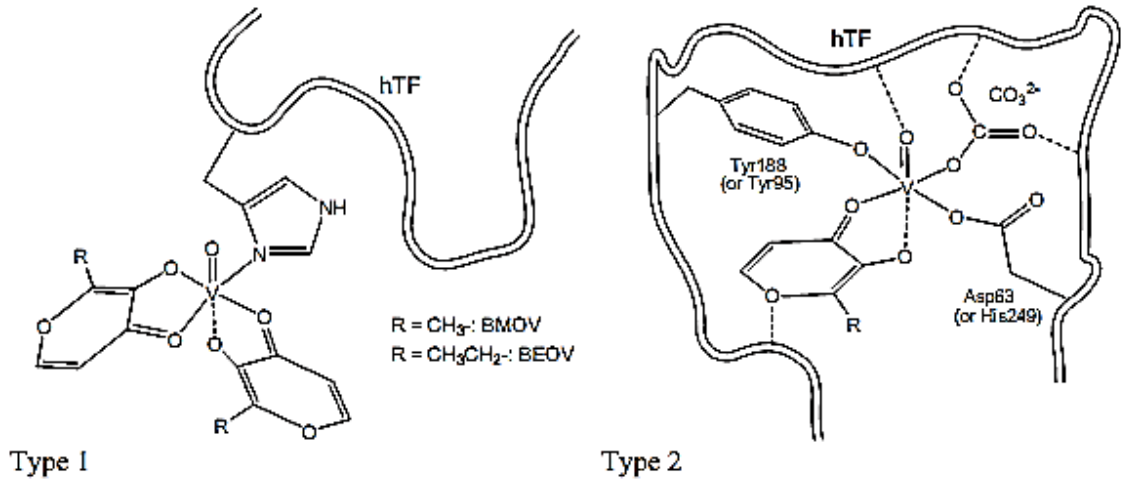

Figure 15. Proposed two binding types of $V^{IV}O$ - complexes to hTF. Bis(maltolato)oxidovanadium(IV), BMOV, and bis(ethylmaltolato) oxidovanadium(IV), BEOV, complexes are shown as examples. In the type 1 binding the VO:carrier ligand ratio is 1:2. It is assumed that in the cis-($V^{IV}O$)(carrier ligand)$_2$(H_2O) structure the water molecule is replaced by N of histidine imidazole group or by COO^- group of surface aspartic or glutamic acid. In the type 2 binding the VO:carrier ligand ratio is 1:1. It is assumed that iron-binding sites donors coordinated around vanadium are any two among the following: Asp-63, Tyr-95, Tyr-188, His-249. From ref. [97]

$V^{IV}O^{2+}$ binding by apo-hTF has been studied[96] by circular dichroism (CD), electron paramagnetic resonance (EPR) and urea gel electrophoresis. Several $V^{IV}O$(carrier)$_n$ complexes were chosen for the experiment: carrier ligand is maltolato- , dhp(1,2-dimethyl-3-hydroxy-4-pyridinone) and picolinato-.

The CD spectra showed that:

- two $V^{IV}O^{2+}$ centers bind to one molecule of hTF; [96]
- $V^{IV}O^{2+}$ centers bind exactly at the Fe binding sites, not at surface N (imidazole); [96]
- binding is as shown schematically in Figure 15: type 2 binding; [96]
- experiments with $V^{IV}O(maltol)_2$ (BMOV) show that there is a significant difference in the CD spectra, this meaning that the presence of maltol changes the type of binding of $V^{IV}O^{2+}$ to hTF. Hence, hTF($V^{IV}O(maltol)_m)_m$ species are being formed upon addition of the ligand. Further ligand addition after $V^{IV}O$:maltol ratios of 1:1 do not change the CD spectra,

however, the signal intencity decreases a little. The reason is that with increasing of maltol concentration in solution $V^{IV}O^{2+}$ unbinds hTF and goes to the solution forning $V^{IV}O$–maltol complexes which do not give CD spectra; [96]

- maltol and dhp ligands may delay the oxidation of V^{+4} to V^{+5}; [96]
- dhp or maltol, when added alone to apo-hTF, cause no changes in the CD spectra. The explanation is that these ligands cannot be in close interaction with hTF chiral centers when not bound to $V^{IV}O^{2+}$;[96]
- CD spectra of $V^{IV}O^{2+}$ complexes with different ligands follow different patterns as, for example, $V^{IV}O$-dhp complexes have higher binding strengths than the $V^{IV}O$-maltol, and their λ_{max} are different; [96]
- $V^{IV}O^{2+}$, when binding to apo-hTF, cause the change of its conformation from open to the closed form as well as the iron does. However, when V^{V} binds to apo-hTF, this change does not occur; [96]
- for both iron binding sites with $V^{IV}O^{2+}$ bound, the CD spectra are not much different. [96]

1.6.0. Techniques used in vanadium-serum proteins studies.

There is a range of techniques considered to be useful in the investigation of structure, conformation and binding nature in the vanadium-serum protein systems. Among them are the following: electron paramagnetic resonance (EPR), ^{51}V nuclear magnetic resonance (^{51}V NMR), circular dichroism (CD), UV-Vis absorption, X-ray absorption spectroscopy, inductively coupled plasma – mass spectrometry (ICP), high performance liquid chromatography coupled to mass spectrometry (HPLC-MS), capillary electrophoresis (electrospray ionization sourse) coupled to mass spectrometry (CE-ESI-MS). In this section only techniques used in this study (electron paramagnetic resonance, circular dichroism, UV-Vis absorption and fluorescence spectroscopy) are shortly described.

1.6.1. Electron paramagnetic resonance (EPR)

In EPR the sample undergoes irradiation by an external electromagnetic field induced by microwaves. In many cases the sample is frozen in liquid nitrogen since polar solvents (like H_2O, MeOH and others) absorb most of the microwaves at room temperature. The complex concentration should be ≥700 μM to ensure a good quality of spectrum (high signal-to-noise ratio).[1]

To be analyzed by this technique the metal must be paramagnetic, i.e. to have unpaired electrons. The electron configuration of vanadium in $V^{IV}O^{2+}$ ion is $1s^2 2s^2 2p^6 3s^2 3p^6 4s^2 3d^1$ so it has one unpaired d-electron with the spin S=1/2, being EPR active.

If the complex molecule contains one vanadium atom V^{IV} (mononuclear) it gives simple EPR spectra. However, in di- and polynuclear complexes (with 2 or more vanadium atoms, e.g. $(V^{IV})_2$-μ-O, $(V^{IV}V^{V})$μ-O) the interactions between centers occur and it affects the nature of the EPR spectrum.[1]

The external magnetic field (B) causes the unpaired electron spin energy level splitting in two levels (or energy states): parallel and perpendicular(anti-parallel) in regard to the field B. This is called Zeeman Effect. The energy difference is expressed by the following equation (1.1.):

$$\Delta E = E_B = h\nu = g\beta B\Delta m_s \qquad (1.1.)$$

Where ΔE – energy difference between two states;

E_B – electromagnetic radiation energy;

h – Planck's constant;

ν – field frequency;

g is a g-factor or g-value which characterizes the electron magnetic moment and gyromagnetic ratio (for free electron g = 2.0023, for $V^{IV}O^{2+}$ complexes g usually ranges from 1.94 to 1.98);

β – Bohr magneton;

B – magnetic field applied;

Δm_s– electron spin quantum number difference between two states. [1,104,105]

The nucleus also has its spin *I*. When electron couples to the nucleus with *I*>0 (hyperfine coupling) spin energy levels split further (hyperfine splitting). The electron spin energy levels are split into sublevels. The number of sublevels equals to $2nI + 1$ where n is nuclei number involved in coupling. The number of splits results in the same number of allowed transitions. [1,104,105]

The parameter used to characterize the hyperfine coupling and splitting is hyperfine coupling constant A. Under isotropic (homogeneous in all the directions) conditions (usually room temperature) for mononuclear $V^{IV}O^{2+}$ the spin energy level is split into 8 lines ranging from m_I=-7/2 transition at low field to m_I= +7/2 transition at high field. Anisotropic (heterogeneous in all the directions) conditions take place when the sample is in solid state or frozen, and the

additional splitting occurs. Z axis is assigned to be axis parallel to the V=O bond, whereas x and y are perpendicular axes. Hence, the g-value perpendicular components are g_x and g_y while parallel component is g_z. Similarly, the A value perpendicular components are A_x and A_y, and parallel component is A_z. For each $V^{IV}O^{2+}$complex 5 sets each made of eight lines are observed: two having axial symmetry (x=y≠z) and three having rhombic symmetry (x≠y≠z). As the V=O bond is quite strong $V^{IV}O^{2+}$complexes usually give axial or nearly axial spectra. [1,104,105]

A and g values can be estimated or calculated from spectra simulation using corresponding software.[1]

In systems containing paramagnetic metals ($V^{IV}O^{2+}$ - hTF and $V^{IV}O^{2+}$ - HSA in our case) EPR spectrum gives the information about the changes in vanadium coordination sphere. The hyperfine coupling constant A_z can provide the information on donor atoms bound to $V^{IV}O^{2+}$. [1,104,105]

1.6.2. Circular dichroism (CD).

This technique is based on the different absorbtion of the left- and right- circularly polarized light by the chiral moiety of the compound (vanadium as the coordination center or the protein moiety). The wavelength range for CD usually is UV–Vis (100-1000 nm). Chiral compounds are able to rotate the plane of linearly polarised light which is passing through them. This light may be considered to consist of two circularly polarised components: left and right circularly polarised waves with the same amplitude and in phase. When crossing a chiral medium, their propagation pace is different as they have different refractive indices. Both beams intensities reach the detector where they are being measured and compared. Hence, the plane of polarisation is rotated by a certain angle (α) which may vary with λ. The change of α with λ is called optical rotary dispersion (ORD). At the λ used the extinction coefficient for the left (L) and right (R) circular polarized light may be different. The term circular dichroism (CD) is the difference between the left and right circularly polarised light molar absorption coefficients $\Delta\varepsilon=\varepsilon_L - \varepsilon_R$. The CD phenomenon can be observed only within an absorption band and the Δε values vary with λ. The CD and ORD phenomena are called the Cotton effect. The plot may be presented in the form of $\Delta\varepsilon/M^{-1}cm^{-1}$ (molecular CD) as a function of the wavelength (nm) with both positive and negative bands depending on the absorption nature ($\varepsilon_L > \varepsilon_R$ or $\varepsilon_L < \varepsilon_R$). [1,106-109]

Circular dichroism can be applied in e.g.:

- proving of $V^{IV}O^{2+}$ binding to hTF or HSA;

- determination of protein : $V^{IV}O^{2+}$: ligand binding ratios;
- determination of protein vanadium binding sites;
- protein conformation change studies;
- estimation of complex-protein bond strength.[1,106-109]

1.6.3. Ultraviolet-visible absorption (UV-Vis).

This technique is based on the selective absorption of the electromagnetic waves in the ultraviolet, normally (190-390 nm) and "visible" (400-1000 nm) region by the compounds.[1] The UV-Vis absorption spectra can be caused by the following electronic transitions:

- metal d–d transitions which are parity-forbidden (give the most important information);
- metal-to-ligand charge transfer (MLCT);
- ligand-to-metal charge transfer (LMCT);
- intra-ligand transitions and inter-valence charge transfer (IVCT) (for complexes with more than one vanadium centre in different oxidation states).

In this work UV-Vis absorption spectra were applied for e.g.:

- vanadium or vanadium-protein solution stability studies (absorption bands change in time);
- determination of protein exact concentration;
- as a complementary technique to fluorescence spectroscopy of protein-complex systems.[1]

1.6.4. Fluorescence spectroscopy (fluorometry, spectrofluorometry).

This technique is based on excitement of groups of the protein using a beam of ultraviolet light at a certain wavelength (usually 280 or sometimes 295 nm) and subsequent detection of the radiation emitted. Three aromatic amino acids contribute to the protein fluorescence: tyrosine, phenylalanine and tryptophan (exception: green fluorescent proteins). Ultraviolet light excites the electrons in the fluorophore groups of these amino acids and causes them to emit light in a certain λ range. Most of the emission is due to tryptophan. The plot is presented in the form of fluorescence intensity as a function of wavelength at which the emission occurs. In this work fluorescence spectroscopy was mostly used to get information about:

- probe binding of compounds to HSA or hTF;
- number and amino acid composition of vanadium binding sites (by binding to hTF or HSA vanadium occupies their sites and thus may cause concentration-dependent fluorescence quenching);
- estimate vanadium binding constants.[1,110]

2.0. OBJECTIVES

Since $V^{IV}O(oda)(H_2O)_2$, $V^{IV}O(oda)(bipy)$,$V^{IV}O(oda)(phen)$ and $V^{IV}O(acac)_2$ complexes are reported to have anticancer activity, it is important to understand their binding to blood serum proteins hTF and HSA, which are known to play key roles in drug transport to the target cells and distribution in the organism. A range of studies[26,66-68,72-74] reported their antitumor activity, mainly focusing on the investigation of cytotoxicity, genotoxicity, apoptotic action, suppression of mitochondria activity, cell morphological changes, DNA cleavage, role of oxidative stress and possible mechanisms of these actions. Some studies[79,96-103,111-115] report about the interaction of other $V^{IV}O^{2+}$ complexes with HSA and hTF, but not of $V^{IV}O(oda)(H_2O)_2$, $V^{IV}O(oda)(bipy)$,$V^{IV}O(oda)(phen)$.

In this study our first objective was to synthesize the complexes $V^{IV}O(oda)(H_2O)_2$, $V^{IV}O(oda)(bipy)$,$V^{IV}O(oda)(phen)$ which are not commercially available.

A second objective was to study the stability of solutions of the complexes in conditions close to those observed in blood serum.

Thirdly, by means of CD, EPR and fluorescence spectroscopies and modeling some physiological conditions, e.g. pH=7.4, we aimed to investigate the possible binding sites, binding modes and number and type of different chelate species formed between all four studied complexes and HSA and hTF. It was important to know if the particular complex binds to the protein in the form as it was administered, i.e. with ligands, or it partially loses some ligand, or if it binds only as $V^{IV}O^{2+}$.

To have additional confirmation of binding of the studied complexes binding to serum proteins some studies were done with solutions containing V^{IV}-complexes and hTF after passing by PD-10 columns. UV-Vis absorption, EPR and CD spectroscopies and ICP were used here.

A complication we had to take into account is the oxidation of V^{IV} to V^{V} in the solutons during the experiments which could distort all the results. For this reason most manipulations involving $V^{IV}O^{2+}$ compounds were done excluding oxygen. This delays the oxidation processes, but might not have avoided them completely.

Experimental Part

3.0. EXPERIMENTAL PART

3.1.0. Materials

Water.

Millipore water was used for the preparation of solutions of the complexes for studies and buffer solutions. The water was produced using a Mili-Q water purification system. Distilled water was used in the synthetic procedures. Deionized water was used in some CD and EPR experiments.

Solvents. Solvents were purchased from Sigma-Aldrich, Carlo-Erba, Panreac or Fisher and used as received.

Buffers.

Two main buffer systems were used in the solution studies and studies of interaction with the serum proteins: Tris (2-Amino-2-hydroxymethyl-propane-1,3-diol, $(HOCH_2)_3CNH_2$) and PBS (Phosphate buffered saline). Sodium carbonate used in Tris preparation was purchased from Reagente Puro ERBA. Tris was purchased from Aldrich Chemistry. PBS was purchased from Sigma Aldrich.

Ligands.

The ligand used in the synthesis was diglycolic acid (2-(carboxymethyloxy)acetic acid, or oda ($O(CH_2COOH)_2$)) purchased from Aldrich Chemistry.

Oxidovanadium (IV).

Oxidovanadium(IV) acetylacetonate (oxobis(2,4-pentanedionato)vanadium(IV), or $V^{IV}O(acac)_2$ was used in the synthesis. $V^{IV}O(acac)_2$ was purchased from Fluka® Analytical.

Vanadium(IV) oxide sulfate pentahydrate, $V^{IV}OSO_4{\cdot}5H_2O$, was purchased from Riedel-de Haën.

Reagents.

2,2'-bipyridine ($(C_5H_4N)_2$), or bipy, 1,10-phenanthroline ($C_{12}H_8N_2$), or phen and 1,10-phenanthroline hydrochloride, or *o*-phen· HCl ($C_{12}H_8N_2$ · HCl) were used in the synthesis. 2,2'-bipyridine was purchased from ACROS ORGANICS. 1,10-phenanthroline was purchased from Alfa Aesar®. 1,10-phenanthroline hydrochloride was purchased from MERCK.

Proteins.

Apo-Transferrin human (apo-hTF) (ATF2011-07; >95%), lyophilized from sodium phosphate with a molecular mass of 78.5 kDa and fatty acid and globulin free human serum albumin (HSA) (A3782-5G; ≥99%), lyophilized powder with a molecular mass of 67 kDa were used. hTF was purchased from Akron™ bio tech. HSA was purchased from Sigma Aldrich.

PD-10 Desalting Columns containing 8.3 mL of Sephadex™ G-25 Medium were purchased from GE Healthcare.

All the reagents and proteins used in this study were used as received from supplier without further purification.

3.2.0. Synthesis and characterization of oxidovanadium(IV) complexes

3.2.1. Synthesis

Synthesis of the $V^{IV}O(oda)(H_2O)_2$

To a solution of $[V^{IV}O(acac)_2]$ (1.325 g, 5 mmol) in water (20 mL) diglycolic acid (0.6706 g, 5 mmol) was added. The resulting solution was refluxed in a glycerol bath for 3 h. The reaction was conducted with exclusion of oxigen. The hot solution was filtered from impurities and then concentrated in order to remove Hacac, cooled to room temperature, and left overnight at ≈ 4 ° C to let the blue crystals form. Then, the blue crystals were filtered off, washed with cold water, acetone and diethyl ether, and then dried under vacuum. Yield: 0.7487 g (63.7%). Elemental analysis found, C, 20.32; H, 3.38; $C_4H_8VO_8$ (235.04 g mol^{-1}) requires, C, 20.44; H, 3.43. FT-IR (KBr, cm^{-1}): 3057 vs vbr (ν, OH), 1587 vs br (ν_{asymm}, COO^-), 993 vs (ν, V=O) (see *Appendices B 1 and B2*).

Synthesis of the $V^{IV}O(oda)(bipy)$

A solution of $[V^{IV}O(oda)(H_2O)_2]$ (0,47025 g, 2 mmol) in methanol (20 mL) was slowly added to solution of 2,2'-bipyridine (0,31238 g, 2 mmol) in methanol (20 mL). The reaction was conducted with exclusion of oxigen. The yellow-brownish solid was obtained immediately. The solid was filtered, washed with cold methanol, and dried under vacuum. Yield: 0.6462 g (90.96%). Elemental analysis found, C, 44.08; H, 3.47; N, 7.24; $C_{14}H_{12}N_2VO_6 \cdot 1.5H_2O$ (419.28 g mol^{-1}) requires, C, 43.99; H, 3.96; N, 7.33. Found: FT-IR (KBr, cm^{-1}): 3423m vbr (ν, OH), 1635 s br (ν_{asymm}, COO^-), 997 vs (ν, V=O) (see *Appendices B 3 and B 4*).

Synthesis of the $V^{IV}O(oda)(phen)$

A solution of $[V^{IV}O(oda)(H_2O)_2]$ (0,30097 g, 1,28 mmol) in water (8 mL) was slowly added to a solution of *o*-phen· HCl (0,30064 g, 1,28 mmol) in water (3,2 mL). The reaction was conducted with exclusion of oxigen. The yellow-green solid was obtained immediately. The solid was filtered, washed with cold water, acetone, and diethyl ether, and dried under vacuum. Yield: 0.18084 g (37.25%). Elemental analysis found, C, 47.12; H, 3.40; N, 6.78; $C_{16}H_{12}N_2VO_6 \cdot 1.6H_2O$ (408.05 g mol^{-1}) requires C, 47.1; H, 3.75; N, 6.87. FT-IR (KBr, cm^{-1}):

3567 m br, 3406,64 m vbr (ν, OH), 1678 vs br (ν_{asymm}, COO^-), 999vs (ν, V=O) (see *Appendices B 5 and B 6*).

3.2.2. Preparation of solutions

Buffers.

The Tris buffer was prepared by dissolving the Tris powder in Millipore water. Sodium carbonate (Na_2CO_3) was added to Tris buffer in the *experiment 5.1*. Freshly prepared Tris buffer was used in each experiment. pH adjustment to pH=7.4 was made with conc. HCl. For details on the preparation of Tris buffer see *Appendix A.*

PBS buffer was prepared by dissolving a PBS tablet in 200 mL of Millipore water. Each solution was replaced with the new one once turbidity appeared.

All the pH readings were recorded by means of Denver Model 15 pH meter calibrated at pH = 7.0 and pH= 4.0.

$V^{IV}O(oda)(H_2O)_2$ solution for stability studies.

The solution was prepared by dissolving of $V^{IV}O(oda)(H_2O)_2$ in MeOH and subsequent addition of Tris buffer. Freshly prepared solutions were used in each experiment. For details on the preparation of the $V^{IV}O(oda)(H_2O)_2$ solution see *Appendix A.*

Solutions of $V^{IV}O(oda)(H_2O)_2$, $V^{IV}O(oda)(bipy)$, $V^{IV}O(oda)(phen)$ and $V^{IV}O(acac)_2$ for CD, EPR and fluorescence spectroscopy studies.

Stock solutions of $V^{IV}O(oda)(H_2O)_2$ were prepared by dissolving the complex in MeOH. Stock solutions of $V^{IV}O(oda)(bipy)$ were prepared by dissolving the complex in DMSO and EtOH. Stock solutions of $V^{IV}O(oda)(phen)$ were prepared by dissolving complexes in H_2O while $V^{IV}O(acac)_2$ solutions were prepared in PBS buffer and DMSO (*experiments 2.5 and 2.6.*). Freshly prepared solutions were used in each experiment.

Solutions of hTF and HSA for CD, EPR and fluorescence spectroscopy studies.

Stock solutions of hTF and HSA were prepared by dissolving the proteins in PBS buffer. hTF in Tris buffer was used in the *experiment 5.1*. Freshly prepared solution was used in each experiment.

While preparing all the solutions containing V^{IV} compounds nitrogen gas was bubbled through all the solvents to prevent the oxidation of V^{IV} to V^{V}.

3.3.0. Spectroscopic measurements

3.3.1. Fourier transform infrared spectroscopy (FTIR).

All the IR measurements were recorded with Jasco FT/IR-4100 spectrometer in the range of 4400-400 cm^{-1}, baseline was made with the air. The sample was prepared by mixing of the compound with KBr powder and pressing into a thin tablet at a Perkin Elmer press under 10 kg · 1000. The IR spectra with the interpretation can be found in the *Appendix B*.

3.3.2. Ultraviolet–visible absorption spectroscopy.

All the UV-Vis absorption spectra were recorded with Perkin Elmer Lambda 35 UV - Vis spectrometer at the wavelength range of 1000–250/300 nm for stability studies and 500 – 250 nm as a complementary technique for fluorescence studies. Baseline was made with air. 10 mm (chamber volume 3500 µL) cells made of Quartz SUPRASIL® from Hellma® Analytics were used in all the measurements. 1 mm cells (chamber volume 350 µL) made of Quartz SUPRASIL® from Hellma® and 1 mm cell (chamber volume 350 µL) from Starna® were used in the *experiment 5.1*.

3.3.3. Circular dichroism spectroscopy.

CD spectra were recorded on a Jasco J-720 spectropolarimeter either using the usual photomultiplier with a red-sensitive photomultiplier (EXWL-308) in the visible range. The measurements were performed at ~25 ° C using either a 20 mm (chamber volume ~5.0 mL) absorption cells from Hellma®, or a Macro Suprasil® quartz and 3.5 mm I.D. ×50 mm cylindrical quartz cell (Jasco Parts Center, CQ3-50, chamber volume ~ 800 µL) or a 2 mm cell (chamber volume ~600 µL) made of Quartz SUPRASIL® from Hellma®.

3.3.4. Electron paramagnetic resonance spectroscopy (EPR).

The EPR spectra were obtained with a Bruker ESP 300E spectrometer at 77 K. The samples (ca. 300-400 µL) were placed in 3 mm quartz tubes (Wilmad 707-SQ-250M) and frozen in liquid nitrogen.

3.3.5. Fluorescence spectroscopy.

The fluorescence spectra were obtained on a Fluorolog® Horiba Jobin Yvon Spectrofluorometer with single proton counting controller - FluoroHub from Horiba Scientific™. The samples were excited at the wavelength of 280 nm (slit width 5 nm) and the emission spectra were measured in the 290 – 500 nm range, and at 295 nm (slit width 9 nm) with the emission spectra measured in the 305-515 nm range. The samples from the systems $V^{IV}O(oda)(H_2O)_2$ + hTF, $V^{IV}O(oda)(H_2O)_2$ + HSA, and $V^{IV}O(oda)(phen)$ + HSA were

excited at 280 nm only. All the measurements were done in 10 mm fluorescence quartz cells from Hellma® Analytics with the chamber volume of ~ 3500 µL at room temperature except *experiment 4.9* (at 25, 30, 35, 40º C).

3.4.0. Procedure.

3.4.1. Stability studies.

The stability studies were carried out with $V^{IV}O(oda)(H_2O)_2$ in MeOH.

Experiment 1.1. For details on the preparation of the solution see *Appendix A*. The UV-Vis spectra were recorded immediately after preparation of the solution, after 10, 20, 30, 40, 50, 60, 90, 120, 150, 180, 210, 240, 270 and 300 min.

3.4.2. Studies of complex-human serum protein interaction by circular dichroism (CD).

The part of each protein stock solution in each experiment was previously diluted to determine the exact stock solution concentration by UV absorption at λ=280 nm and adjust the complex stepwise additions to the protein. Then, another part of the stock solution was diluted, constituting the initial protein solution with the ratio complex : protein=0. In *experiments 2.1., 2.4., 2.6.and 2.7.* the protein stock solution was used without dilution. In each experiment the complex solution was prepared immediately before use and the solvent was previously bubbled with nitrogen to minimize the dissolved complex contact with air and thus prevent the oxidation of V^{IV} to V^{V}.

Experiment 2.1. $V^{IV}O(oda)(H_2O)_2$ + hTF system.

To the solution of hTF (7.23×10^{-4} M) in PBS were progressively added controlled volumes of a 6.32×10^{-2} M solution of $V^{IV}O(oda)(H_2O)_2$ in MeOH to obtain $V^{IV}O(oda)(H_2O)_2$: hTF ratios ranging from 1 to 4. EPR samples (400 µL each) were taken at $V^{IV}O(oda)(H_2O)_2$: hTF ratios of 1, 2 and 4. For additional information on concentrations of each sample see *Appendix C 1*.

Experiment 2.2. $V^{IV}O(oda)(bipy)$ + hTF system (continuous addition).

To the 5.77×10^{-4} M solution of hTF in PBS were progressively added controlled volumes of a 3.58×10^{-2} M solution of $V^{IV}O(oda)(bipy)$ in DMSO to obtain $V^{IV}O(oda)(bipy)$: hTF ratios ranging from 0.36 to 4.7. For additional information on concentrations of each sample see *Appendix C 2*.

Experiment 2.3. $V^{IV}O(oda)(bipy)$ + HSA system (continuous addition).

To the 5.37×10^{-4} M solution of HSA in PBS were progressively added controlled volumes of a 4.8×10^{-2} M solution of $V^{IV}O(oda)(bipy)$ in DMSO to obtain $V^{IV}O(oda)(bipy)$: HSA ratios ranging from 0.26 to 5.05. For additional information on concentrations of each sample see *Appendix C 3*.

Experiment 2.4. $V^{IV}O(oda)(phen)$ + hTF system (continuous addition).

To the 5.32×10^{-4} M solution of hTF in PBS were progressively added 1.2, 1.2 and 1.2 mg of solid $V^{IV}O(oda)(phen)$ to obtain $V^{IV}O(oda)(phen)$: hTF ratios of 1, 2.01 and 3.09 respectively. The EPR samples (400 µL each) were taken at $V^{IV}O(oda)(phen)$: TF ratios of 2.01 and 3.09. For additional information on concentrations of each sample see *Appendix C 4.*

Experiment 2.5. $V^{IV}O(acac)_2$ + hTF system (continuous addition).

To the 4.8×10^{-4} M solution of hTF in PBS were progressively added controlled volumes of a 3.77×10^{-2} M solution of $V^{IV}O(acac)_2$ in DMSO to obtain $V^{IV}O(acac)_2$: hTF ratios ranging from 0.28 to 5.01. For EPR sample (240 µL) was taken at $V^{IV}O(acac)_2$: hTF ratio of 5.01. For additional information on concentrations of each sample see *Appendix C 5.*

Experiment 2.6. $V^{IV}O(acac)_2$ + HSA system (continuous addition).

To the 6.02×10^{-4} M solution of HSA in PBS were progressively added controlled volumes of a 3.64×10^{-2} M solution of $V^{IV}O(acac)_2$ in DMSO to obtain $V^{IV}O(acac)_2$: HSA ratios ranging from 0.51 to 5. The EPR samples (400 µL each) were taken at $V^{IV}O(acac)_2$: HSA ratios of 3 and 5. For additional information on concentrations of each sample see *Appendix C 6.*

Experiment 2.7. hTF + $V^{IV}O^{2+}$ + phen system.

To the 5.32×10^{-4} M solution of hTF in PBS were progressively added controlled volumes of a 0.795 M solution of $V^{IV}OSO_4$ in H_2O and 0.111 M solution of o-phenantroline(phen) in EtOH to obtain hTF : $V^{IV}OSO_4$: phen ratios of 1:1:1, 1:2:2, 1:3:3 and 1:3:5. The EPR samples (400, 500, 400 µL) were taken at hTF:$V^{IV}OSO_4$: phen ratios of 1:2:2, 1:3:3 and 1:3:5 For additional information on concentrations of each sample see *Appendix C 7.*

3.4.3. Studies of complex-human serum protein interaction by electron paramagnetic resonance (EPR).

Some of the EPR samples (240, 400 and 500 µL) (e*xperiments 3.4, 3.5, 3.6, and 3.7*) were taken from some solutions used for CD experiments at certain stages (certain complex : protein ratios) of addition of complexes to the protein. Some samples (e*xperiments 3.1., 3.2., 3.3, 3.8 and 3.9*) were prepared separately for EPR analysis.

Experiment 3.1. $V^{IV}O(oda)(H_2O)_2$ + hTF system.

To prepare samples (240 µL each) with $V^{IV}O(oda)(H_2O)_2$: hTF ratios of 0.73, 2.89 and 4.28 to 4.94×10^{-4} M solution of hTF in PBS were added different amounts of a solution of $V^{IV}O(oda)(H_2O)_2$ (4.34×10^{-2} M) in MeOH. For additional information on concentrations of each sample see *Appendix C 8.*

Experiment 3.2. $V^{IV}O(oda)(H_2O)_2$ in MeOH.

To prepare a 2.8×10^{-3} M solution, 0.00134 g of $V^{IV}O(oda)(H_2O)_2$ was dissolved in 2×10^{-3} L of MeOH. A sample of 240 µL was used for the analysis.

Experiment 3.3. $V^{IV}O(oda)(bipy)$ + hTF system.

To four equal solutions with concentration of hTF (4.91×10^{-4} M) in PBS of was added different amounts of a solution of $V^{IV}O(oda)(bipy)$ (4.77×10^{-2} M) in DMSO to obtain $V^{IV}O(oda)(bipy)$: hTF ratios ranging from 0.49 to 4.02. For additional information on concentrations of each sample see *Appendix C 9.*

Experiment 3.4. $V^{IV}O(oda)(phen)$ + hTF system.

The samples were taken from the CD *Experiment 2.4.*, with VO(oda)(phen):hTF ratios of 2.01 and 3.09. For additional information on concentrations of each sample see *Appendix C 10.*

Experiment 3.5. hTF + $V^{IV}O^{2+}$ + phen system.

The samples were taken from the CD *Experiment 2.7.*, with hTF: $V^{IV}O^{2+}$: phen ratios of 1:2:2, 1:3:3 and 1:3:5. For additional information on concentrations of each sample see *Appendix C 11*.

Experiment 3.6. $V^{IV}O(acac)_2$ + hTF system.

The sample was taken from the CD *Experiment 2.5.*, with $V^{IV}O(acac)_2$: hTF ratio of 5.01. For additional information on concentrations of each sample see *Appendix C 12.*

Experiment 3.7. $V^{IV}O(acac)_2$ + HSA system.

The sample was taken from the CD *Experiment 2.6.*, with $V^{IV}O(acac)_2$:HSA ratios of 3 and 5. For additional information on concentrations of each sample see *Appendix C 13.*

Experiment 3.8. $V^{IV}O(oda)(bipy)$ in EtOH.

To prepare a 1.431×10^{-3} M solution, 0.00120 g of $V^{IV}O(oda)(bipy)$ was dissolved in 2×10^{-3} L of EtOH (absolute). A sample of 400 µL was used for the analysis.

Experiment 3.9. $V^{IV}O(oda)(phen)$ in H_2O+DMSO.

To prepare a 1.47×10^{-3} M solution, 0.00132 g of $V^{IV}O(oda)(phen)$ was dissolved in total of 2.2×10^{-3} L of H_2O (90%) and DMSO (10%). A sample of 400 µL was used for the analysis.

3.4.4. Studies of complex-human serum protein interaction by fluorescence spectroscopy.

The part of each protein stock solution in each experiment was previously diluted to determine the exact stock solution concentration and adjust the complex additions to the protein. Then, another part of the stock solution was diluted to make an initial protein solution with the ratio complex:protein=0. In each experiment the complex solution was prepared immediately before use and the solvent was previously bubbled with nitrogen gas to minimize

the dissolved complex contact with air and thus prevent the oxidation of V^{IV} to V^{V}. The blanks having same content except the protein were measured in order to be subtracted from the samples to obtain the fluorescence of the pure protein. The UV-Vis absorption measurements were done with each sample to be further used in the data corrections.

Experiment 4.1. $V^{IV}O(oda)(H_2O)_2$ + hTF system.

To a solution of hTF (2.46×10^{-6} M) in PBS was progressively added a solution of $V^{IV}O(oda)(H_2O)_2$ (8.51×10^{-4} M) in MeOH to obtain $V^{IV}O(oda)(H_2O)_2$:hTF ratios ranging from 0.23 to 3.46.

Experiment 4.2. $V^{IV}O(oda)(H_2O)_2$ + HSA system.

To a solution of HSA (2.6×10^{-6} M) in PBS was progressively added solution of $V^{IV}O(oda)(H_2O)_2$ (9.8×10^{-4} M) in MeOH to obtain $V^{IV}O(oda)(H_2O)_2$:HSA ratios ranging from 0.25 to 18.86.

Experiment 4.3. $V^{IV}O(oda)(bipy)$ + hTF system.

To a solution of hTF (1×10^{-6} M) in PBS was progressively added a solution of $V^{IV}O(oda)(bipy)$ (1.96×10^{-4} M) in DMSO to obtain $V^{IV}O(oda)(bipy)$:hTF ratios ranging from 0.13 to 3.26.

Experiment 4.4. $V^{IV}O(oda)(bipy)$ + HSA system.

To a solution of HSA (1.03×10^{-6} M) in PBS was progressively added a solution of $V^{IV}O(oda)(bipy)$ (1.86×10^{-4} M) in DMSO to obtain $V^{IV}O(oda)(bipy)$:HSA ratios ranging from 0.12 to 9.03.

Experiment 4.5. $V^{IV}O(oda)(phen)$ + hTF system.

To a solution of hTF (2.46×10^{-6} M) in PBS was progressively added a solution of $V^{IV}O(oda)(phen)$ (8.58×10^{-4} M) in DMSO to obtain $V^{IV}O(oda)(phen)$:hTF ratios ranging from 0.23 to 1.28.

Experiment 4.6. $V^{IV}O(oda)(phen)$ + HSA system.

To a solution of HSA (2.55×10^{-6} M) in PBS was progressively added a solution of $V^{IV}O(oda)(phen)$ (1.14×10^{-3} M) in DMSO to obtain $V^{IV}O(oda)(phen)$:HSA ratios ranging from 0.59 to 2.97.

Experiment 4.7. $V^{IV}O(acac)_2$ + hTF system.

To a solution of hTF (1.02×10^{-6} M) in PBS was progressively added a solution of $V^{IV}O(acac)_2$ (1.89×10^{-4} M) in PBS to obtain $V^{IV}O(acac)_2$:hTF ratios ranging from 0.12 to 3.08.

Experiment 4.8. $V^{IV}O(acac)_2$ + HSA system.

To a solution of HSA (1×10^{-6} M) in PBS was progressively added solution of $V^{IV}O(acac)_2$ (2.34×10^{-4} M) in PBS to obtain $V^{IV}O(acac)_2$:HSA ratios ranging from 0.15 to 19.33.

Experiment 4.9. $V^{IV}O(oda)(phen)$ + hTF system at 25, 30, 35 and 40 ° C.

To a solution of hTF (1.005×10^{-6} M) in PBS was progressively added solution of $V^{IV}O(oda)(phen)$ (1.96×10^{-4} M) in DMSO to obtain $V^{IV}O(oda)(phen)$:hTF ratios ranging from 0.13 to 1.95. The experiment was done at 25 º C.

To a solution of hTF (1.005×10^{-6} M) in PBS was progressively added solution of $V^{IV}O(oda)(phen)$ (2.27×10^{-4} M) in DMSO to obtain $V^{IV}O(oda)(phen)$:hTF ratios ranging from 0.15 to 3.76. The experiment was done at 30 º C.

To a solution of hTF (1.018×10^{-6} M) in PBS was progressively added solution of $V^{IV}O(oda)(phen)$ (1.96×10^{-4} M) in DMSO to obtain $V^{IV}O(oda)(phen)$:hTF ratios ranging from 0.13 to 4.17. The experiment was done at 35 º C.

To a solution of hTF (1.018×10^{-6} M) in PBS was progressively added solution of $V^{IV}O(oda)(phen)$ (2.02×10^{-4} M) in DMSO to obtain $V^{IV}O(oda)(phen)$:hTF ratios ranging from 0.13 to 3.31. The experiment was done at 40 º C.

3.4.5. Studies of complex-human serum protein interaction by gel filtration, ICP, CD, EPR and UV-Vis.

Experiment 5.1. hTF + $V^{IV}O(oda)(bipy)$ system; hTF + $V^{IV}O(acac)_2$ system.

Tris buffer (0.10 M) containing Na_2CO_3 (2.5×10^{-2} M), hereinafter referred to as buffer, was used in the experiment. Nine PD-10 desalting columns were equilibrated by passing 25 mL of the buffer throught each of them.

2.5 mL of solution of hTF (1.41×10^{-4} M) in buffer was passed through the column and eluted with 3.5 mL of the buffer. The UV-Vis absorption spectra (250-500 nm) of the hTF solution were recorded before and after passing through the column using 1 mm cells. The CD spectrum (2 mm cell, 250-400 nm) of the solution after passing the column was also recorded.

To the four equal solutions (2.5 mL each) of hTF (140.87×10^{-6} M) in buffer adequate volumes of solution of $V^{IV}O(oda)(bipy)$ (2.96×10^{-2} M) in DMSO was added to obtain solutions with hTF:$V^{IV}O(oda)(bipy)$ ratios of 1:1.05, 1:2.1, 1:4.21 and 1:8.41.

To each of the four equal solutions (2.5 mL each) of hTF (1.41×10^{-4} M) in buffer adequate volumes of solution of $V^{IV}O(acac)_2$ (2.78×10^{-2} M) in DMSO was added to obtain solutions with hTF:$V^{IV}O(acac)_2$ ratios of 1:1.01, 1:2.05, 1:4.02 and 1:7.89.

Each of the eight resulting solutions were passed throught (eight) equilibrated columns and each eluted with 3.5 mL of the buffer. The CD spectra (2 mm cell, 250-400 nm) of solutions after passing the column were also recorded. The CD spectra of the solutions with ratios hTF:$V^{IV}O$(oda)(bipy)=1:4.21 (10 mm cell, 325-800 nm) and hTF:$V^{IV}O(acac)_2$=1:7.89 (20 mm cell, 250-800 nm) after passing the column were also recorded. The eight samples (~240 µL) from solutions after passing the column were taken for EPR measurements. Eight samples (1 mL each) were taken from each solution that passed the column for ICP analysis (determination of V content).

3.5.0. Data processing.

Circular dichroism (CD). All the CD spectra were processed by means of JASCO 32 software. From the recorded CD data the baseline was firstly subtracted (buffer or protein in buffer in some cases). Then, the ellipticity, θ, millidegrees was converted to the molecular CD, $\Delta\varepsilon$, $M^{-1}cm^{-1}$ using the protein concentration and cell light pathway length. Then, adaptive smoothing was applied to some of the samples, and mean-movement smoothing was applied to the hTF - $V^{IV}O(acac)_2$ due to the characteristics of the noise in these spectra.

Electron paramagnetic resonance (EPR). The EPR data obtained were processed by means of Bruker WinEPR SimFonia software. Then, all the spectra were simulated with Roki software.[116]

Fluorescence spectroscopy. The final fluorescence data obtained is fluorescence intensity, expressed in CPS/MicroAmps plotted versus wavelength. Then, this data was further corrected by the subtraction of the blanks fluorescence and also corrected with UV-Vis absorption data at 2 excitement wavelengths and at 2 wavelength of maximum emission correspondingly. The Stern-Volmer plots were obtained and the best fittings found. For systems with hyperbolic dependence the corresponding equations were applied. To find the best fitting for some systems TableCurve software was used.

Results and discussion

4.0. Results and Discussion.

4.1.0. Solution stability studies.

4.1.1. Background.

The bands in UV-Vis region, and particularly in the Vis range give the information about the transitions of d – electrons (d-d transitions) of vanadium (IV) in the complex. If the spectra in the visible range remain approximately the same for certain periods of time, this means that the complex does not decompose or changes during that period, namely by hydrolysis and/or by oxidation. Thus recording the UV-Vis spectrum as a function of time provides information on the stability of the complexes in the medium where the compound is dissolved.

4.1.2. UV-Vis spectra of $V^{IV}O(oda)(H_2O)_2$ in MeOH and Tris buffer.

The change in absorption of $V^{IV}O(oda)(H_2O)_2$ in 5% MeOH and 95% Tris buffer with time in the 300-1000 nm range is presented in Figure 16 (*experiment 1.1.*).

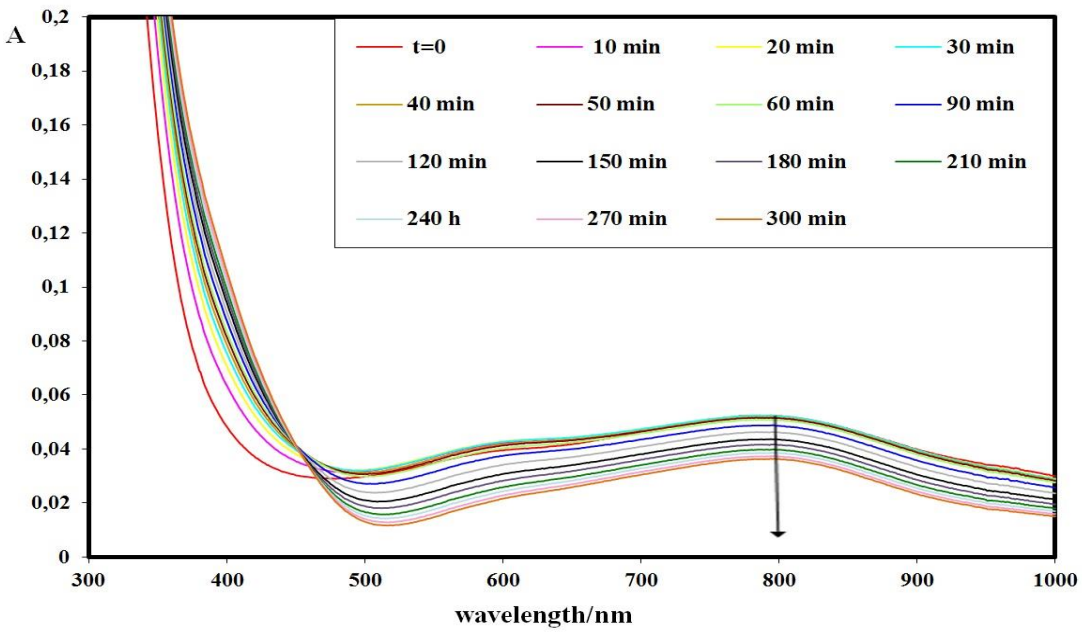

Figure 16. Ultraviolet-visible absorption spectra measured with time of a solution of $V^{IV}O(oda)(H_2O)_2$ (1.8×10^{-3} M) in 5% MeOH and 95% Tris buffer. The cell path length used was 10 mm.

In Figure 16 it may be observed that d-d transitions are observed at ~600 nm and ~785 nm. The solution of $V^{IV}O(oda)(H_2O)_2$ was reasonably stable at least for ~60 minutes. After this period of time there is a tendency for a decrease in the absorption with time, but the λ_{max} of the bands remain the same. Probably there is some progressive hydrolysis and oxidation of $V^{IV}O$ to V^{V} species. The absorption vs time of this system is depicted in Figure 17.

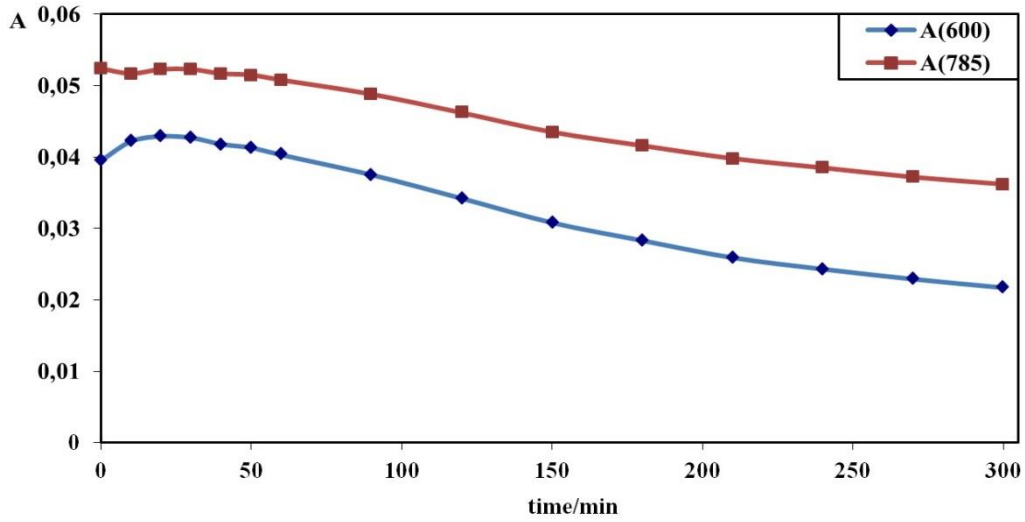

Figure17. Representation of absorption vs time for λ = 600 and 785 nm of a solution of $V^{IV}O(oda)(H_2O)_2$ (1.8×10^{-3} M) in 5% MeOH and 95% Tris buffer. The cell path length used was 10 mm.

4.2.0. Studies of the interaction of the complexes with hTF.

4.2.1. Studies by circular dichroism (CD). Background.

In the visible range $V^{IV}O$-d-d electronic transitions are observed (the protein does not absorb); thus, CD signals different from zero can only be recorded in the visible range of the spectrum when there is coordination of donor atoms of the protein to vanadium(IV). Globally, the higher the extinction coefficient (ε) of a particular band, the higher the CD bands intensities. The final CD spectrum recorded is the sum of CD signals of all the $V^{IV}O$-complexes formed in the system being studied. It is important to know if the complex binds to the hTF together with ligands or as $V^{IV}O^{2+}$ $^{+}$, and if the hTF closes its conformation or not upon binding of the complex. [96]

4.2.1.1. CD spectra of $V^{IV}O$-oda–hTF complexes.

Figure 18 depicts the changes in the visible CD spectra of titration of hTF with 1 – 4 mol equivalents of $V^{IV}O(oda)(H_2O)_2$ (*experiment 2.1.*). The complexes formed in the system produce both positive and negative d-d bands. One positive band approximately at 915 - >1000 nm with unclear spectra maxima at >1000 nm and can be attributed to either $d_{xy}\rightarrow d_{xz}$ or $d_{xy}\rightarrow d_{yz}$ transitions, one negative band approximately at 700 - 936 nm with the spectra minima at ~ 858 nm can be attributed to either $d_{xy}\rightarrow d_{xz}$ or $d_{xy}\rightarrow d_{yz}$ transitions, one slightly positive (see *Appendix D* 1) band approximately at 650 - 800 nm with the spectra maxima at ~ 700 nm can be attributed to $d_{xy}\rightarrow d_{x2-y2}$ transitions, one negative band approximately at 494 -

678 nm with the spectra minima at ~ 590 nm can be possibly attributed to $d_{xy} \rightarrow d_{z2}$ transitions.

Solutions of pure hTF in PBS produce no CD spectra in the visible range as hTF does not absorb in this wavelength range. After addition of 1 mol equivalent of $V^{IV}O(oda)(H_2O)_2$ the CD signal intensity starts globally increasing and keeps on increasing up to 4 mol equivalents of $V^{IV}O(oda)(H_2O)_2$ added. This means that: (i) V^{IV} ions bind to chiral groups of hTF and that induced CD (ICD) is observed, (ii) the ligand(s) are coordinated to the V^{IV} centers and they are close to the hTF chiral centers. Comparison of these CD spectra and the CD spectra of hTF:$V^{IV}O^{2+}$ = 1:2 from ref.[96,109,106] also confirms the conclusion (ii) as the bands of this spectra do not completely match the bands of hTF-$V^{IV}O^{2+}$ spectrum (in the absence of ligand); thus, the ligand(s) are coordinated to the V^{IV} centers and they are close to the hTF chiral centers, (iii) the spectra measured do not allow concluding if hTF only binds 2 mole equivalents of the $V^{IV}O$-complex (at the Fe^{III} binding sites) or if additional binding occurs also at surface His groups.

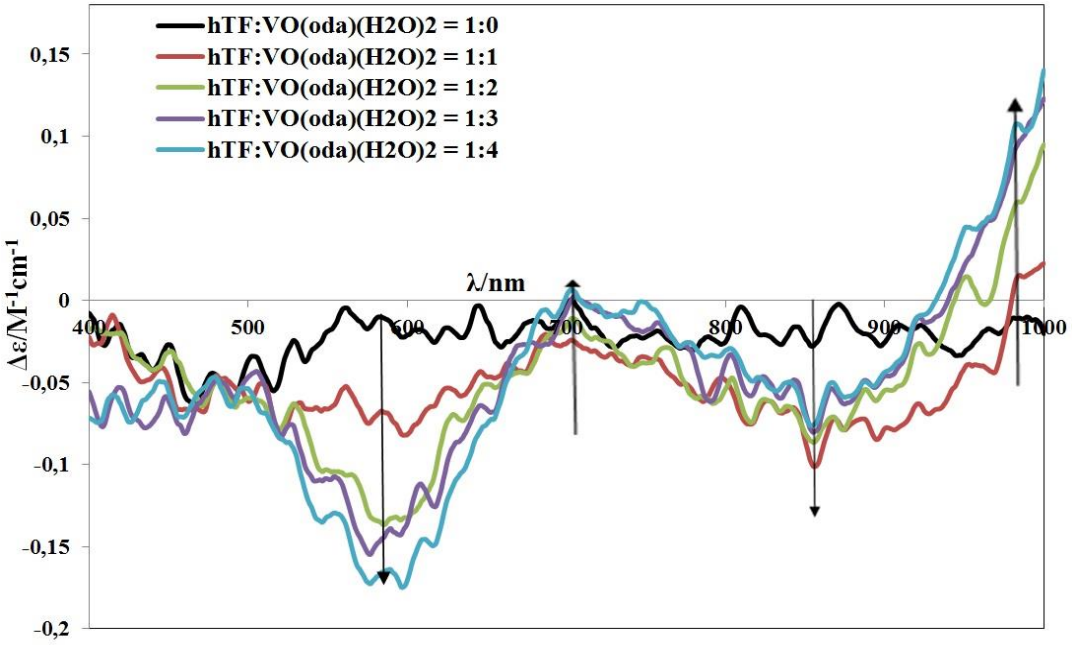

Figure 18. The CD spectra of solutions containing hTF (7.23×10^{-4} M) in PBS upon stepwise additions of adequate volumes of a solution of $V^{IV}O(oda)(H_2O)_2$ (6.32×10^{-2} M) in MeOH. Maximum % of MeOH added was 4.03; cell path length was 20 mm.

Figure 19 depicts the changes in the UV-Vis range of the CD spectra of solutions containing apo-hTF upon stepwise additions of $V^{IV}O(oda)(bipy)$ (*experiment 2.2.*). The samples with the $V^{IV}O(oda)(bipy)$:hTF ratios of up to 1.14 were measured in the range of 330-700 nm while samples with the rest of ratios, up to 4.7, in the range of 330-800 nm.

The complexes formed in the system produce both positive and negative bands in the range of 330-800 nm. One negative band approximately at 730 - >800 nm with the spectra minima at ~ 787 nm can be attributed to either $d_{xy} \rightarrow d_{xz}$ or $d_{xy} \rightarrow d_{yz}$ transitions, one positive band approximately at 670 - 780 nm with the spectra maxima at ~707 nm can be attributed to either $d_{xy} \rightarrow d_{xz}$ or $d_{xy} \rightarrow d_{yz}$ transitions, one negative band approximately at 520 - 675 nm with the spectra minima at ~594 nm can be attributed to $d_{xy} \rightarrow d_{x2-y2}$ transitions, one positive band approximately at 420- 525 nm with the spectra maxima at ~500 nm can be attributed to $d_{xy} \rightarrow d_{z2}$ transitions, one negative band approximately at 330 - 420 nm with the spectra minima at ~ 390 nm and one positive band with the spectra maxima at ~340 nm can possibly be charge-transfer (CT) bands.

Solutions of pure hTF in PBS produce no CD spectra in the 350-1000 nm region as it does not absorb in this wavelength range. In Figure 18 the spectrum of hTF is taken as a baseline. After addition of 0.36 mol equivalents of $V^{IV}O$(oda)(bipy) a clear CD spectrum is already measured. From Figure 19 it can be concluded that: (i) V^{IV} ions are bound to chiral groups of hTF and that induced CD (ICD) is observed, (ii) the ligand(s) are coordinated to the V^{IV} centers and they are close to the hTF chiral centers. Comparison of these CD spectra with the CD spectra of hTF:$V^{IV}O^{2+}$ = 1:2 from ref. [96,106,109] also confirms the conclusion (ii) as the bands of this spectra do not match with the bands of hTF-$V^{IV}O^{2+}$ spectrum (in the absence of ligand).

Then, further addition of 0.6 and 0.84 mol equivalents of $V^{IV}O$(oda)(bipy) causes small changes as well. Then, CD signal intensity starts increasing more at ratios of 1.14 and 1.75, and their spectra are very similar. The most significant changes are observed when hTF is loaded by 2.35 - 4.7 mol equivalents of $V^{IV}O$(oda)(bipy). Upon the increase of the ratio complex:hTF, the CD spectra measured progressively change. First, the concentration of the 1:1 increases, then the concentration of the 2:1 also increases; the binding at each binding site is not exactly equal, thus, the corresponding CD spectra are not the same. Hence, (iii) the spectra measured do not allow concluding if hTF only binds 2 mol equivalents of $V^{IV}O$(oda)(bipy) (at the iron binding sites) or if additional binding occurs also at surface His groups. What is clear is that the 2:1 ($V^{IV}O$(oda)(bipy):hTF) complex has negative bands with λ_{max} at ~390 nm, at ~594 nm and at ~787 nm. The 1:1 complex probably has positive bands with λ_{max} at ~340 nm, at ~500 nm and at ~680 nm.

For $V^{IV}O$(oda)(bipy):hTF ratios higher than 4, the intensity of bands at λ_{max} at ~ 390 nm, at ~ 594 nm and at ~ 707 nm clearly decrease. This is possibly due to (iv) some hydrolytic

oxidation of $V^{IV} \rightarrow V^{V}$- species, (v) the increase of ligand concentration in the bulk solution probably contributes to removal of V^{IV} bound to hTF.

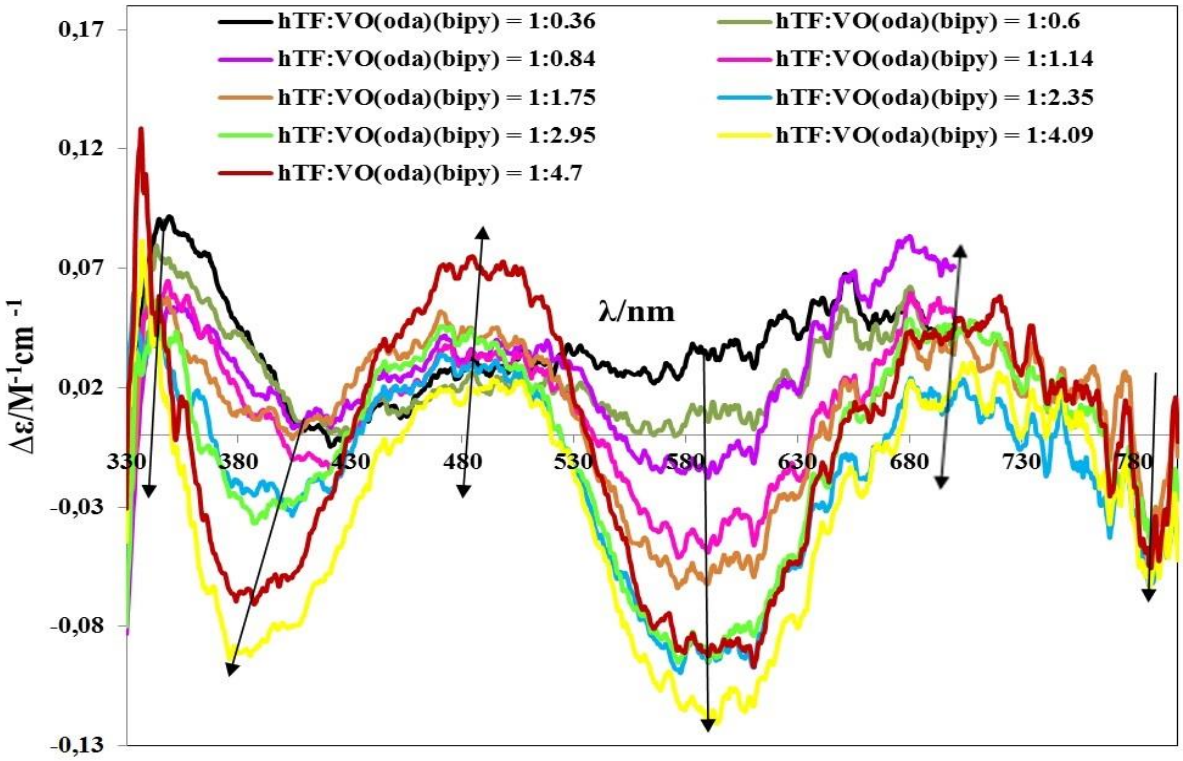

Figure 19. CD spectra of solutions containing hTF (5.77×10^{-4} M) in PBS upon stepwise additions of adequate volumes of a solution of $V^{IV}O$(oda)(bipy) (3.58×10^{-2} M) in DMSO. Maximum % of DMSO added was 5.28; the cell path length was 50 mm.

Figure 20 depicts the changes in the UV-Vis CD spectra of hTF in PBS upon addition of 1-3 mol equivalents of $V^{IV}O^{2+}$ and 1-5 mol equivalents of o-phenantroline (phen) (*experiment 2.7.*). The spectra of pure hTF was taken as a baseline.

The complexes formed in the system produce one negative band (λ_{max}= ~592 nm) and two positive bands (λ_{max}= ~700 nm, ~461 nm). The band at λ_{max}= ~700 nm can be attributed to $d_{xy} \rightarrow d_{xz}$ or $d_{xy} \rightarrow d_{yz}$ transitions, at λ_{max}= ~592 nm can be attributed to $d_{xy} \rightarrow d_{x2-y2}$ transitions. The positive band at~461 nm may correspond to the $d_{xy} \rightarrow d_{z2}$ transitions and/or to a CT band.

Pure hTF in PBS produces no CD spectra as it does not absorb in this wavelength range. After addition of 1 mol equivalents of $V^{IV}O^{2+}$ and phen the CD spectral intensity increases and keeps on increasing up to ratio of 1:3:3. From this it can be concluded that: (i) V^{IV} ions are bound to chiral groups of hTF and that induced CD (ICD) is observed, (ii) the phen ligands are coordinated to the V^{IV} centers and they are close to the hTF chiral centers. Each

molecule of hTF becomes loaded by 2 mol equivalents of vanadium (IV) approximately at the ratio of 1:3:3. The pattern of the spectra is always the same, (iii) suggesting that the environment around each V^{IV} (possibly one at each iron binding site) is always the same. Addition of 2 more mol equivalents of phen does not change much the spectra intensity so the spectra at ratios of 1:3:3 and 1:3:5 almost coincide. It can be assumed that (iv) the phen ligand binds to $V^{IV}O^{2+}$ at the ratio 1:1 forming mononuclear species so the further addition of phen does not make any change to the spectrum. Comparison of this CD spectra and the CD spectra of hTF:$V^{IV}O^{2+}$ = 1:2 from ref. [96,106,109] shows that (v) phen ligand is bound to the $V^{IV}O^{2+}$ centers as the bands of these spectra significantly differ from the bands of hTF-VO^{2+} spectrum (in the absence of ligand).

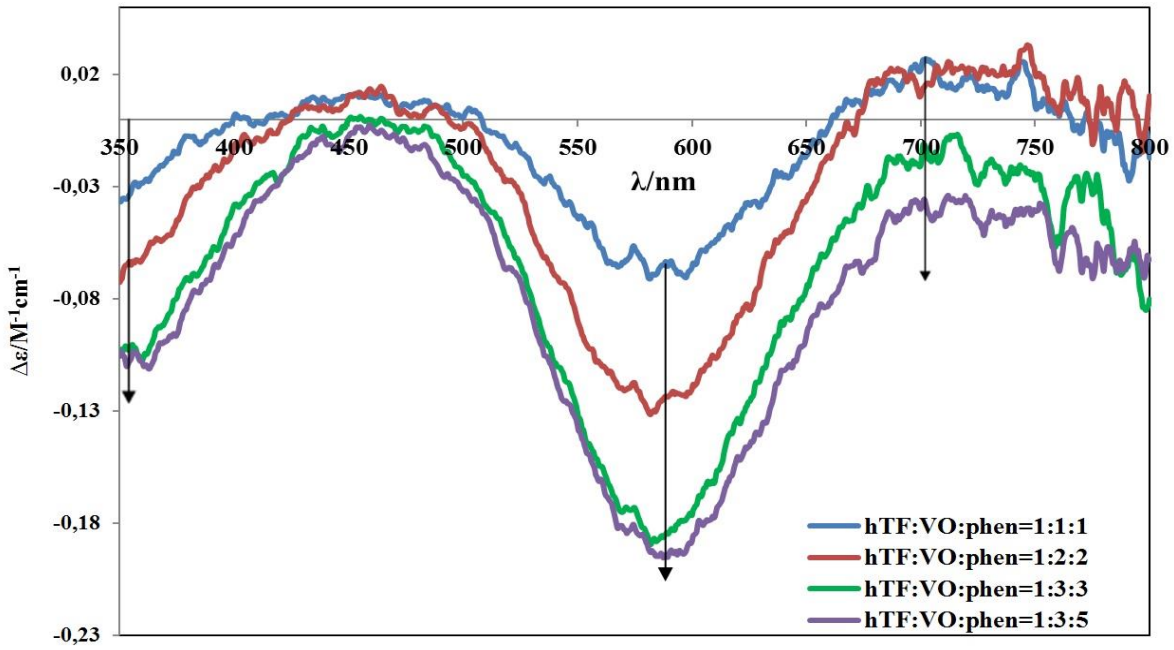

Figure 20. CD spectra of solutions containing hTF (5.32×10^{-4} M) in PBS upon stepwise additions of adequate volumes of a solution of $V^{IV}OSO_4$ **(**0.795 M) in H_2O and solution of o-phenantroline (phen) (1.1×10^{-1} M) in EtOH. Maximum % of EtOH added was 2.2; cell path length was 20 mm.

The Figure 21 depicts the changes in the UV-Vis CD spectra upon addition of 1-3.09 mol equivalents of $V^{IV}O$(oda)(phen) to a hTF solution in PBS (*experiment 2.4.*). The spectra of pure hTF was taken as a baseline.The complexes formed in the system produce two negative bands in the range of 350-800 nm, with λ_{max}= ~375 nm and λ_{max}= ~558 nm and two positive bands, with λ_{max}= ~485 nm and λ_{max}= ~696 nm. The band at λ_{max}= ~696 nm can be attributed to $d_{xy} \rightarrow d_{xz}$ or $d_{xy} \rightarrow d_{yz}$ transitions, at λ_{max}= ~558 nm can be attributed to $d_{xy} \rightarrow d_{x2-y2}$ transitions, at 485 nm may correspond to the $d_{xy} \rightarrow d_{z2}$ transitions and/or to a CT band, at λ_{max}= ~375 may correspond to a CT band.

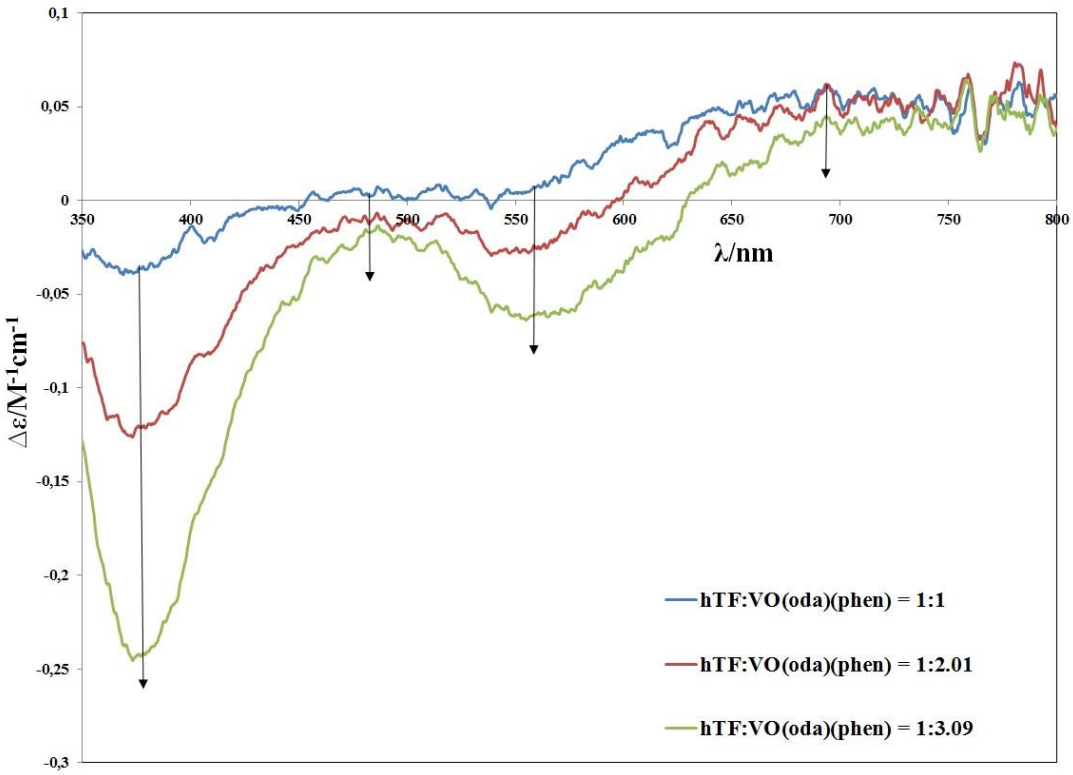

Figure 21. CD spectra of solutions containing hTF (5.32×10^{-4} M) in PBS upon stepwise additions of adequate amounts of solid $V^{IV}O$(oda)(phen). Cell path length was 20 mm.

Pure hTF in PBS produces no CD spectra as it does not absorb in this wavelength range. After addition of 1 mol equivalent of $V^{IV}O$(oda)(phen) a slight change occurs and the CD signal intensity starts increasing and keeps on increasing up to ratio of 1:3.09. The most significant change is observed at ratio of 1:3.09. From this it can be concluded that: (i) V^{IV} ions are bound to chiral groups of hTF and that induced CD (ICD) spectra are observed, (ii) the ligand(s) are coordinated to the V^{IV} centers and they are close to the hTF chiral centers, (iii) it is plausible that each molecule of hTF becomes loaded by 2 mol equivalents of vanadium (IV) (one at each iron binding site) approximately at the ratio of 1:3.09. Comparison of these CD spectra and the CD spectrum of hTF:$V^{IV}O^{2+}$ = 1:2 from ref. [96,106,109] and the CD spectrum from *experiment 2.7* shows that, probably, (iv) $V^{IV}O$(oda)(phen) binds to hTF together with the ligand oda and at least partly retains the phen ligand in the binding process, as the bands of these spectra do not match with the bands of hTF-$V^{IV}O^{2+}$ spectrum in the absence of ligand and with the bands of hTF-$V^{IV}O^{2+}$-phen spectra.

4.2.1.2. CD spectra of solutions containing hTF and $V^{IV}O(acac)_2$.

The Figure 22 shows the changes in the visible range of the CD spectra of solutions containing apo-hTF upon stepwise additions of $V^{IV}O(acac)_2$ (*experiment 2.5.*). The spectra of pure hTF was taken as a baseline.

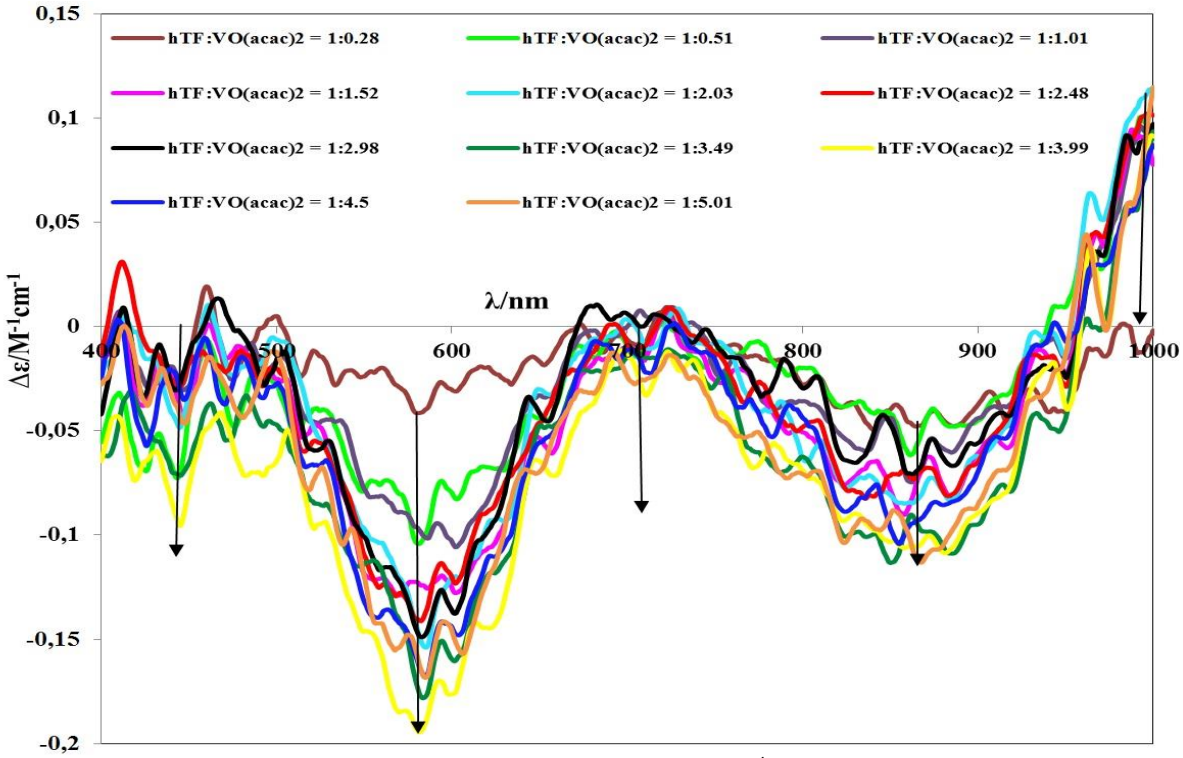

Figure 22. CD spectra of of solutions containing hTF (4.8×10^{-4} M) in PBS upon stepwise additions of adequate volumes of a solution of $V^{IV}O(acac)_2$ (3.77×10^{-2} M) in DMSO. Maximum % of DMSO added was 5.9. The cell path length was 50 mm.

As in the region 400-1000 nm pure hTF does not absorb, the CD bands observed are due to the formation of hTF-$V^{IV}O$ complexes. It is interesting to observe that the pattern of all CD spectra appears to be the same, this suggesting that the type of binding does not change upon additions of complex. The CD spectra are rather noisy, it is not clear if there are isodichroic points or not. It also appears that the intensity of the spectra is also approximately the same for all spectra for ratios $V^{IV}O(acac)_2$:hTF higher than 1.52.

The complexes formed in the system produce both positive and negative bands in the range of 400-1000 nm. One positive band is observed approximately at 945 - >1000 nm with unclear spectra maxima which can be attributed either to $d_{xy} \rightarrow d_{xz}$ or to $d_{xy} \rightarrow d_{yz}$ transitions, one negative band approximately at 700 - 954 nm with the spectra minima at ~870 nm which can be attributed either to $d_{xy} \rightarrow d_{xz}$ or to $d_{xy} \rightarrow d_{yz}$ transitions, one positive band approximately at 650 - 812 nm with the spectra maxima at ~714 nm, one negative band approximately at 500 - 700 nm with the spectra minima at ~585 nm which can be attributed to $d_{xy} \rightarrow d_{x2-y2}$ transitions and one positive band approximately at 400-582 nm with the spectra maxima at ~ 447 nm which can be attributed to $d_{xy} \rightarrow d_{z2}$ transitions. Clearly (i) $V^{IV}O(acac)_2$ binds hTF, contradicting previous reports that such binding does not occur.[117,118] The fact that the

intensity of the CD spectra almost does not change for $V^{IV}O(acac)_2$:hTF ratios > 1.52 also indicates that (ii) $V^{IV}O$-complexes responsible for the CD spectra measured are bound at the Fe^{III} binding sites of hTF. However, (iii) this does not rule out the binding of $V^{IV}Oacac$ – complexes for $V^{IV}O(acac)_2$:hTF ratios > 1.52 at surface His residues, as these are not expected to yield significant CD spectra. [117,118]

4.2.2. Studies of the interaction by EPR. Background.

The main objective of the discussion of the results obtained in this work is to compare the EPR spectra of each system analyzed with the EPR spectrum of the corresponding complex alone and with the EPR spectrameasured for the hTF (or HSA) -$V^{IV}O^{2+}$ systems to check if the complex binds to hTF (or HSA) and if so, whether it binds to the protein as $V^{IV}O^{2+}$ or with the ligand(s). In some cases it is possible to suggest the hTF (or HSA):$V^{IV}O^{2+}$:ligand ratio.

4.2.2.1. The EPR spectra of $V^{IV}O$-oda–hTF complexes.

Figure 23 depicts the X-band EPR spectra of the solutions containing hTF in PBS and $V^{IV}O(oda)(H_2O)_2$ in MeOH (*experiment 3.1.*), of solution containing $V^{IV}O(oda)(H_2O)_2$ in MeOH (*experiment 3.2.*). The X-band EPR spectra of solutions containing hTF and $V^{IV}OSO_4$ (ratios 1:1 and 1:2) are also presented for comparison. The series of spectra being analyzed do not superimpose completely with the spectrum of solution of $V^{IV}O(oda)(H_2O)_2$ in MeOH. This means that (i) V^{IV} of $V^{IV}O(oda)(H_2O)_2$ binds to hTF. Due to the high level of noise in the parallel region of the spectra being analyzed, it is not clear if the spectra superimpose with the spectra of solutions of hTF:$V^{IV}O^{2+}$=1:1 and hTF:$V^{IV}O^{2+}$=1:2 although they look similar. However, differences are seen in the perpendicular region and distinct CD spectra.

Figure 24 depicts the amplification of the low and high field ranges of the X-band EPR spectra presented in the Figure 23. Spin Hamiltonian parameters (g_x, g_y, g_z, A_x, A_y and A_z) of the samples being analyzed and the sample of $V^{IV}O(oda)(H_2O)_2$ in MeOH are presented in the Table 1. The EPR spectra of hTF-$V^{IV}O^{2+}$ systems are composed by two sets of resonances, A and B.[93,119] These resonances were attributed to $V^{IV}O^{2+}$ bound in the N-and C-terminal sites respectively, reported by different authors, and are presented in Table 1 for comparison.[105,120] It is clearer that the peaks in the parallel region in both low and high field of the samples being analyzed do not completely superimpose with the peaks of the the spectra of solutions of hTF:$V^{IV}O^{2+}$=1:1 and hTF:$V^{IV}O^{2+}$=1:2 which means that (ii) $V^{IV}O(oda)(H_2O)_2$ possibly binds to hTF with at least one ligand.

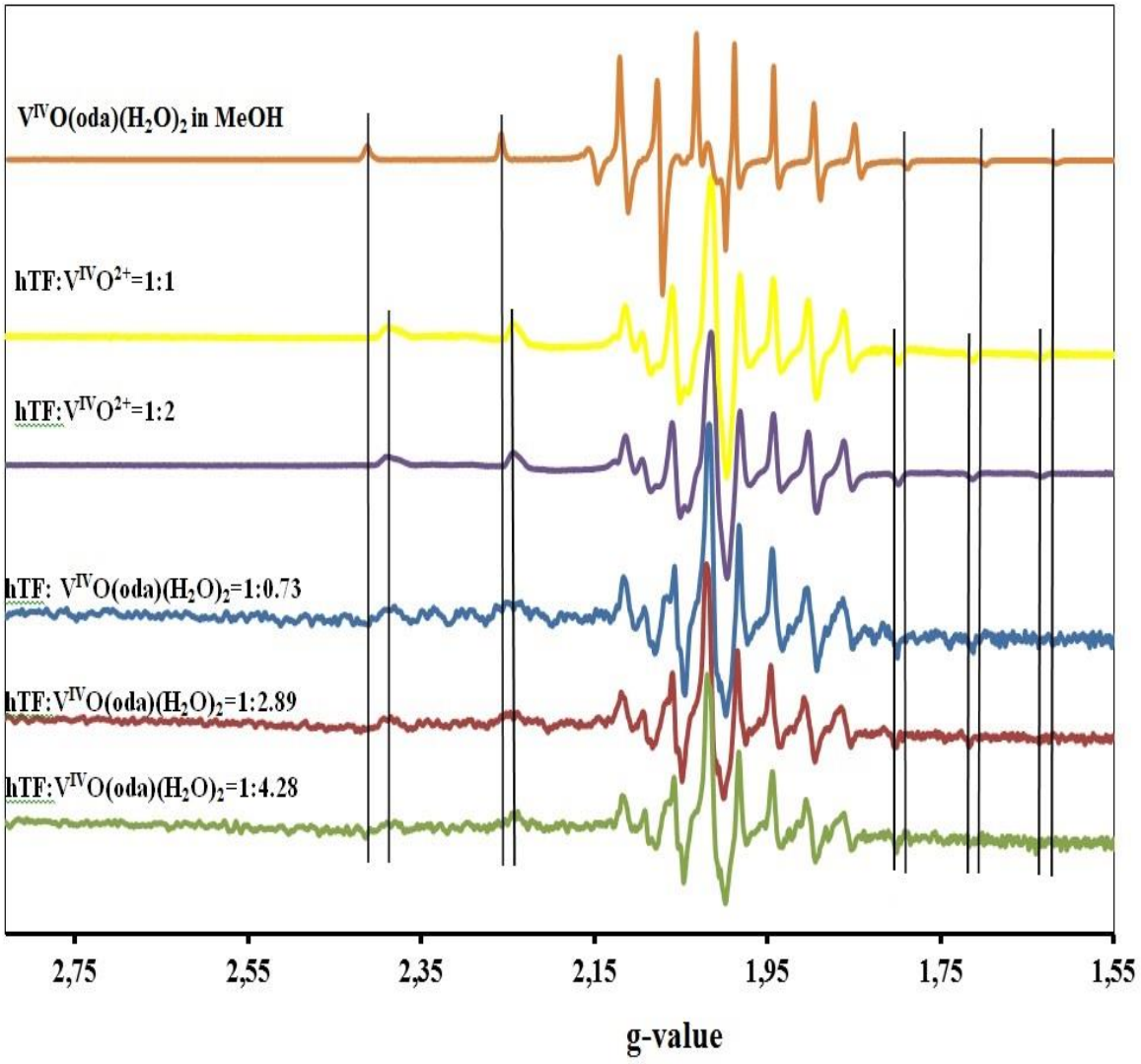

Figure 23. X-band EPR spectra of solutions containing hTF (4.9×10^{-4} M, 4.78×10^{-4} M, 4.7×10^{-4} M) in PBS and $V^{IV}O(oda)(H_2O)_2$ (3.58×10^{-4} M, 1.38×10^{-3} M, 2.02×10^{-3} M) in MeOH respectively. The X-band EPR spectra of the solution containing $V^{IV}O(oda)(H_2O)_2$ (2.85×10^{-3}) in MeOH and solutions containing hTF (6×10^{-4} M) and $V^{IV}OSO_4$ ($C=C_{hTF}$ and $C= C_{hTF}\times2$) in HEPES-S buffer are included for comparison. Maximum % of DMSO added was 4.3; T= 77 K.

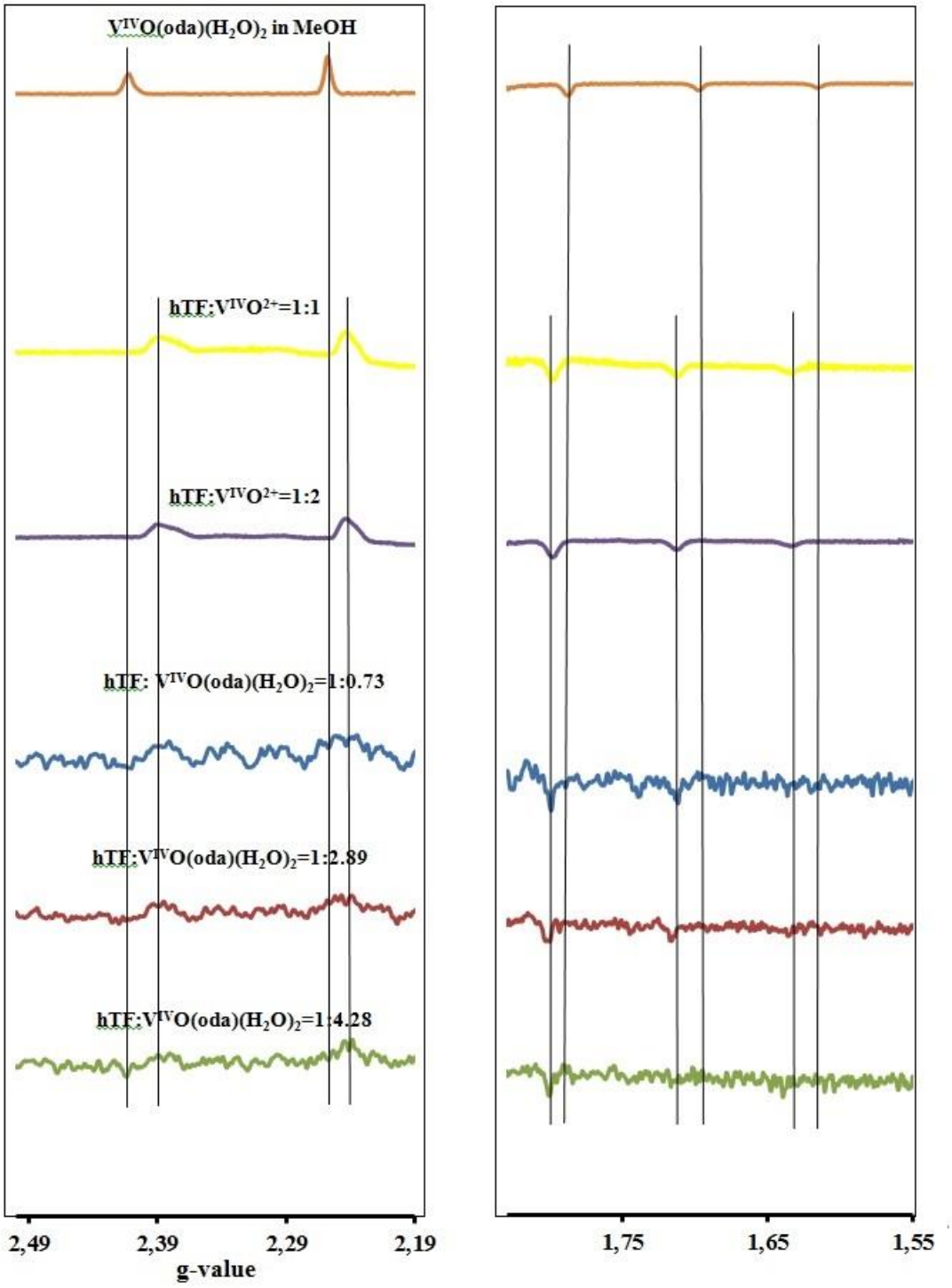

Figure 24. Amplification of the low and high field ranges of the X-band EPR spectra of solutions containing hTF (4.9×10^{-4} M, 4.78×10^{-4} M, 4.7×10^{-4} M) in PBS and $V^{IV}O(oda)(H_2O)_2$ (3.58×10^{-4} M, 1.38×10^{-3} M, 2.02×10^{-3} M) in MeOH respectively. Amplification of the low and high field ranges of the X-band EPR spectra of solution containing $V^{IV}O(oda)(H_2O)_2$ (2.85×10^{-3}) in MeOH and of solutions containing hTF (6×10^{-4} M) and $V^{IV}OSO_4$ ($C=C_{hTF}$ and $C= C_{hTF}\times2$) in HEPES-S buffer are included for comparison. Maximum % of DMSO added was 4.3; T= 77 K.

Table 1. Spin Hamiltonian parameters (g_x, g_y, g_z, A_x, A_y and A_z) of samples for the hTF-$V^{IV}O(oda)(H_2O)_2$ system, the $V^{IV}O(oda)(H_2O)_2$ in MeOH, obtained by simulation of the experimental EPR spectra with the computer program of Rockenbauer and Korez[116], and those reported by other authors for $V^{IV}O$–hTF species (A and B).

System		**g_x, g_y**	**g_z**	**A_x, A_y ($\times 10^4$ cm^{-1})**	**A_z($\times 10^4$ cm^{-1})**
$V^{IV}O(oda)(H_2O)_2$ in MeOH		1.982	1.937	68.1	178.5
$V^{IV}O$–hTF species A	ref[96]		1.939		168.5
	ref[121]		1.937		168.3
	ref[122]		1.938		168
	ref[123]		1.938		168
	ref[124]		1.940		166.8
$V^{IV}O$–hTF species B	ref[96]		1.940		171.1
	ref[122]		1.941		170.3
	ref[123]		1.938		170
	ref[124]		1.934		170
	ref[121]		1.941		170.5
	ref[121]		1.935		171.8
hTF:$V^{IV}O(oda)(H_2O)_2$=1:0.73		1.978	1.943	58	168.8
hTF:$V^{IV}O(oda)(H_2O)_2$=1:2.89		1.980	1.945	58	169.3
hTF:$V^{IV}O(oda)(H_2O)_2$=1:4.28		1.978	1.942	58	168.3

The g_z values obtained in this work for all the samples hTF:$V^{IV}O(oda)(H_2O)_2$ are higher than those obtained for $V^{IV}O(oda)(H_2O)_2$ in MeOH and for both $V^{IV}O$–hTF species A and B. The A_z values obtained in this work for the same samples differ from all the A_z values obtained for $V^{IV}O(oda)(H_2O)_2$ in MeOH and for both $V^{IV}O$–hTF species A and B except the one for the sample hTF:$V^{IV}O(oda)(H_2O)_2$=1:4.28, the A_z of which matches with A_z of $V^{IV}O$–hTF species A from ref[121]. This corroborates the conclusions (i) V^{IV} of $V^{IV}O(oda)(H_2O)_2$ binds to hTF and (ii) $V^{IV}O(oda)(H_2O)_2$ possibly binds to hTF with at least one ligand and is in agreement with the results obtained from CD analyses of this system (*experiment 2.1.*, *Appendix E* (Figure E 1)).

Figure 25 depicts the X-band EPR spectra of the solutions containing hTF in PBS and $V^{IV}O(oda)(bipy)$ in DMSO (*experiment 3.3.*), of the solution containing $V^{IV}O(oda)(bipy)$ in EtOH (*experiment 3.8.*); the X-band EPR spectra of solutions containing hTF and $V^{IV}OSO_4$ (ratios 1:1 and 1:2) are included for comparison. The series of spectra being analyzed do not superimpose with the spectrum of solution of $V^{IV}O(oda)(bipy)$ in EtOH which contains at least two species of V^{IV}. This means that (i) V^{IV} of $V^{IV}O(oda)(bipy)$ binds to hTF. Moreover, they do not superimpose with the spectra of solutions of hTF and $V^{IV}O^{2+}$ (ratios 1:1 and 1:2)

which means that (ii) $V^{IV}O$(oda)(bipy) possibly binds to hTF with at least one ligand (oda or both).

Figure 26 depicts the amplification of the low and high field ranges of the X-band EPR spectra presented in the Figure 25. Spin Hamiltonian parameters (g_x, g_y, g_z, A_x, A_y and A_z) of the samples being analyzed, the sample of $V^{IV}O$(oda)(bipy) in EtOH and of $V^{IV}O$–hTF species A and B reported by different authors are also presented in the Table 2. It is clear that the peaks in the parallel region in both low and high field of the samples being analyzed do not superimpose with the peaks of the the spectra of solutions of hTF:$V^{IV}O^{2+}$=1:1 and hTF:$V^{IV}O^{2+}$=1:2, this confirming the conclusion (ii) above.

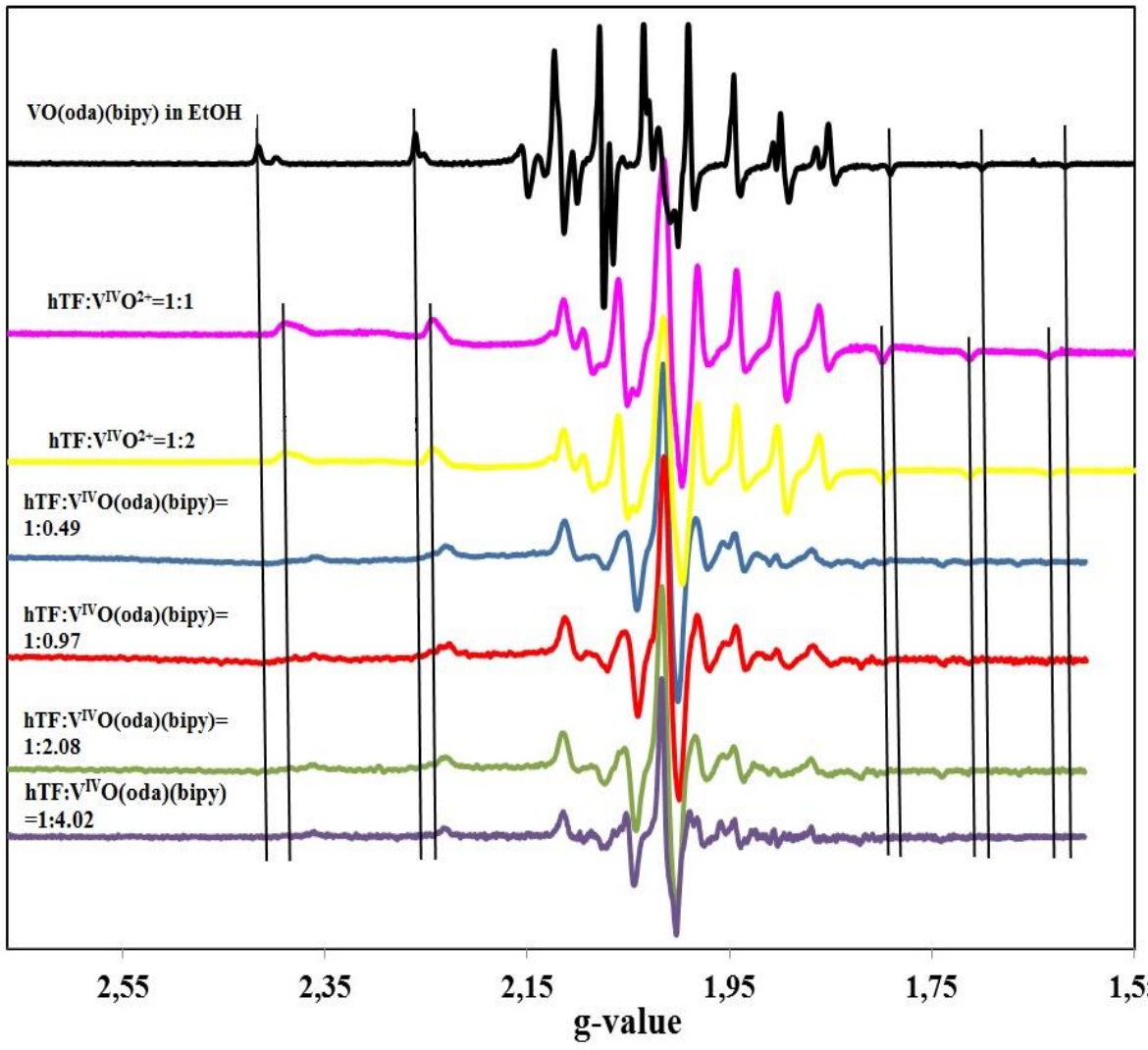

Figure 25. X-band EPR spectra of solutions containing hTF (4.89×10^{-4} M, 4.86×10^{-4} M, 4.81×10^{-4} M and 4.72×10^{-4} M) in PBS and $V^{IV}O$(oda)(bipy) (2.37×10^{-4} M, 4.72×10^{-4} M, 1×10^{-3} M and 1.9×10^{-3} M) in DMSO respectively. The X-band EPR spectra of solution containing $V^{IV}O$(oda)(bipy) (1.43×10^{-3} M) in EtOH and solutions containing hTF (6×10^{-4} M) and $V^{IV}OSO_4$ (C=C_{hTF} and C= $C_{hTF}\times2$) in HEPES-S buffer are included for comparison. Maximum % of DMSO added was 3.98; T= 77 K.

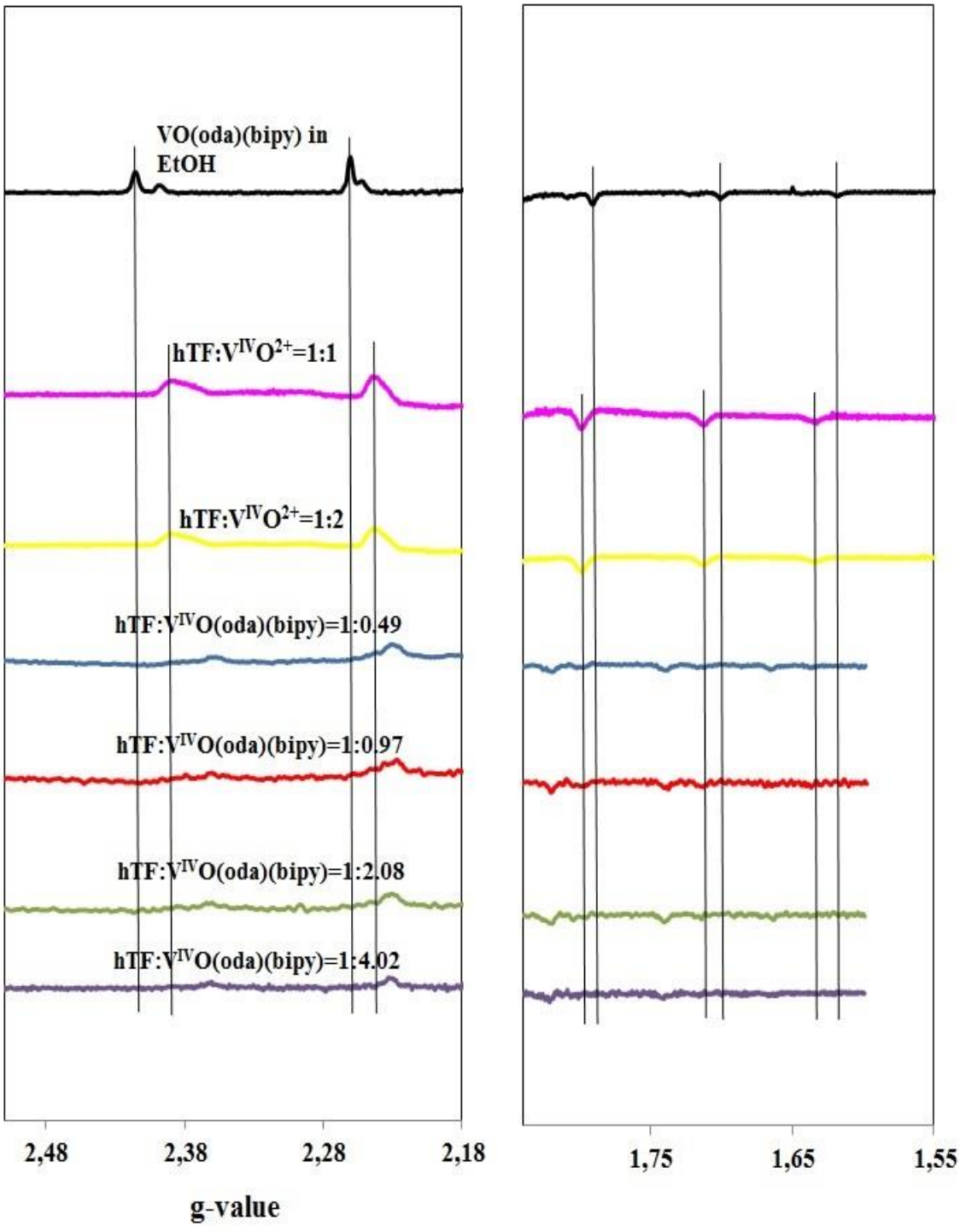

Figure 26. Amplification of the low and high field ranges of the X-band EPR spectra of solutions containing hTF (4.89×10^{-4} M, 4.86×10^{-4} M, 4.81×10^{-4} M and 4.72×10^{-4} M) in PBS and $V^{IV}O$(oda)(bipy) (2.37×10^{-4} M, 4.72×10^{-4} M, 1×10^{-3} M and 1.9×10^{-3} M) in DMSO respectively. Amplification of the low and high field ranges of the X-band EPR spectra of solution containing $V^{IV}O$(oda)(bipy) (1.43×10^{-3} M) in EtOH and solutions containing hTF (6×10^{-4} M) and $V^{IV}OSO_4$ ($C=C_{hTF}$ and $C= C_{hTF}\times2$) in HEPES-S buffer are included for comparison. Maximum % of DMSO added was 3.98; T= 77 K.

Table 2. Spin Hamiltonian parameters (g_x, g_y, g_z, A_x, A_y and A_z) of samples for the hTF-VO(oda)(bipy) system, the $V^{IV}O$(oda)(bipy) in EtOH, obtained by simulation of the experimental EPR spectra with the computer program of Rockenbauer and Korez[116], and those reported by other authors for $V^{IV}O$–hTF species (A and B).

System		**g_x, g_y**	**g_z**	**A_x, A_y ($\times 10^4$ cm^{-1})**	**A_z ($\times 10^4$ cm^{-1})**
$V^{IV}O$(oda)(bipy) in EtOH		1.975	1.942	60.3	170.7
$V^{IV}O$–hTF species A	ref[96]		1.939		168.5
	ref[121]		1.937		168.3
	ref[122]		1.938		168
	ref[123]		1.938		168
	ref[124]		1.940		166.8
$V^{IV}O$–hTF species B	ref[96]		1.940		171.1
	ref[122]		1.941		170.3
	ref[123]		1.938		170
	ref[124]		1.934		170
	ref[121]		1.941		170.5
	ref[121]		1.935		171.8
hTF:$V^{IV}O$(oda)(bipy)=1:0.49		1.978	1.954	52	168.7
hTF:$V^{IV}O$(oda)(bipy)=1:0.97		1.977	1.953	53	168.8
hTF:$V^{IV}O$(oda)(bipy)=1:2.08		1.981	1.953	52	169
hTF:$V^{IV}O$(oda)(bipy)=1:4.02		1.980	1.956	51	169.2

The g_z values obtained in this work for all the samples hTF:$V^{IV}O$(oda)(bipy) are higher than those obtained for $V^{IV}O$(oda)(bipy) in EtOH and for both VO–hTF species A and B. A_z values obtained in this work for the same samples significantly differ from all the A_z values obtained for $V^{IV}O$(oda)(bipy) in EtOH and for both VO–hTF species A and B. This fact corroborates the conclusions (i) and (ii) above and is in agreement with the results obtained from CD analyses of this system (*experiment 2.3.*).

Figure 27 depicts the X-band EPR spectra of the solutions containing hTF and $V^{IV}O$(oda)(phen) in PBS (*experiment 3.4.*), and of other related systems (*experiments 3.5.* and *3.9.*). The series of spectra being analyzed do not superimpose with the spectrum of solution of $V^{IV}O$(oda)(phen) in H_2O+10% DMSO which contains at least two species of V^{IV}. This means that (i) V^{IV} of $V^{IV}O$(oda)(phen) binds to hTF. Moreover, it is obvious that they do not superimpose with the spectra of solutions of hTF and $V^{IV}O^{2+}$ (ratios 1:1 and 1:2) which means that (ii) $V^{IV}O$(oda)(phen) probably binds to hTF with at least one ligand. It is not clear from Figure 27 if the spectra of solutions containing hTF and $V^{IV}O$(oda)(phen) in PBS (*experiment*

3.4.) superimpose with the spectra of solutions containing hTF in PBS, $VOSO_4$ in H_2O and o-phenantroline·H_2O in EtOH (*experiment 3.5.*).

Figure 28 depicts the amplification of the low and high field ranges of the X-band EPR spectra presented in the Figure 27. Spin Hamiltonian parameters (g_x, g_y, g_z, A_x, A_y and A_z) of the samples being analyzed, the sample of $V^{IV}O$(oda)(phen) in H_2O+10% DMSO and of $V^{IV}O$–hTF species A and B reported by different authors are presented in the Table 3.

The g_z values obtained in this work for all the samples from hTF-VO(oda)(phen) and hTF-$V^{IV}O$-phen systems are higher than those obtained for $V^{IV}O$(oda)(phen) in H_2O+10% DMSO and for both $V^{IV}O$–hTF species A and B. The A_z values obtained in this work for the same samples differ from all the A_z values obtained for $V^{IV}O$(oda)(phen) in H_2O+10% DMSO and for both $V^{IV}O$–hTF species A and B. This corroborates the conclusions (i) and (ii). The peaks in the parallel region in both low and high field of the samples containing hTF and $V^{IV}O$(oda)(phen) in PBS (*experiment 3.4.*) seem to superimpose with the spectra of the samples containing hTF in PBS, $VOSO_4$ in H_2O and o-phenantroline·H_2O in EtOH (*experiment 3.5.*). This suggests that $V^{IV}O$(oda)(phen) when binding to hTF probably loses one ligand (oda) and is bound in the form of $V^{IV}O$(phen). This suggestion is supported by the values of spin Hamiltonian parameters of both systems: g_x and g_z are the same for all the samples being compared; g_y, A_x, A_y and A_z values are very similar for all the samples being compared. However, it contradicts to the results obtained from the CD analyses of these two systems (*experiments 2.4.* and *2.7.*) which suggest that $V^{IV}O$(oda)(phen) loses phen ligand when binding to hTF. Hence, (iii) the binding of $V^{IV}O$(oda)(phen) to hTF does not correspond to simple binding of $V^{IV}O$(oda) or $V^{IV}O$(phen) to hTF. The ratio of ($V^{IV}O$):(phen) in the species formed is (iv) probably 1:1 as the spectra of the samples hTF:$V^{IV}O$:phen=1:3:3 and hTF:$V^{IV}O$:phen=1:3:5 completely superimpose and the spin Hamiltonian parameters for these two samples are very similar.

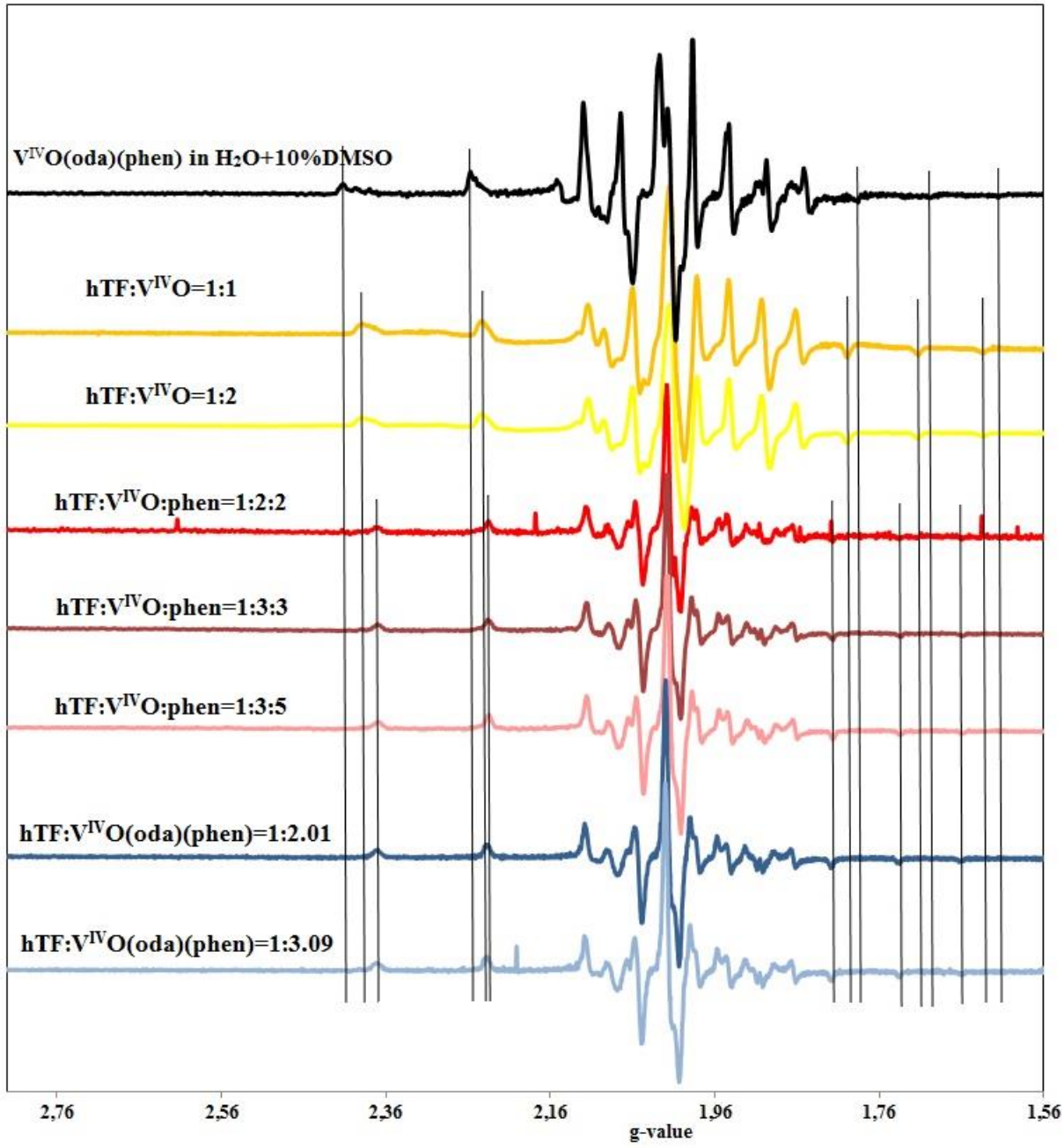

Figure 27. X-band EPR spectra of solutions containing hTF (5.32×10^{-4} M) and $V^{IV}O$(oda)(phen) (1.07×10^{-3} M and 1.65×10^{-3} M) in PBS (*experiment 3.4.*), of the solutions containing hTF (5.26×10^{-4} M, 5.24×10^{-4} M and 5.19×10^{-4} M) in PBS, $V^{IV}OSO_4$ (1.06×10^{-3} M, 1.57×10^{-3} M and 1.56×10^{-3} M) in H_2O and o-phenantroline (1.05×10^{-3} M, 1.57×10^{-3} M and 2.59×10^{-3} M) in EtOH (maximum % of EtOH added was 2.16) (*experiment 3.5.*), of the solution containing $V^{IV}O$(oda)(phen) (1.47×10^{-3} M) in H_2O+10% DMSO (*experiment 3.9.*). The X-band EPR spectra of solutions containing hTF (6×10^{-4} M) and $V^{IV}OSO_4$ ($C=C_{hTF}$ and $C=C_{hTF}\times2$) in HEPES-S buffer are included for comparison. T= 77 K.

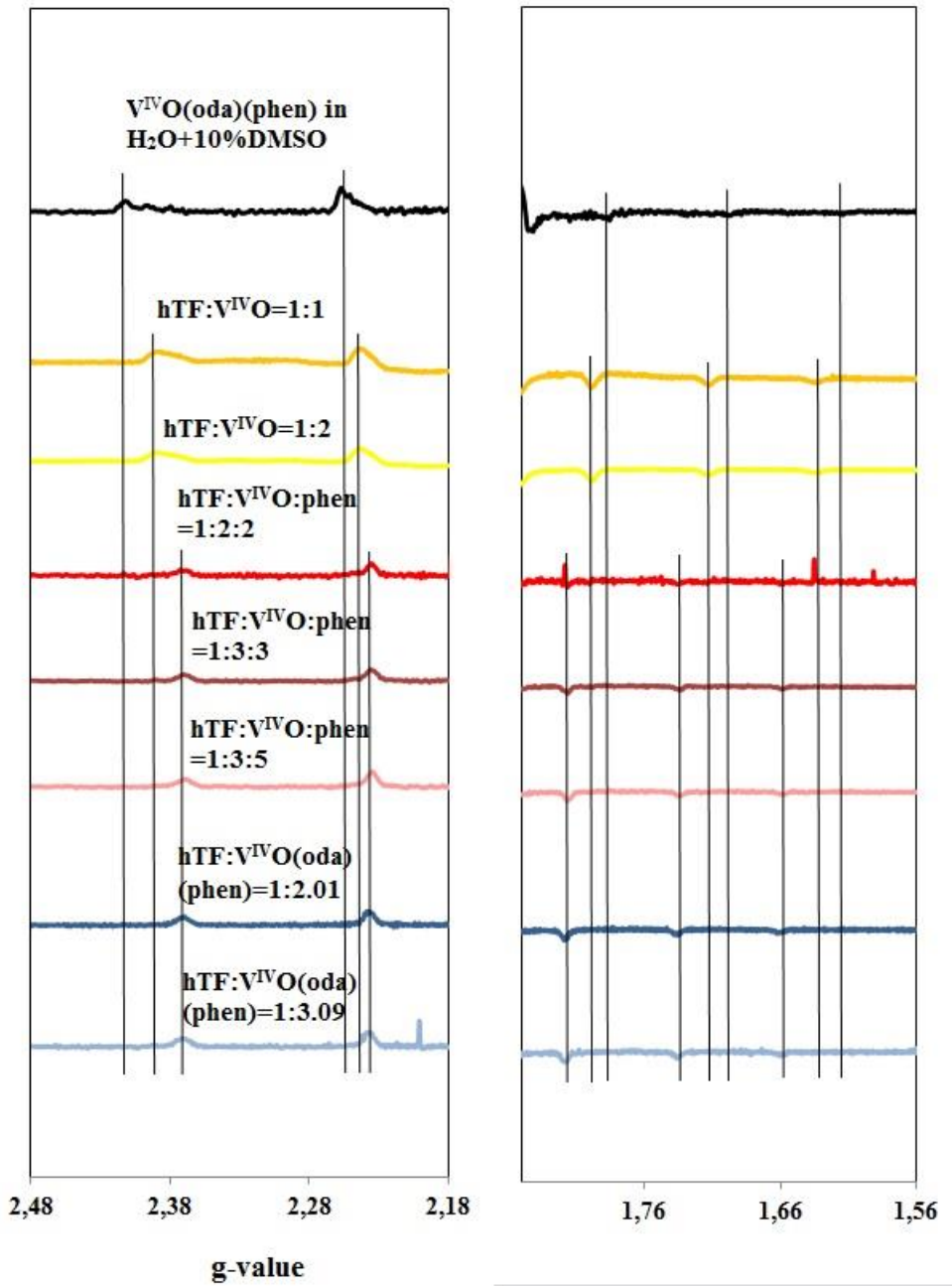

Figure 28. Amplification of the low and high field ranges of the X-band EPR spectra of solutions containing hTF (5.32×10^{-4} M) and $V^{IV}O$(oda)(phen) (1.07×10^{-3} M and 1.65×10^{-3} M) in PBS (*experiment 3.4.*), of the solutions containing hTF (5.26×10^{-4} M, 5.24×10^{-4} M and 5.19×10^{-4} M) in PBS, $V^{IV}OSO_4$ (1.06×10^{-3} M, 1.57×10^{-3} M and 1.56×10^{-3} M) in H_2O and o-phenantroline (1.05×10^{-3} M, 1.57×10^{-3} M and 2.59×10^{-3} M) in EtOH (maximum % of EtOH added was 2.16) (*experiment 3.5.*), of the solution containing $V^{IV}O$(oda)(phen) (1.47×10^{-3} M) in H_2O+10% DMSO (*experiment 3.9.*). The amplification of the X-band EPR spectra of solutions containing hTF (6×10^{-4} M) and $V^{IV}OSO_4$ ($C=C_{hTF}$ and $C= C_{hTF}\times2$) in HEPES-S buffer are included for comparison. T= 77 K.

Table 3. Spin Hamiltonian parameters (g_x, g_y, g_z, A_x, A_y and A_z) for the hTF-VO(oda)(phen) system, the hTF-$V^{IV}O$-phen system and for the $V^{IV}O$(oda)(phen) in H_2O+10% DMSO, obtained by simulation of the experimental EPR spectra with the computer program of Rockenbauer and Korez[116], and those reported by other authors for $V^{IV}O$–hTF species (A and B).

System		g_x	g_y	g_z	A_x ($\times 10^4$ cm^{-1})	A_y ($\times 10^4$ cm^{-1})	A_z ($\times 10^4$ cm^{-1})
$V^{IV}O$(oda)(phen) in H_2O+10% DMSO		1.984	1.984	1.939	65.6	65.6	178.4
$V^{IV}O$–hTF species A	ref[96]			1.939			168.5
	ref[121]			1.937			168.3
	ref[122]			1.938			168
	ref[123]			1.938			168
	ref[124]			1.940			166.8
$V^{IV}O$–hTF species B	ref[96]			1.940			171.1
	ref[122]			1.941			170.3
	ref[123]			1.938			170
	ref[124]			1.934			170
	ref[121]			1.941			170.5
	ref[121]			1.935			171.8
hTF:$V^{IV}O$:phen=1:2:2		1.986	1.990	1.961	59	50	160.8
hTF:$V^{IV}O$:phen=1:3:3		1.986	1.990	1.961	59	50	160.8
hTF:$V^{IV}O$:phen=1:3:5		1.986	1.990	1.961	59	50.1	161
hTF:$V^{IV}O$(oda)(phen)=1:2.01		1.986	1.989	1.961	58.7	49.6	160.6
hTF:$V^{IV}O$(oda)(phen)=1:3.09		1.986	1.990	1.961	58.9	49.8	160.9

4.2.2.2. The EPR spectra of solutions containing hTF and $V^{IV}O(acac)_2$.

Figure 29 depicts the X-band EPR spectra of the solutions containing hTF in PBS and $V^{IV}O(acac)_2$ in DMSO (*experiment 3.6.*) and of the solution containing $V^{IV}O(acac)_2$ in MeOH. The EPR spectra of solutions containing hTF and $V^{IV}O^{2+}$ (ratios 1:1 and 1:2) are also included for comparison. The spectrum of the sample hTF:$V^{IV}O(acac)_2$=1:5.01 does not superimpose with the spectrum of solution of $V^{IV}O(acac)_2$ in MeOH. This means that (i) V^{IV} of $V^{IV}O(acac)_2$ binds to hTF; moreover, it is obvious that it does not superimpose with the spectra of solutions of hTF and $V^{IV}O^{2+}$ (ratios 1:1 and 1:2), which means that (ii) $V^{IV}O(acac)_2$ possibly binds to hTF with at least one $acac^-$ ligand.

Figure 30 depicts the amplification of the low and high field ranges of the X-band EPR spectra presented in the Figure 29. Spin Hamiltonian parameters (g_x, g_y, g_z, A_x, A_y and A_z) of the sample hTF:$V^{IV}O(acac)_2$=1:5.01 and the sample of $V^{IV}O(acac)_2$ in MeOH are presented in the Table 4. The peaks in the parallel region in both low and high field of the spectrum of the sample hTF:$V^{IV}O(acac)_2$=1:5.01 do not completely superimpose with the peaks of the the

spectra of solutions of hTF:$V^{IV}O^{2+}$=1:1 and hTF:$V^{IV}O^{2+}$=1:2. The A_z values of the solution of $V^{IV}O(acac)_2$ in MeOH and in the presence of hTF appear quite similar, but the spectra differ in the perpendicular region.

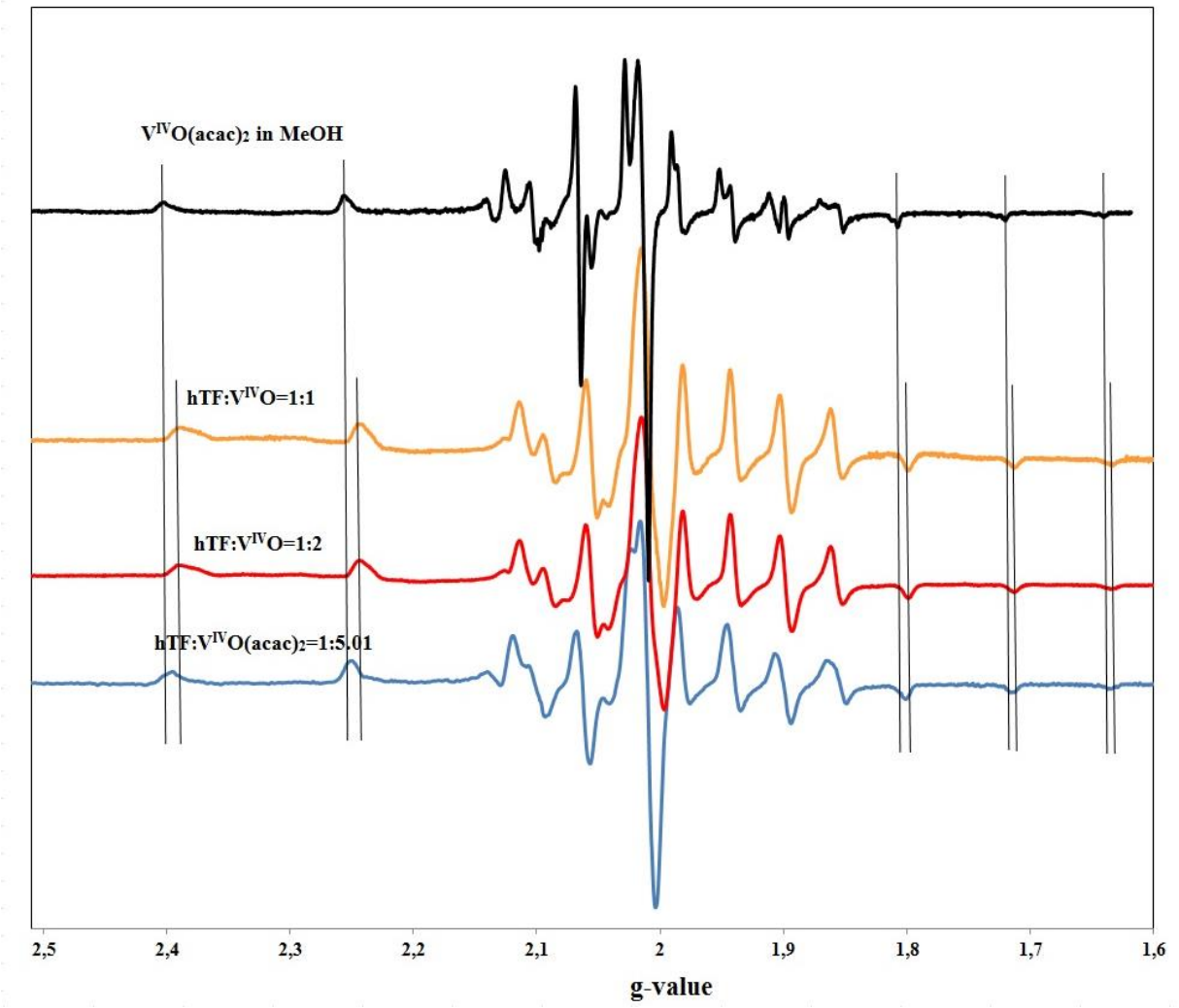

Figure 29. X-band EPR spectra of the solution containing hTF (4.5×10^{-4} M) in PBS and $V^{IV}O(acac)_2$ (2.25×10^{-3} M) in DMSO. The X-band EPR spectra of solution containing $V^{IV}O(acac)_2$ in MeOH, solutions containing hTF (6×10^{-4} M) and $V^{IV}OSO_4$ (C=C_{hTF} and C= $C_{hTF}\times2$) in HEPES-S buffer are included for comparison. Maximum % of DMSO added was 5.98; T= 77 K.

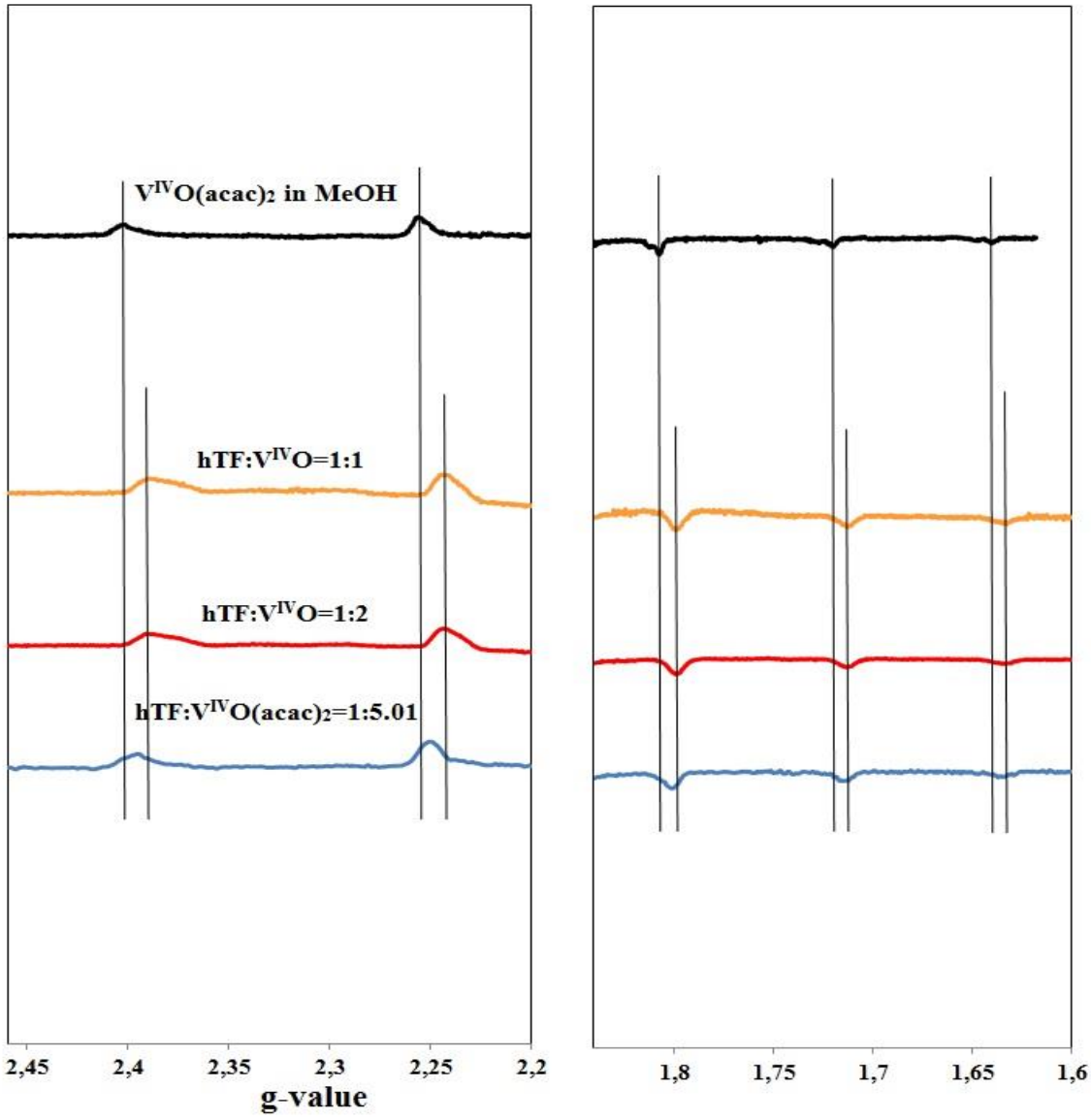

Figure 30. Amplification of the low and high field ranges of the X-band EPR spectra of the solution containing hTF (4.5×10^{-4} M) in PBS and $V^{IV}O(acac)_2$ (2.25×10^{-3} M) in DMSO. The amplification of the X-band EPR spectra of solution containing $V^{IV}O(acac)_2$ in MeOH, solutions containing hTF (6×10^{-4} M) and $V^{IV}OSO_4$ ($C=C_{hTF}$ and $C= C_{hTF}\times2$) in HEPES-S buffer are included for comparison. Maximum % of DMSO added was 5.98; T= 77 K.

The g_z value obtained in this work for the sample hTF:$V^{IV}O(acac)_2$=1:5.01 are higher than those obtained for both VO–hTF species A and B and is lower than that of the sample of $V^{IV}O(acac)_2$ in MeOH. The A_z value of the sample hTF:$V^{IV}O(acac)_2$=1:5.01 is equal to the A_z values obtained for $V^{IV}O$–hTF species B in ref[123] and ref[124], however, the g_z values of the corresponding samples differ. This corroborates the conclusions (i) and (ii) and is in agreement with the results obtained from CD analysis of this system (*experiment 2.5.*), while contradicting previous reports that such binding does not occur. [117,118]

Table 4. Spin Hamiltonian parameters (g_x, g_y, g_z, A_x, A_y and A_z) of the sample from hTF-$V^{IV}O(acac)_2$ system (hTF:$V^{IV}O(acac)_2$=1:5.01) and of the sample of $V^{IV}O(acac)_2$ in MeOH, obtained by simulation of the experimental EPR spectra with the computer program of Rockenbauer and Korez[116], and those reported by other authors for $V^{IV}O$–hTF species (A and B).

System		**g_x, g_y**	**g_z**	**A_x, A_y ($\times 10^4$ cm^{-1})**	**A_z($\times 10^4$ cm^{-1})**
$V^{IV}O(acac)_2$ in MeOH		1.984	1.954	60.8	171.2
$V^{IV}O$–hTF species A	ref[96]		1.939		168.5
	ref[121]		1.937		168.3
	ref[122]		1.938		168
	ref[123]		1.938		168
	ref[124]		1.940		166.8
$V^{IV}O$–hTF species B	ref[96]		1.940		171.1
	ref[122]		1.941		170.3
	ref[123]		1.938		170
	ref[124]		1.934		170
	ref[121]		1.941		170.5
	ref[121]		1.935		171.8
hTF:$V^{IV}O(acac)_2$=1:5.01		1.979	1.946	60.4	170

4.2.3. Studies of the interaction of $V^{IV}O(oda)(bipy)$ and $V^{IV}O(acac)_2$ complexes with hTF by size-exclusion gel-filtration chromatography, ICP, CD, EPR and UV-Vis absorption (*experiment 5.1.*).

The results of the ICP analysis are presented in Table 5. It is obvious from Table 5 that for each sample the concentration of vanadium determined in the eluate is lower than that added, this meaning that not all the V^{IV} added to hTF solution binds to hTF, and that a significant amount of V^{IV} in solution stayed in the pores of the PD-10 columns. The vanadium:hTF ratios presented in the last column of table approximately correspond to the mol equivalents of V^{IV} bound per 1 molecule of hTF in each sample. There is a clear tendency for both systems, that with the increase of the complex:hTF ratio the difference between the "expected" and found mol equivalents of V^{IV} increases.

It is clear from the data of Table 5 that hTF binds more than 2 mol equivalents of either $V^{IV}O(oda)(bipy)$ or $V^{IV}O(acac)_2$, possibly at two iron binding sites and at some surface histidine residues.

Table 5. The results of the ICP analysis of the samples from the *experiment 5.1*. (hTF-$V^{IV}O$(oda)(bipy) and hTF-$V^{IV}O(acac)_2$ systems). As determined by UV absorption, the hTF concentration before running through the column was 1.41×10^{-4} M and after running through the column 9.43×10^{-5} M; the dilution factor is ~67 % upon elution through the PD-10 columns.

Molar ratios of hTF:complex in the samples prepared	**Found V^{IV} concentration/M after passing by the PD-10 column**	**Vanadium:hTF ratio found in the eluate**
hTF:$V^{IV}O$(oda)(bipy)=1:1.05	0.84×10^{-4}	0.9
hTF:$V^{IV}O$(oda)(bipy)=1:2.1	1.4×10^{-4}	1.5
hTF:$V^{IV}O$(oda)(bipy)=1:4.21	2.3×10^{-4}	2.5
hTF:$V^{IV}O$(oda)(bipy)=1:8.41	3.7×10^{-4}	4
hTF: $V^{IV}O(acac)_2$=1:1.01	0.84×10^{-4}	0.9
hTF: $V^{IV}O(acac)_2$=1:2.05	1.4×10^{-4}	1.5
hTF: $V^{IV}O(acac)_2$=1:4.02	1.9×10^{-4}	2.1
hTF: $V^{IV}O(acac)_2$=1:7.89	2.9×10^{-4}	3.1

The solution of apo-hTF has bands in 250–330 nm range. These bands are due to hTF aromatic amino acid residues and the CD spectra reflect short-range interactions between these aromatic side groups with other optically active groups of hTF.[96] The bands at approximately 250–265 nm are usually associated with phenylalanine, at approximately 265–280 nm with tyrosine and at approximately 270–290 nm with tryptophan. At wavelength of >350 nm hTF does not absorb so no induced CD can be observed for solutions only containing hTF.[96] The extinction coefficients of the Trp bands are much higher than those Tyr, and Phe (much lower). Probably Δε values follow a similar trend.

Figure 31 depicts the CD spectra in the UV (250-400 nm) range of solutions containing apo-hTF and of $V^{IV}O$(oda)(bipy) prepared in separate batches.

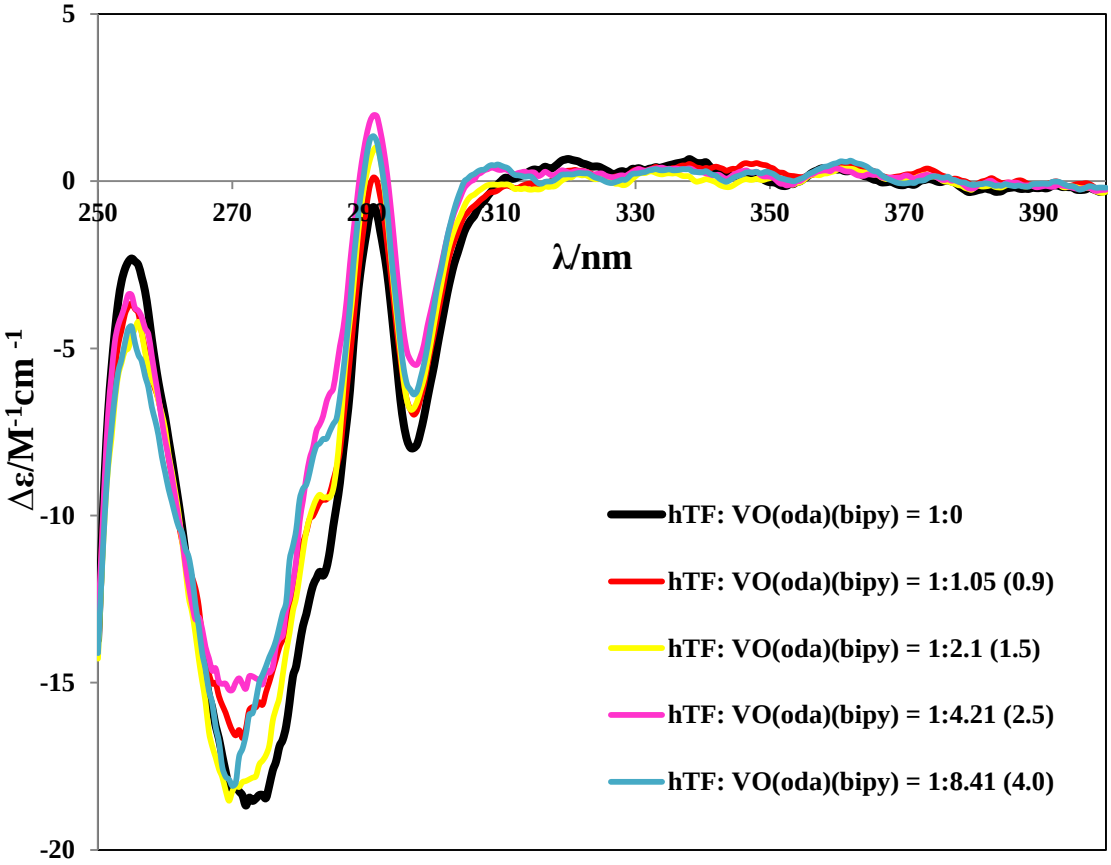

Figure 31. CD spectra of the solutions after passing through the PD-10 columns and elution with 3.5 mL of Tris buffer. The solutions contain apo-hTF (9.43×10^{-5} M) and different concentrations of $V^{IV}O$(oda)(bipy) (initially obtained by addition of $V^{IV}O$(oda)(bipy) (2.96×10^{-2} M) in DMSO to solutions of hTF(1.41×10^{-4} M) in Tris buffer). Maximum % of DMSO added was 4; the cell path length was 2 mm. The ratio of V^{IV}:hTF as found by ICP (for V) is indicated in brackets.

The absorption of the samples is high in the 260-300 nm range, so the signal-to-noise ratio is not favorable, and it is not easy to detect a clear trend in the bands as the complex is added.

It is possible that (i) $V^{IV}O$(oda)(bipy) binds close to some tyrosine residue(s), but Trp, expected to yield higher Δε values, is not much affected. Moreover, (ii) some oxidation of $V^{IV} \rightarrow V^{V}$-species may occur and (iii) as ligands concentration increases, some of $V^{IV}O^{2+}$ may unbind from the hTF. The most "complete" interaction between hTF and $V^{IV}O$(oda)(bipy) happens at the ratio of 4.21 (2.5).

The comparison of these CD spectra with the CD spectrum of the $V^{IV}O$-hTF system at the hTF: $V^{IV}O$(oda)(bipy) ratio of 1:2 from ref.[96] shows that (iv) $V^{IV}O^{2+}$ possibly binds with at least one ligand, as the spectra differ. Particularly, the difference is obvious in the 270-285 nm range and in the visible range (*experiment 2.3.*).

Figure 32 depicts the X-band EPR spectra of the solutions whose CD spectra are depicted in Figure 31. The EPR spectra of solutions containing $V^{IV}O$(oda)(bipy) in EtOH and of solutions containing hTF and $V^{IV}O^{2+}$ are presented for comparison. The series of spectra being analyzed do not superimpose completely with the spectrum of solution of $V^{IV}O$(oda)(bipy) in EtOH which contains at least two V^{IV} species. This means that the V^{IV} of $V^{IV}O$(oda)(bipy) binds to hTF (confirmation of conclusion (i)); as the spectra being analyzed are noisy and the peaks in the parallel region in both low and high fields are not very clear, it cannot be concluded for sure if these spectra superimpose with the spectra of solutions of hTF:$V^{IV}OSO_4$=1:1 and 1:2. However, it seems that they do not superimpose which allows to suggest that (iv) $V^{IV}O$(oda)(bipy) is bound to hTF with at least one of the ligands, thus confirming the conclusions previously made from the CD spectra of this system (*experiment 2.2.*).

Figure 33 depicts the amplification of the low and high field ranges of the EPR spectra presented in the Figure 32. It is clearer that the peaks in the parallel region in both low and high field do not superimpose. Due to the high noise level it was only possible to simulate samples with ratios hTF:$V^{IV}O$(oda)(bipy) of 1:2.1 (1.5) and 8.41 (4.0). The spin Hamiltonian parameters (g_x, g_y, g_z, A_x, A_y and A_z) of these samples are presented in the Table 6.

The g_z values obtained in this work for the samples hTF:$V^{IV}O$(oda)(bipy)=2.1 (1.5) and hTF:$V^{IV}O$(oda)(bipy)=8.41 (4.0) are higher than those obtained for $V^{IV}O$(oda)(bipy) in EtOH and for both VO–hTF species A and B. A_z values obtained in this work for the same samples differ from all the A_z values obtained for $V^{IV}O$(oda)(bipy) in EtOH and for both VO–hTF species A and B. However, A_z values from this work are somewhat close to A_z values obtained for VO–hTF species B from ref[119,121-124]. These results support previously suggested conclusion (iv) which is also in agreement with the results obtained in this work from CD (*experiment 2.2.*) and EPR (*experiment 3.3.*) analyses of this system.

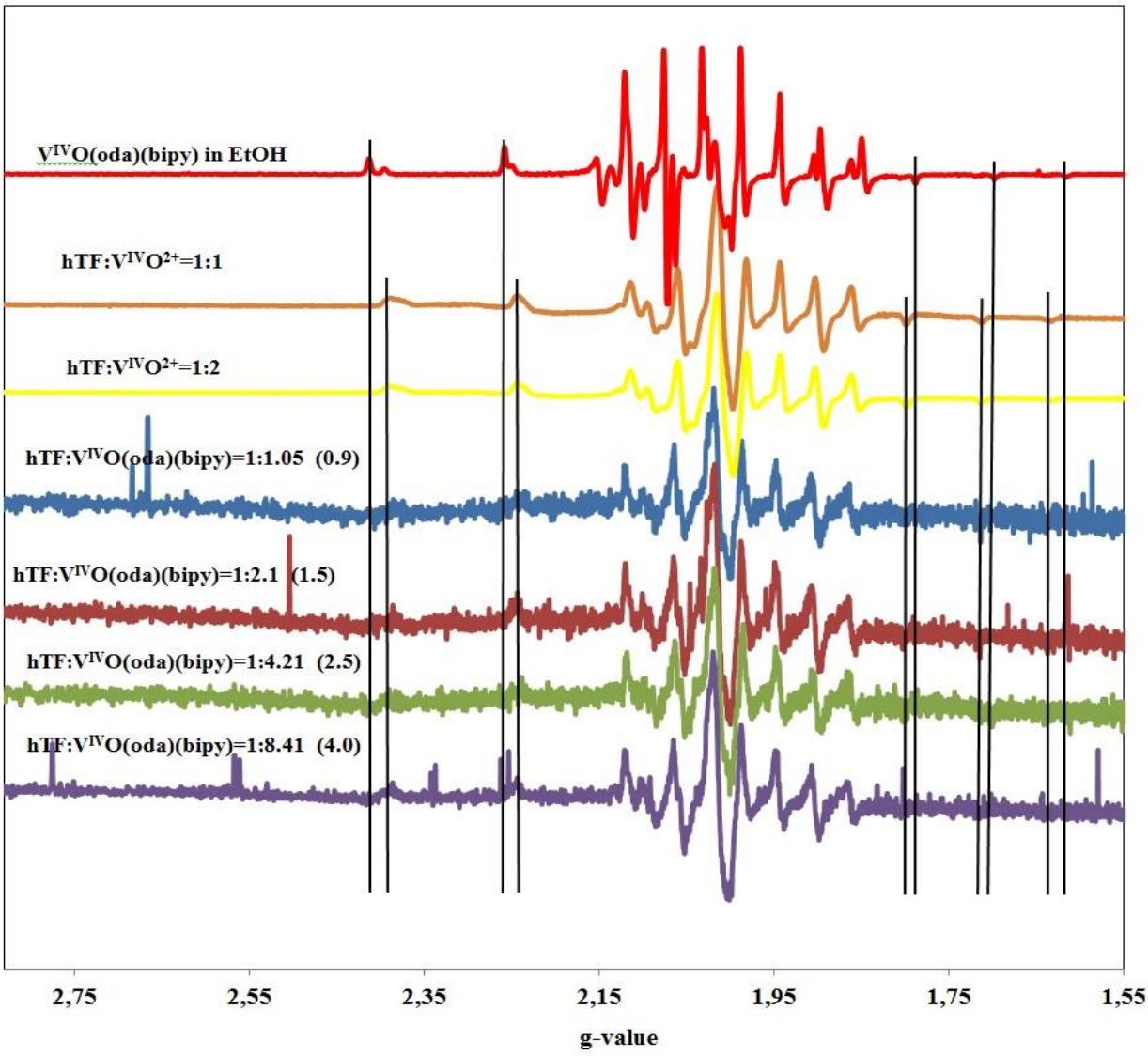

Figure 32. X-band EPR spectra of solutions containing hTF (9.43×10^{-5} M) and different concentrations of $V^{IV}O$(oda)(bipy), obtained by addition of $V^{IV}O$(oda)(bipy) (2.96×10^{-2} M) in DMSO to separate solutions of apo-hTF (1.41×10^{-4} M) in Tris buffer, and passing them through PD-10 columns with elution with 3.5 mL of Tris buffer. Maximum % of DMSO added was 4; T= 77 K. The content of V^{IV} found by ICP is indicated in brackets. The X-band EPR spectra of solution containing $V^{IV}O$(oda)(bipy) (1.43×10^{-3} M) in EtOH, solutions containing hTF (6.0×10^{-4} M) and $V^{IV}OSO_4$ ($C=C_{hTF}$ and $C= C_{hTF}\times2$) in HEPES-S buffer are included for comparison.

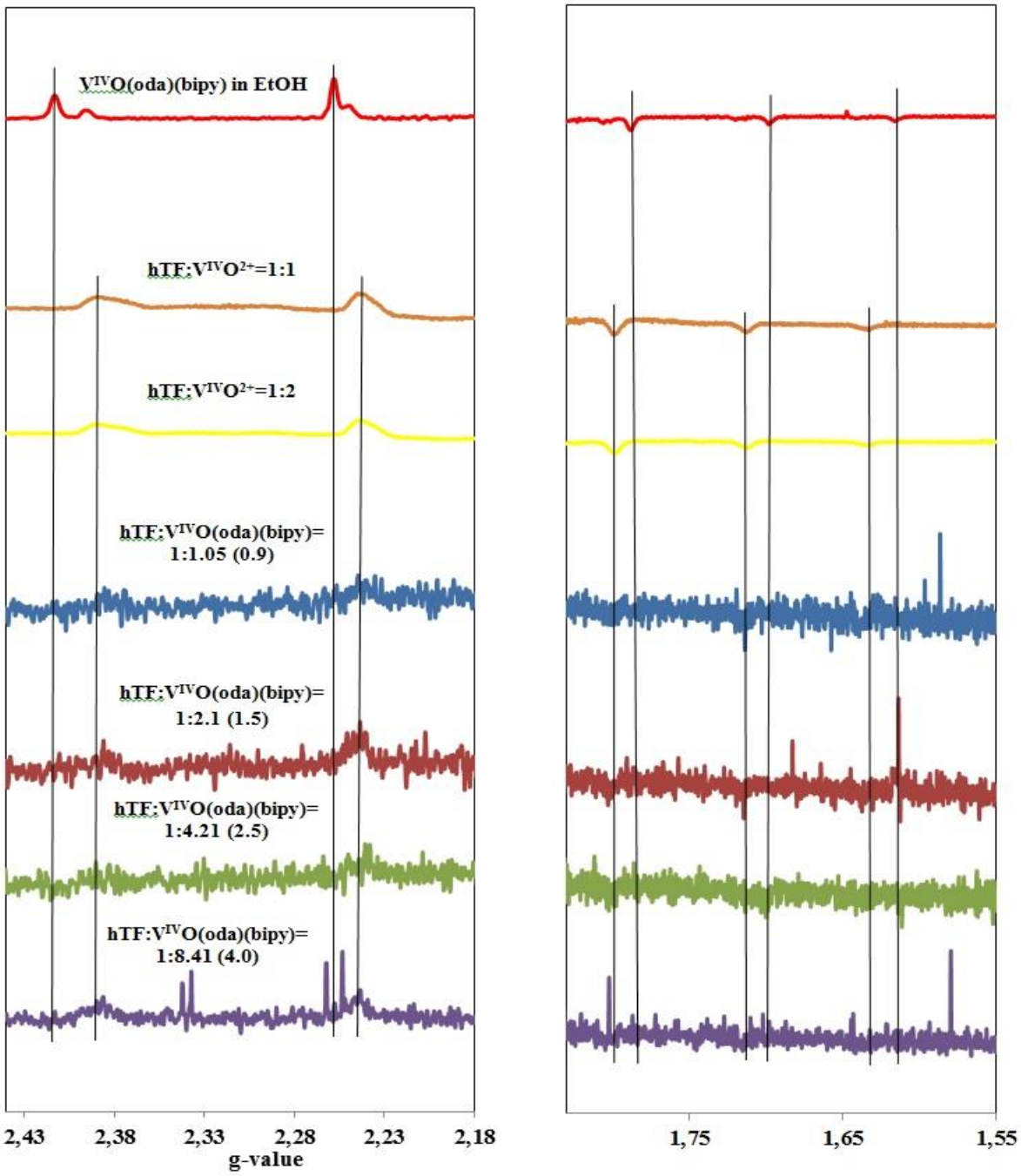

Figure 33. Amplification of the low and high field ranges of the X-band EPR spectra of solutions containing hTF (9.43×10^{-5} M) and different concentrations of $V^{IV}O$(oda)(bipy) obtained by addition of $V^{IV}O$(oda)(bipy) (2.96×10^{-2} M) in DMSO to separate solutions of apo-hTF (1.41×10^{-4} M) in Tris buffer and passing through PD-10 columns with elution with 3.5 mL of Tris buffer. Maximum % of DMSO added was 4; T= 77 K. Content of V^{IV} found by ICP is indicated in brackets. The amplification of the X-band EPR spectra of solution containing $V^{IV}O$(oda)(bipy) in EtOH, solutions containing hTF (6.0×10^{-4} M) and $V^{IV}OSO_4$ (C=C_{hTF} and C= $C_{hTF}\times2$) in HEPES-S buffer are included for comparison.

Table 6. Spin Hamiltonian parameters (g_x, g_y, g_z, A_x, A_y and A_z) of samples for hTF- $V^{IV}O$(oda)(bipy) system and for $V^{IV}O$(oda)(bipy) in EtOH, obtained by simulation of the experimental EPR spectra with the computer program of Rockenbauer and Korez[116], and those reported by other authors for $V^{IV}O$–hTF species (A and B).

System		g_x, g_y	g_z	A_x, A_y ($\times 10^4$ cm^{-1})	A_z($\times 10^4$ cm^{-1})
$V^{IV}O$(oda)(bipy) in EtOH		1.975	1.942	60.3	170.7
	ref[96]		1.939		168.5
	ref[121]		1.937		168.3
	ref[122]		1.938		168
	ref[123]		1.938		168
	ref[124]		1.940		166.8
$V^{IV}O$–hTF species B	ref[96]		1.940		171.1
	ref[122]		1.941		170.3
	ref[123]		1.938		170
	ref[124]		1.934		170
	ref[121]		1.941		170.5
	ref[121]		1.935		171.8
hTF:$V^{IV}O$(oda)(bipy)= 2.1 (1.5)		1.986	1.962	51.3	169
hTF:$V^{IV}O$(oda)(bipy)=8.41 (4.0)		1.984	1.951	56.7	169.5

Figure 34 depicts the changes in the UV range (250-400 nm) of the CD spectra of solutions containing apo-hTF and of $V^{IV}O(acac)_2$ with ratios hTF:$V^{IV}O(acac)_2$ = 1:1.01 (0.9), 1:2.05 (1.5), 1:4.02 (2.1) and 1:7.89 (3.1) prepared in separate batches (in brackets the correct ratio found for the samples by ICP, after elution from PD-10 columns).

No clear trend can be found. As mentioned above, the CD spectra in this range is probably dominated by the Trp bands, and possibly this amino acid residue is not much affected by the binding of the $V^{IV}O$-complex. However, the binding is clearly confirmed by the CD spectra measured in the visible range and by the analysis of Vanadium content in the samples eluted.

The absorption of the samples is high in the 255-290 nm range, so the signal-to-noise ratio is not favorable, and it is not easy to detect a clear trend in the bands as the complex is added. $V^{IV}O(acac)_2$ possibly binds close to some tyrosine residue(s), possibly to those at iron binding sites. Some removal of V^{IV} bound to hTF due to the increase of ligand concentration in the bulk solution or some change in the conformation of hTF may occur as well as binding to side chain histidine residues.

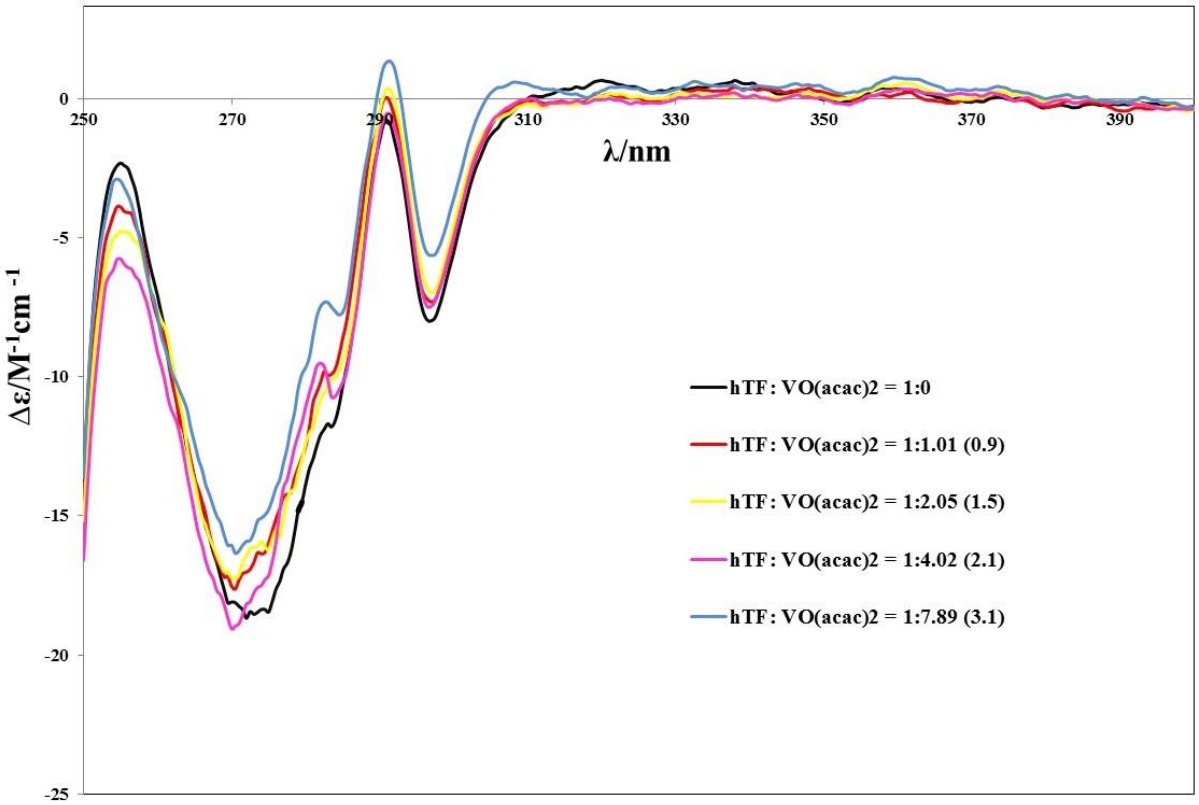

Figure 34. CD spectra of solutions after passing through the PD-10 columns and elution with 3.5 mL of Tris buffer. The solutions contain hTF (9.43×10^{-5} M) and different concentrations of $V^{IV}O(acac)_2$ (obtained by addition of $V^{IV}O(acac)_2$ (2.78×10^{-2} M) in DMSO to separate solutions of hTF (1.41×10^{-4} M) in Tris buffer). Maximum % of DMSO added was 4; the cell path length was 2 mm. Content of V^{IV} found by ICP is indicated in brackets.

The comparison of these CD spectra with the CD spectrum of the $V^{IV}O$-hTF system at the hTF: $V^{IV}O(acac)_2$ ratio of 1:2 from ref.[96] shows that $V^{IV}O^{2+}$ possibly binds together with at least one ligand as the spectra are not completely equal, especially the difference is obvious at 268-285 nm and in the visible range (*experiment 2.5.*).

Figure 35 depicts the X-band EPR spectra of the solutions whose CD spectra are included in Figure 34. The X-band EPR spectra of solution containing $V^{IV}O(acac)_2$ in MeOH, solutions containing hTF and $V^{IV}OSO_4$ (ratios 1:1 and 1:2) are presented for comparison. It is obvious that the series of spectra being analyzed do not superimpose completely with the spectrum of the solution of $V^{IV}O(acac)_2$ in MeOH and with the spectra of solutions of hTF:$V^{IV}O^{2+}$=1:1 and 1:2. The conclusions here that might be made are that (v) $V^{IV}O(acac)_2$ in solutions being analyzed is bound to hTF and (vi) probably keeps at least one $acac^-$ ligand when binding.

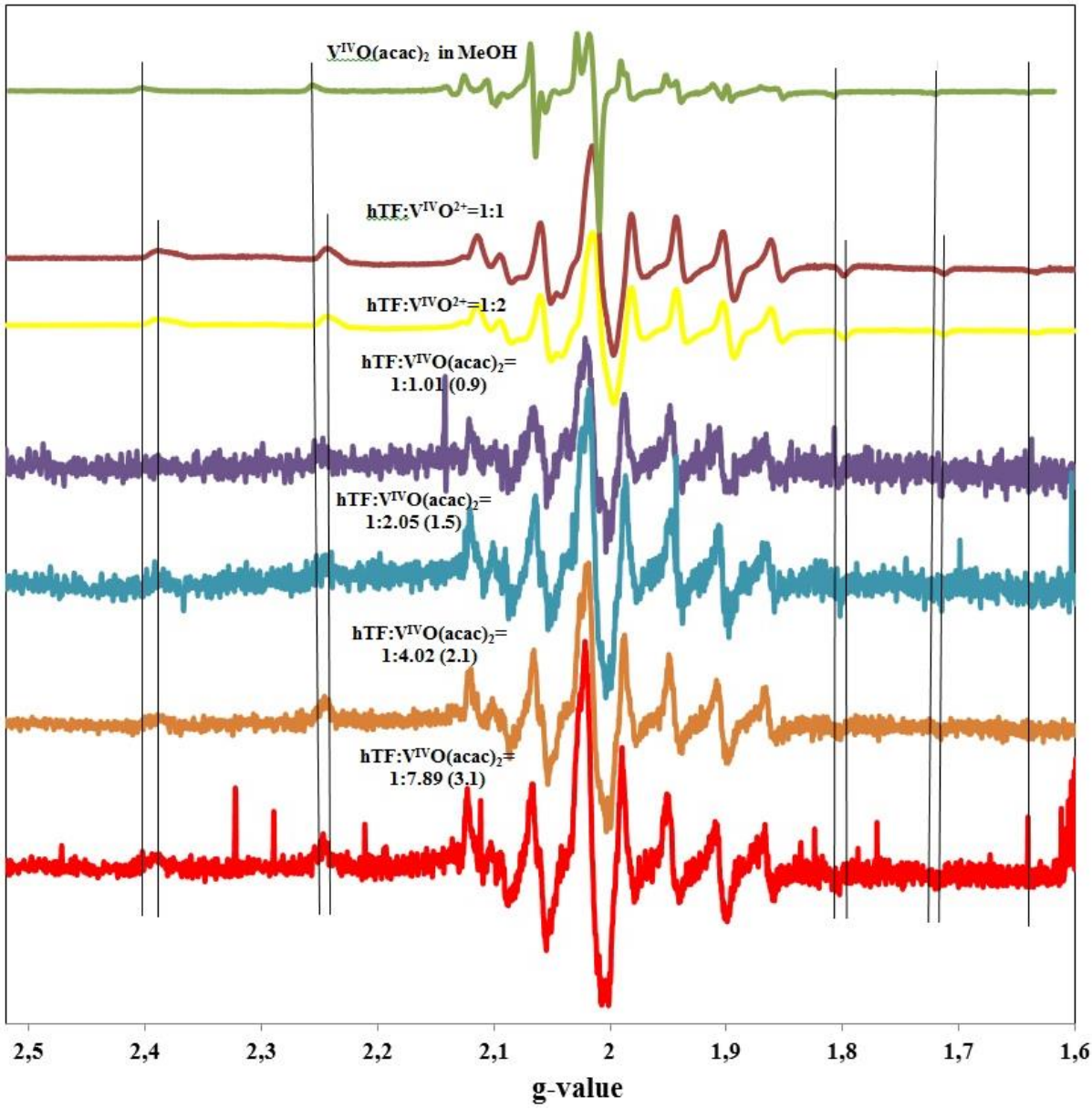

Figure 35. X-band EPR spectra of solutions containing hTF (9.43×10^{-5} M) and different concentrations of $V^{IV}O(acac)_2$ obtained by addition of $V^{IV}O(acac)_2$ (2.78×10^{-2} M) in DMSO to separate solutions of apo-hTF (1.41×10^{-4} M) in Tris buffer and passing through the PD-10 columns with elution with 3.5 mL of Tris buffer. Maximum % of DMSO added was 4; T= 77 K. Content of V^{IV} found by ICP is indicated in brackets. The X-band EPR spectra of solution containing $V^{IV}O(acac)_2$ in MeOH, solutions containing hTF (6.0×10^{-4} M) and $V^{IV}OSO_4$ (C=C_{hTF} and C= $C_{hTF}\times2$) in HEPES-S buffer are included for comparison.

Figure 36 depicts the amplification of the low and high field ranges of the EPR spectra presented in Figure 35. As the concentrations of $V^{IV}O(acac)_2$ in samples are quite low, the spectra are very noisy and the peaks in the parallel region in high field range are not clear. However, it is clear that all peaks in the parallel region of the spectra of samples analyzed do not superimpose with the peaks of the spectrum of the solution of $V^{IV}O(acac)_2$ in MeOH or with the spectra of solutions of hTF:$V^{IV}O^{2+}$=1:1 and 1:2, which corroborates conclusions (iv) and (v). Due to the high noise level it was only possible to simulate spectra of samples with ratios hTF:$V^{IV}O(acac)_2$ of 1:4.02 (2.1) and 1:7.89 (3.1). The spin Hamiltonian parameters (g_x, g_y, g_z, A_x, A_y and A_z) of these samples, the sample of $V^{IV}O(acac)_2$ in MeOH and of $V^{IV}O$–hTF species A and B reported by other authors are included in Table 7.

The g_z values obtained in this work for the samples hTF:$V^{IV}O(acac)_2$=4.02 (2.1) and hTF:$V^{IV}O(acac)_2$=7.89 (3.1) are higher than those obtained for $V^{IV}O(acac)_2$ in MeOH and for both $V^{IV}O$–hTF species A and B. The A_z values obtained in this work for the same samples differ from the A_z values obtained for $V^{IV}O(acac)_2$ in MeOH and for both $V^{IV}O$–hTF species A and B. However, A_z values from this work are close to A_z value obtained for $V^{IV}O$–hTF species A from ref[96]. These results corroborate the conclusions (v) and (vi) previously suggested above which is also in agreement with the results obtained in this work from CD (*experiment 2.5.*) and EPR (*experiment 3.6.*) analyses for this system.

Figure 37 depicts the changes in the UV-Vis range of the CD spectra of the samples hTF: $V^{IV}O(oda)(bipy)$ = 1:4.21 (2.5) and hTF: $VO(acac)_2$ = 1:7.89 (3.1). Only the region at approximately 325-800 nm will be discussed here as the region below 400 nm was discussed above. The spectra appear to correspond to a similar trend in the range of 325-800 nm. One band observed with λ_{max} at ~ 750 nm and can be attributed to either $d_{xy} \rightarrow d_{xz}$ or $d_{xy} \rightarrow d_{yz}$ transitions; the band with λ_{max} at ~ 625 nm can be also attributed to either $d_{xy} \rightarrow d_{xz}$ or $d_{xy} \rightarrow d_{yz}$ transitions; the band with λ_{max} at ~550 nm can be attributed to the $d_{xy} \rightarrow d_{x2-y2}$ transition; the band with λ_{max} at ~454 nm can be attributed to $d_{xy} \rightarrow d_{z2}$ transitions and the band a λ_{max} at ~ 360 nm is probably a charge-transfer (CT) band.

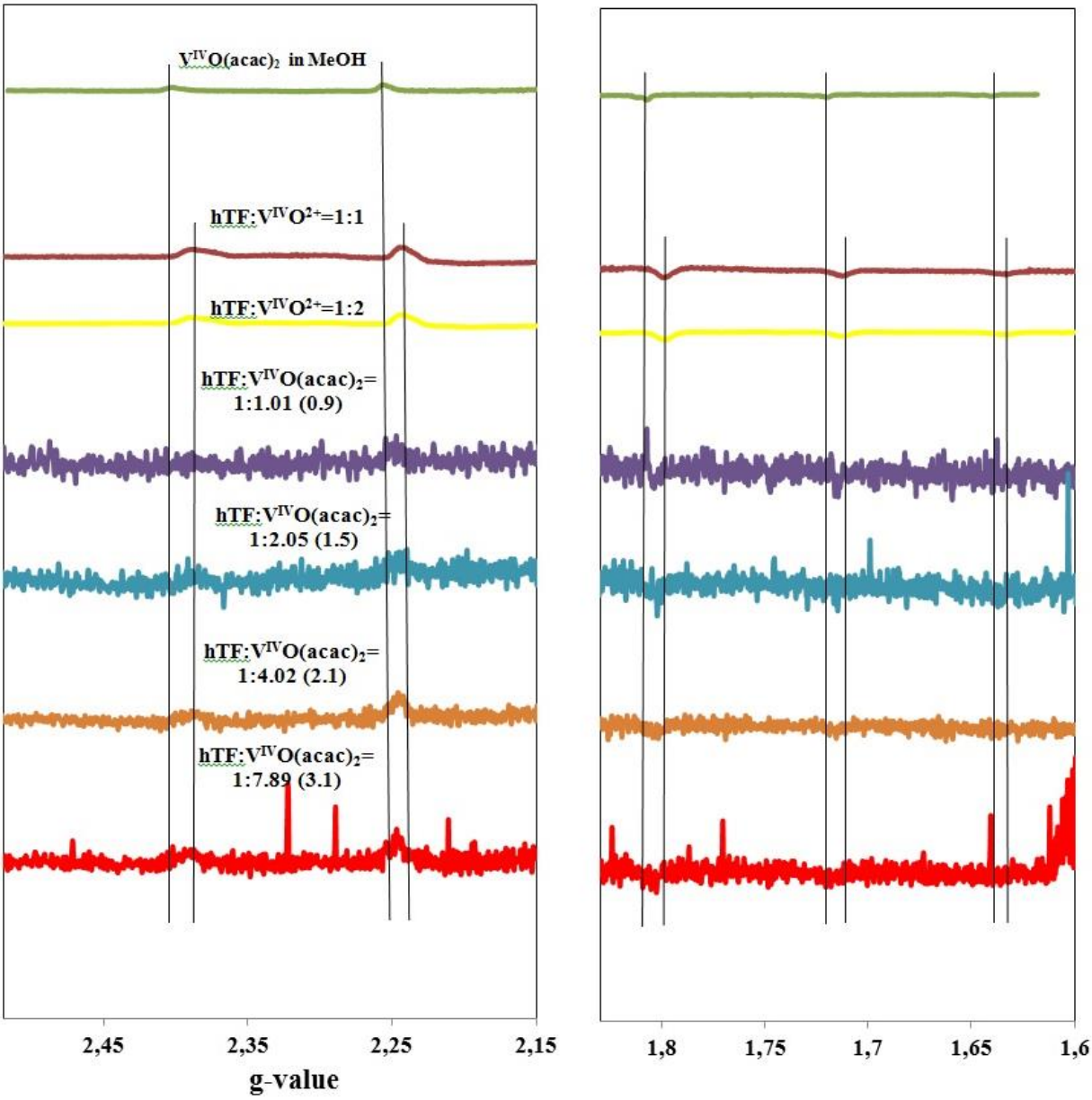

Figure 36. Amplification of the low and high field ranges of the X-band EPR spectra of solutions containing hTF (9.43×10^{-5} M) and different concentrations of $V^{IV}O(acac)_2$ obtained by addition of $V^{IV}O(acac)_2$ (2.78×10^{-2} M) in DMSO to separate solutions of apo-hTF (1.41×10^{-4} M) in Tris buffer after passing through the PD-10 columns and elution with 3.5 mL of Tris buffer. Maximum % of DMSO added was 4; T= 77 K. Content of V^{IV} found by ICP is indicated in brackets. The X-band EPR spectra of solution containing $V^{IV}O(acac)_2$ in MeOH, solutions containing hTF (6.0×10^{-4} M) and $V^{IV}OSO_4$ ($C=C_{hTF}$ and $C= C_{hTF}\times2$) in HEPES-S buffer are included for comparison.

Table 7. Spin Hamiltonian parameters (g_x, g_y, g_z, A_x, A_y and A_z) of samples for the hTF-$V^{IV}O(acac)_2$ system and for $V^{IV}O(acac)_2$ in MeOH, obtained by simulation of the experimental EPR spectra with the computer program of Rockenbauer and Korez[116], and those reported by other authors for VO–hTF species (A and B).

System		**g_x, g_y**	**g_z**	**A_x, A_y ($\times 10^4$ cm^{-1})**	**A_z ($\times 10^4$ cm^{-1})**
$V^{IV}O(acac)_2$ in MeOH		1.984	1.954	60.8	171.2
$V^{IV}O$–hTF species A	ref[96]		1.939		168.5
	ref[121]		1.937		168.3
	ref[122]		1.938		168
	ref[123]		1.938		168
	ref[124]		1.940		166.8
$V^{IV}O$–hTF species B	ref[96]		1.940		171.1
	ref[122]		1.941		170.3
	ref[123]		1.938		170
	ref[124]		1.934		170
	ref[121]		1.941		170.5
	ref[121]		1.935		171.8
hTF:$V^{IV}O(acac)_2$=4.02 (2.1)		1.984	1.949	57.9	168.6
hTF:$V^{IV}O(acac)_2$=7.89 (3.1)		1.985	1.950	57.6	167.7

From Figure 37 it can be concluded that: (vii) the V^{IV} is bound to chiral groups of hTF and induced CD (ICD) is observed, (viii) the ligand(s) are coordinated to the V^{IV} centers and they are close to the hTF chiral centers. Comparison of these CD spectra with the CD spectrum of hTF:$V^{IV}O^{2+}$ = 1:2 from ref.[96,106,109] also confirms the conclusion (viii) as the bands of this spectra do not match with the bands of hTF-$V^{IV}O^{2+}$ spectrum in the absence of ligand. These conclusions are in agreement with conclusions previously made based on the results of CD (*experiments 2.2., 2.5* and *5.1*) and EPR (*experiments 3.3., 3.6.* and *5.1*) analyses of these two systems.

From all the results of *experiment 5.1.* it can be concluded that both complexes $V^{IV}O$(oda)(bipy) and $V^{IV}O(acac)_2$ bind to hTF, and when binding at least one of the ligands is maintained in the V^{IV} coordination shere. In the case of $V^{IV}O(acac)_2$ this contradicts previous reports that such binding does not occur. [117,118] Amino acid residues from the iron binding sites are probably involved in the binding as well as other residues (probably surface His).

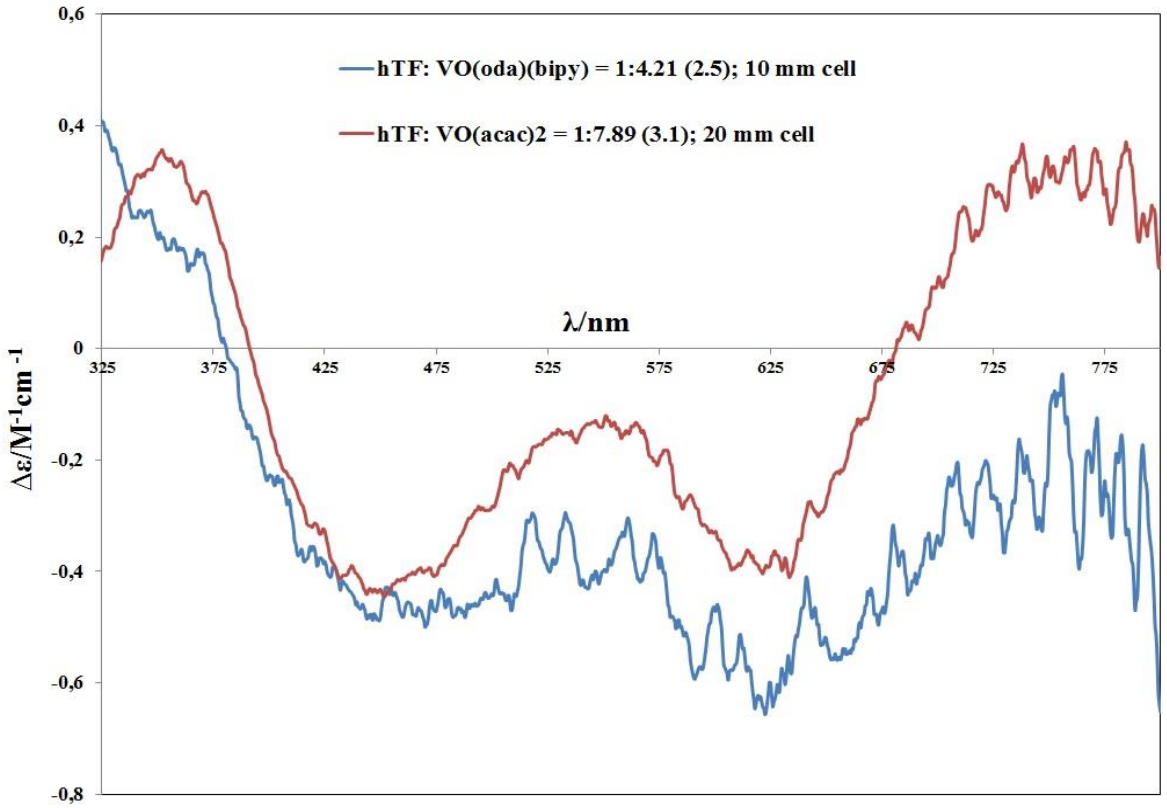

Figure 37. CD spectra of solutions after passing through the PD-10 columns and elution with 3.5 mL of Tris buffer. One spectrum (blue line) corresponds to solution containing hTF (9.43×10^{-5} M) in Tris buffer and $V^{IV}O$(oda)(bipy) (2.3×10^{-4} M, found by ICP) in DMSO. The % of DMSO added was 2; the cell path length was 10 mm. The 2nd spectrum (brown line) corresponds to hTF (9.43×10^{-5} M) in Tris buffer and $V^{IV}O(acac)_2$ (2.9×10^{-4} M, found by ICP) in DMSO. The % of DMSO added was 4; the cell path length was 20 mm. The content of Vanadium found by ICP is indicated in brackets. By mistake the corresponding spectrum of hTF was not measured, therefore, the correct position of the baseline is not known.

4.2.4. Studies by fluorescence spectroscopy. Background.

Three main aromatic amino acids contribute to the hTF fluorescence: tyrosine, phenylalanine and tryptophan. Actually, the intrinsic fluorescence comes almost completely from tryptophan alone. The reason is that phenylalanine's fluorescence has very low quantum yield and the fluorescence of tyrosine is almost completely quenched when ionized or located in the environment of $-NH_2$, -COOH groups or tryptophan. Excitement at two different wavelengths gives different information. At 280 nm both tryptophan and tyrosine residues are excited while at 295 nm only tryptophan is excited.[125] hTF has 8 tryptophan residues (3 in the N-lobe, 5 in the C-lobe), 25 tyrosine residues and 27 phenilalanine residues.[83] The two iron binding sites are located near the junction of two domains formed by Cys-117 to Cys-194 bond in the N-terminus. Tyr-185 and Tyr-188, two of the three histidines - 119, 207 and 249 [91] and

possibly Asp-63 and Tyr-95[97] are possible ligands that may bind to vanadium^{IV}. The partial quenching in the fluorescence of Trp-128 results from the V^{IV} binding to the neighbour His-119 residue. Trp -264 is the major contributor to the hTF fluorescence; however, it is located on the hTF surface and usually does not interact with either metal centre or any other functional residues.[126]

4.2.4.1. The fluorescence spectra of $V^{IV}O$-oda– hTF complexes.

Figure 38 depicts fluorescence emission spectra measured for the hTF-$V^{IV}O(oda)(H_2O)_2$ solution (*experiment 4.1.*) using λ_{ex}=280 nm. hTF demonstrates strong fluorescence emission with λ_{max} at 321 nm. As the complex concentration increases, a hTF fluorescence decrease is observed which means that the fluorescence quenching is concentration-dependent and that $V^{IV}O(oda)(H_2O)_2$ is close enough to the tryptophan and/or tyrosine residues. Hovewer, although quenching is clearly visible, the effect is not much pronounced. Addition of the highest concentration of $V^{IV}O(oda)(H_2O)_2$ (ratio 1:3.46) causes a decrease in the fluorescence intensity of ~21 %.

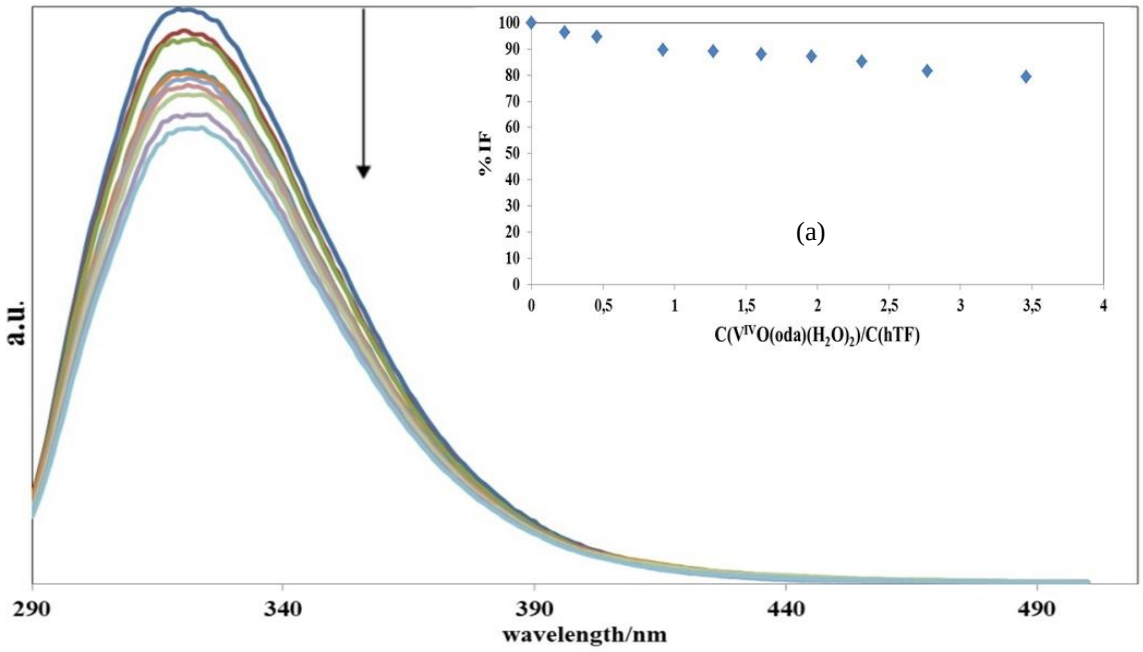

Figure 38. Fluorescence emission spectra measured for the hTF-$V^{IV}O(oda)(H_2O)_2$ solution. The hTF concentration used was 2.46×10^{-6} M and that of $V^{IV}O(oda)(H_2O)_2$ was stepwise increased from 0 to 8.43×10^{-6} M (from hTF: $V^{IV}O(oda)(H_2O)_2$ ratios of 1:0 to 1:3.5). Other conditions: T=298 K; pH=7.4; max % of MeOH added 0.99; λ_{ex}=280 nm. The arrow shows $V^{IV}O(oda)(H_2O)_2$ concentration increase. (a) % of fluorescence intensity decrease versus $V^{IV}O(oda)(H_2O)_2$:hTF ratio.

Figure 39 depicts corrected relative fluorescence intensity of the hTF-$V^{IV}O(oda)(H_2O)_2$ solution measured using λ_{ex}=280 nm. The Stern-Volmer analysis did not give a good fitting to

the data obtained as the dependence is not linear. Since a hyperbolic behavior is observed the following equation was applied: $y=(xa/(1+K_1 \cdot x))+(xc/(1+K_2 \cdot x))$ where *xa* and *xc* are the molar fractions of two different populations of fluorophores with different quenching rate constants K_1 and K_2.

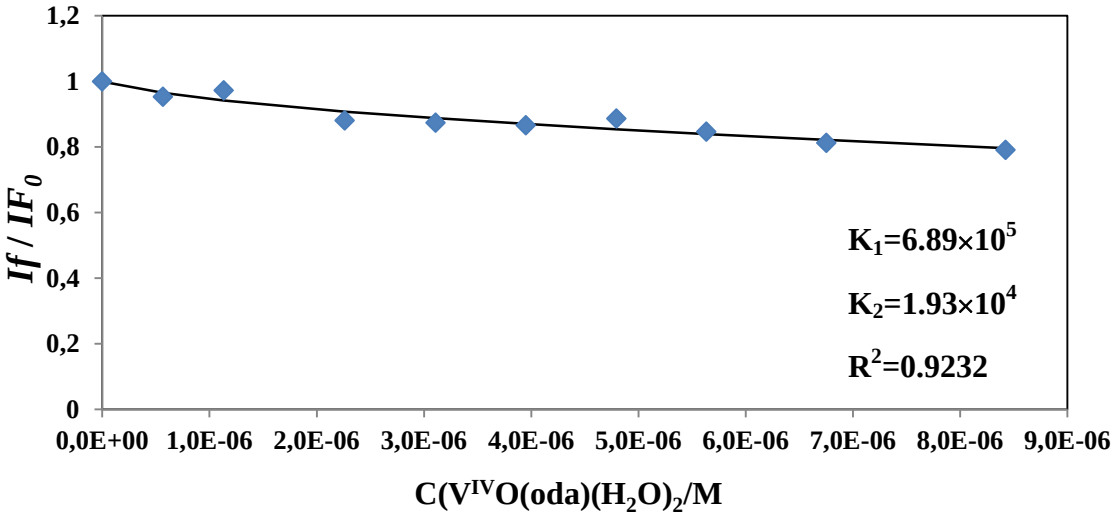

Figure 39. Corrected relative fluorescence intensity of the hTF - $V^{IV}O(oda)(H_2O)_2$ solution (data from Figure 38) vs. concentration of $V^{IV}O(oda)(H_2O)_2$. *If* and IF_0 are the fluorescence intensities at the maximum emission wavelength λ_{em}=321 at the concentration of the complex in a sample and in the absence of the complex respectively. The trendline equation is $y=(0.089/(1+6.89\times10^5 \cdot x))+(0.91/(1+1.93\times10^4 \cdot x))$.

The biphasic dependence suggests that one population of fluorophores is more accessible to the quencher than the other, hence, there is more than one independent binding site, and hTF may be quenched by both quenching mechanisms (static and dynamic) stimultaneously.[125] The quenching rate constants obtained are $K_1=6.89\times10^5$ and $K_2=1.93\times10^4$. The respective fractions expressed in % are 8.9 and 91.

Figure 40 depicts the fluorescence emission spectra measured for the hTF-$V^{IV}O(oda)(bipy)$ solution (*experiment 4.3.*) using λ_{ex}=280 nm. As the complex concentration increases a decrease in the hTF fluorescence is observed which means that the fluorescence quenching is concentration-dependent and that $V^{IV}O(oda)(bipy)$ is close enough to the tryptophan and/or tyrosine residues in the environment near of one or two of the binding sites. Although quenching is clearly visible, the effect is not much pronounced. Addition of 3.26 mol equivalents of $V^{IV}O(oda)(bipy)$ causes a decrease in the fluorescence intensity of ~18 %.

Figure 41 depicts corrected relative fluorescence intensity of the hTF-$V^{IV}O(oda)(bipy)$ solution measured using λ_{ex}=280 nm. Stern-Volmer analysis gave an adequate fitting to the

data obtained as in the concentration ratio measured the dependence is linear. This means that in the given conditions V^{IV} probably binds to one accessible binding site with one Stern-Volmer dynamic quenching constant as quenching is mainly due to dynamic process, dominated by diffusion. The Stern-Volmer dynamic quenching constant from the equation obtained (the slope) is $K_{sv}=5.47x10^4$.[125]

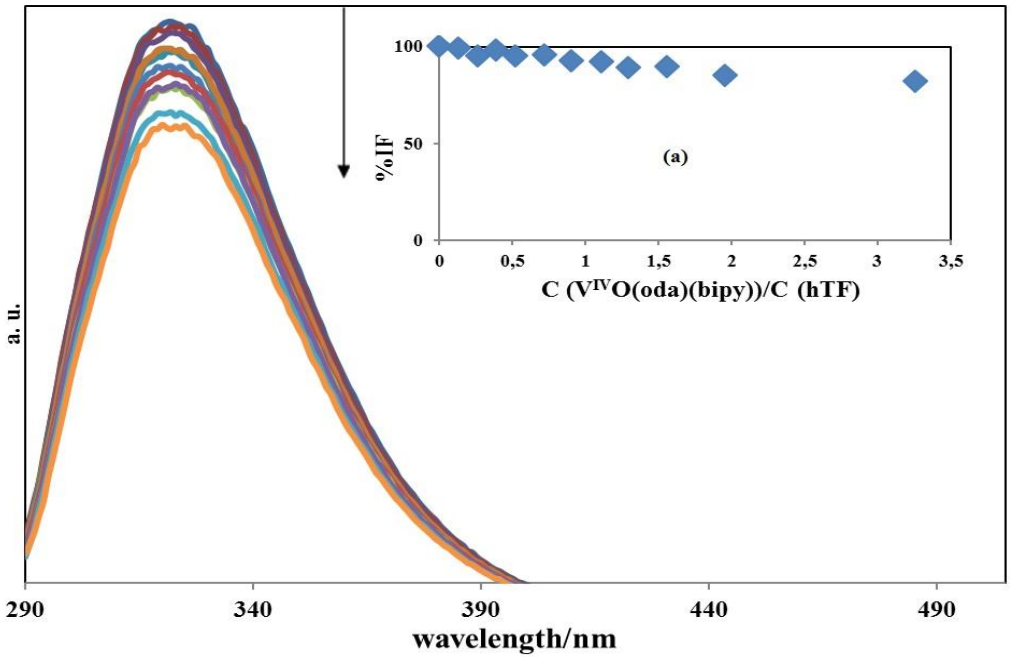

Figure 40. Fluorescence emission spectra for the hTF-$V^{IV}O$(oda)(bipy) solution. The hTF concentration used was 1.0×10^{-6} M and that of $V^{IV}O$(oda)(bipy) was stepwise increased from 0 to 3.2×10^{-6} M (from hTF: $V^{IV}O$(oda)(bipy) ratios 1:0 to 1:3.26). Other conditions: T=298 K; pH=7.4; max % of DMSO added 1.64; λ_{ex}=280 nm. The arrow shows $V^{IV}O$(oda)(bipy) concentration increase. (a) % of fluorescence intensity decrease versus $V^{IV}O$(oda)(bipy):hTF ratio.

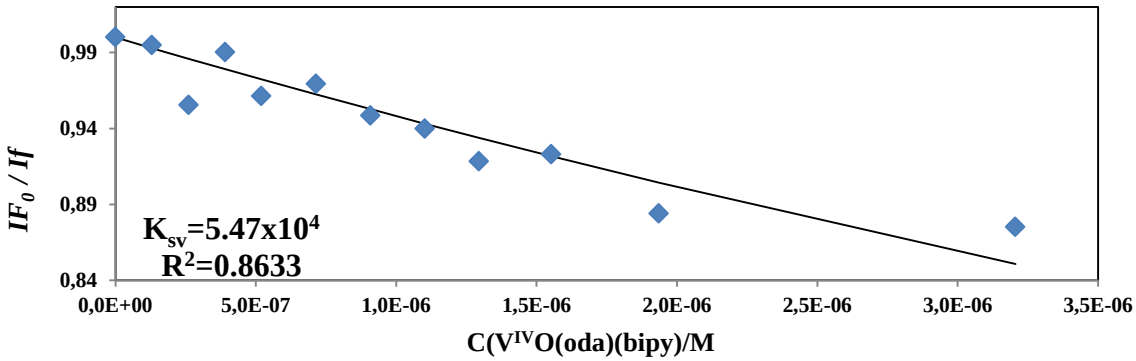

Figure 41. Stern-Volmer plot: corrected relative fluorescence intensity of the hTF-$V^{IV}O$(oda)(bipy) solution (data from Figure 40) vs. concentration of $V^{IV}O$(oda)(bipy). *If* and IF_0 are the fluorescence intensities at the maximum emission wavelength λ_{em}=322 at the concentration of the complex in a sample and in the absence of the complex respectively. The trendline equation is $y=5.47x10^4 \cdot x +1$.

Figure 42 depicts fluorescence emission spectra measured for the hTF-$V^{IV}O$(oda)(bipy) solution (*experiment 4.3.*) using λ_{ex}=295 nm. hTF demonstrates strong fluorescence emission with λ_{max} at 317 nm. The complex causes concentration-dependent hTF fluorescence quenching and is probably close enough to the tryptophan residues. The quenching appears to be stronger than at λ_{ex}=280 nm, this suggesting the presence of several binding sites for $V^{IV}O$(oda)(bipy). [125] Addition of the highest concentration of $V^{IV}O$(oda)(bipy) (ratio 1:1.96) causes a decrease in the fluorescence intensity of ~31.2 %.

Figure 43 depicts corrected relative fluorescence intensity of the hTF - $V^{IV}O$(oda)(bipy) solution measured using λ_{ex}=295 nm. The Stern-Volmer analysis did not give a good fitting to the data obtained as the dependence is not linear. Since a hyperbolic behaviour of the function was observed the following equation was applied: $y=(xa/(1+ K_1 \cdot x))+(xc/(1+ K_2 \cdot x))$ where *xa* and *xc* are the molar fractions of two different populations of fluorophores with different quenching rate constants K_1 and K_2. The biphasic dependence suggests that one population of fluorophores is more accessible to the quencher than the other, hence, there is more than one independent binding site, and hTF may be quenched by both quenching mechanisms (static and dynamic) stimultaneously.[125] The quenching rate constants obtained are $K_1=6.11\times10^6$ and $K_2=1.55\times10^5$. The respective fractions expressed in % are 9.2 and 90.9.

The behavior and the results obtained for this system at both excitation wavelengths (280 and 295 nm) are very different, with much higher quenching constants obtained at 295 nm. This suggests the presence of several binding sites for $V^{IV}O$(oda)(bipy).[125]

Figure 44 depicts fluorescence emission spectra measured for hTF-$V^{IV}O$(oda)(phen) solution (*experiment 4.5.*) using λ_{ex}=280 nm. The complex causes concentration-dependent hTF fluorescence quenching and is probably close enough to the tryptophan and/or tyrosine residues. Although quenching is clearly visible, the effect is not much pronounced. Addition of the highest concentration of $V^{IV}O$(oda)(phen) (ratio 1:1.28) causes a decrease in the fluorescence intensity of ~16%.

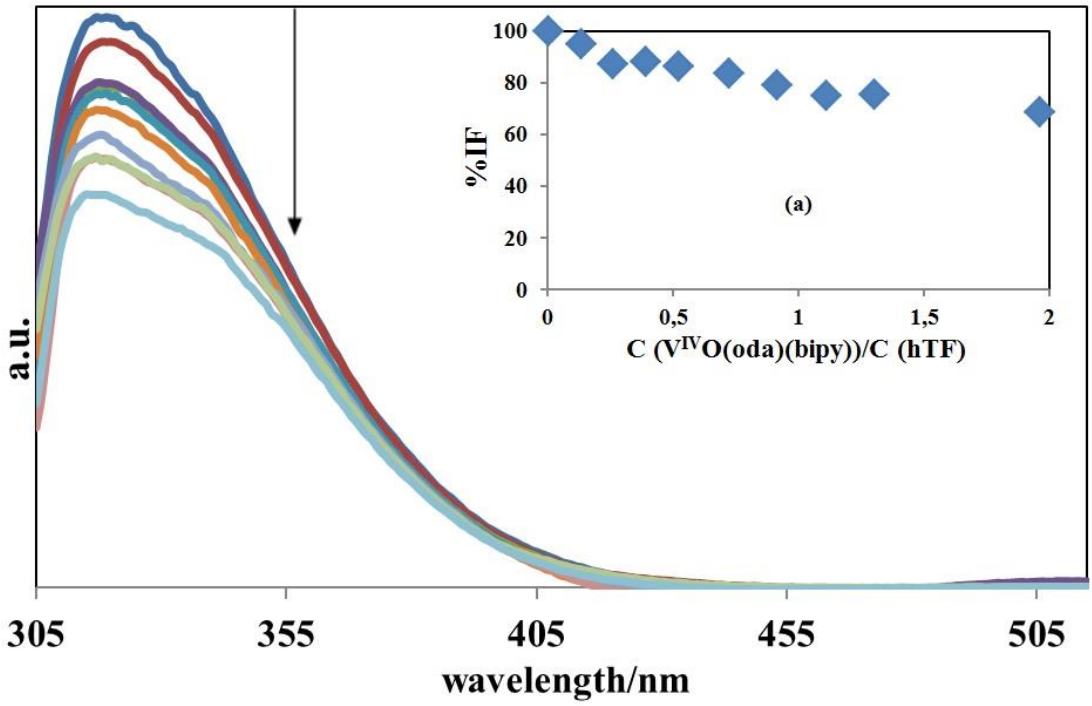

Figure 42. Fluorescence emission spectra measured for the hTF-$V^{IV}O$(oda)(bipy) solution. The hTF concentration used was 1.0×10^{-6} M and that of $V^{IV}O$(oda)(bipy) was stepwise increased from 0 to 1.94×10^{-6} M (from hTF: $V^{IV}O$(oda)(bipy) ratios of 1:0 to 1:1.96). Other conditions: T=298 K; pH=7.4; max % of DMSO added 0.99; λ_{ex}=295 nm. The arrow shows $V^{IV}O$(oda)(bipy) concentration increase. (a) % of fluorescence intensity decrease versus $V^{IV}O$(oda)(bipy):hTF ratio.

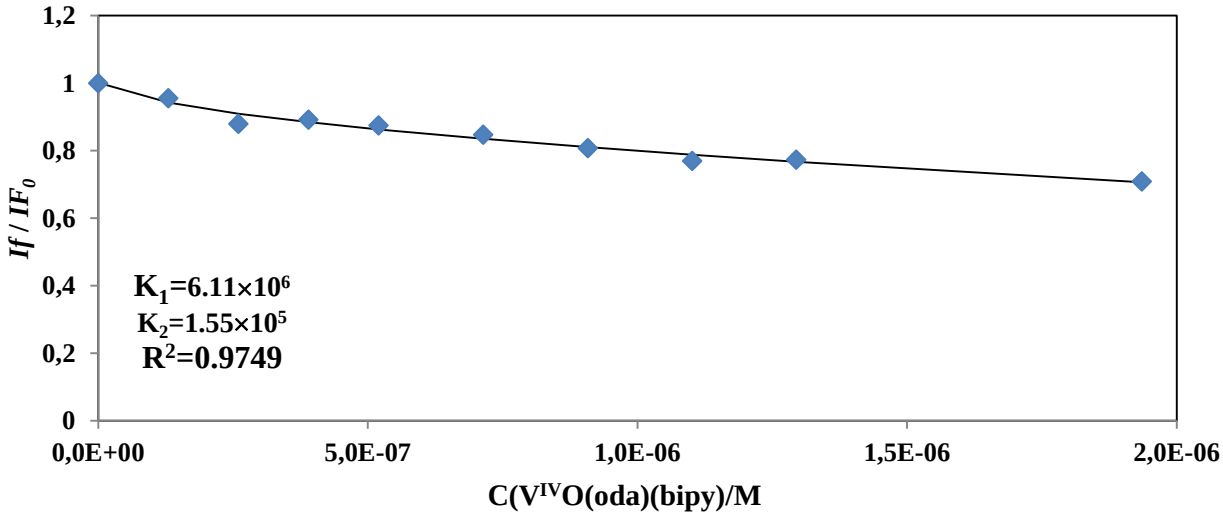

Figure 43. Corrected relative fluorescence intensity of the hTF-$V^{IV}O$(oda)(bipy) solution (data from Figure 42) vs. concentration of $V^{IV}O$(oda)(bipy). *If* and IF_0 are the fluorescence intensities at the maximum emission wavelength λ_{em}=317 at the concentration of the complex in a sample and in the absence of the complex respectively. The trendline equation is $y=(0.092/(1+6.11\times10^6 \cdot x))+(0.909/(1+1.55\times10^5 \cdot x))$.

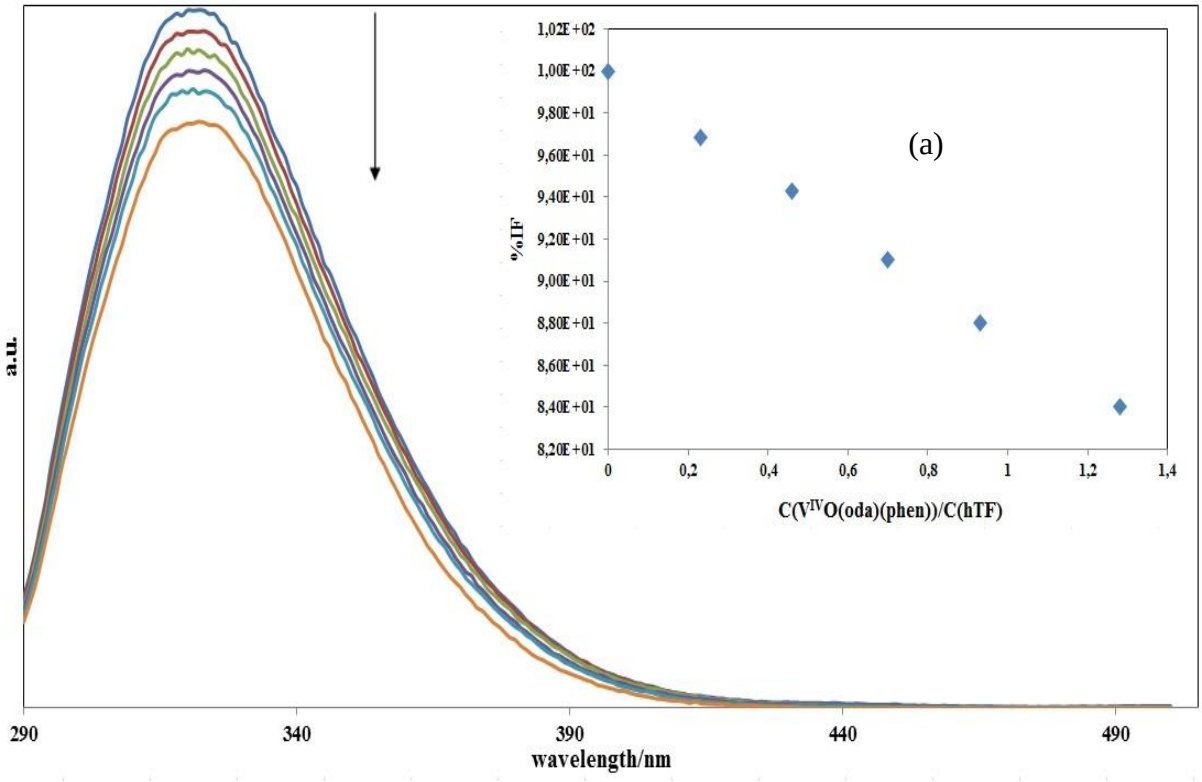

Figure 44. Fluorescence emission spectra measured for the hTF-$V^{IV}O$(oda)(phen) solution. The hTF concentration was 2.46×10^{-6} M and that of $V^{IV}O$(oda)(phen) was stepwise increased from 0 to 3.13×10^{-6} M (from hTF: $V^{IV}O$(oda)(phen) ratios of 1:0 to 1:1.28). Other conditions: T=298 K; pH=7.4; max % of DMSO added 0.36; λ_{ex}=280 m. The arrow shows $V^{IV}O$(oda)(phen) concentration increase. (a) % of fluorescence intensity decrease versus $V^{IV}O$(oda)(phen):hTF ratio.

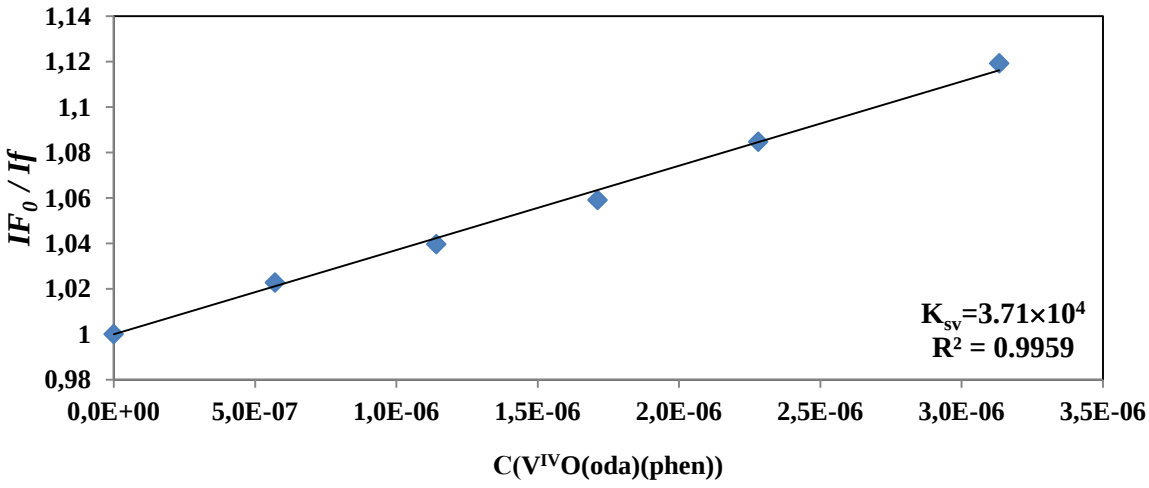

Figure 45. Corrected relative fluorescence intensity of the hTF-$V^{IV}O$(oda)(phen) solution (data from Figure 44) vs. concentration of $V^{IV}O$(oda)(phen). *If* and IF_0 are the fluorescence intensities at the maximum emission wavelength λ_{em}=322 at the concentration of the complex in a sample and in the absence of the complex respectively. The trendline equation is $y=3.71\times10^{4}x+1$.

Figure 45 depicts corrected relative fluorescence intensity of the hTF-$V^{IV}O$(oda)(phen) solution measured using λ_{ex}=280 nm. Stern-Volmer analysis gave adequate fitting to the data obtained as the dependence is linear. This means that in the given conditions V^{IV} probably binds to one accessible binding site with one Stern-Volmer dynamic quenching constant as quenching is mainly due to dynamic process, dominated by diffusion.[125] The Stern-Volmer dynamic quenching constant from the equation obtained (the slope) is $K_{sv}=3.71\times10^4$.

4.2.4.2. The fluorescence spectra of solutions containing hTF and $V^{IV}O(acac)_2$.

Figure 46 depicts fluorescence emission spectra measured for the hTF-$V^{IV}O(acac)_2$ solution (*experiment 4.7.*) using λ_{ex}=280 nm. As the complex concentration increases the hTF fluorescence decrease is observed which means that the fluorescence quenching is concentration-dependent and that $V^{IV}O(acac)_2$ binds close enough to the tryptophan and/or tyrosine residues. Hovewer, although the quenching is clearly visible, the effect is not much pronounced and is lower than for the previous systems described. Addition of the highest concentration of $V^{IV}O(acac)_2$ (ratio 1:3.08) causes a decrease in the fluorescence intensity of ~ 15%.

Figure 47 depicts corrected relative fluorescence intensity of the hTF-$V^{IV}O(acac)_2$ solution measured using λ_{ex}=280 nm. Stern-Volmer analysis did not give a good fitting to the data obtained as the dependence is not linear. Since a hyperbolic behaviour is observed the following equation was applied: $y=(xa/(1+K_1\cdot x))+(xc/(1+K_2\cdot x))$ where *xa* an *xc* are the molar fractions of two different populations of fluorophores with different quenching rate constants K_1 and K_2. The biphasic dependence suggests that one population of fluorophores is accessible to the quencher while the other not, hence, there is more than one independent binding site, and hTF may be quenched by both quenching mechanisms (static and dynamic) stimultaneously.[125] The quenching rate constants obtained are $K_1=8.8\times10^6$ and $K_2=5.13\times10^4$. The corresponding fractions expressed in % are 7.8 and 92.2.

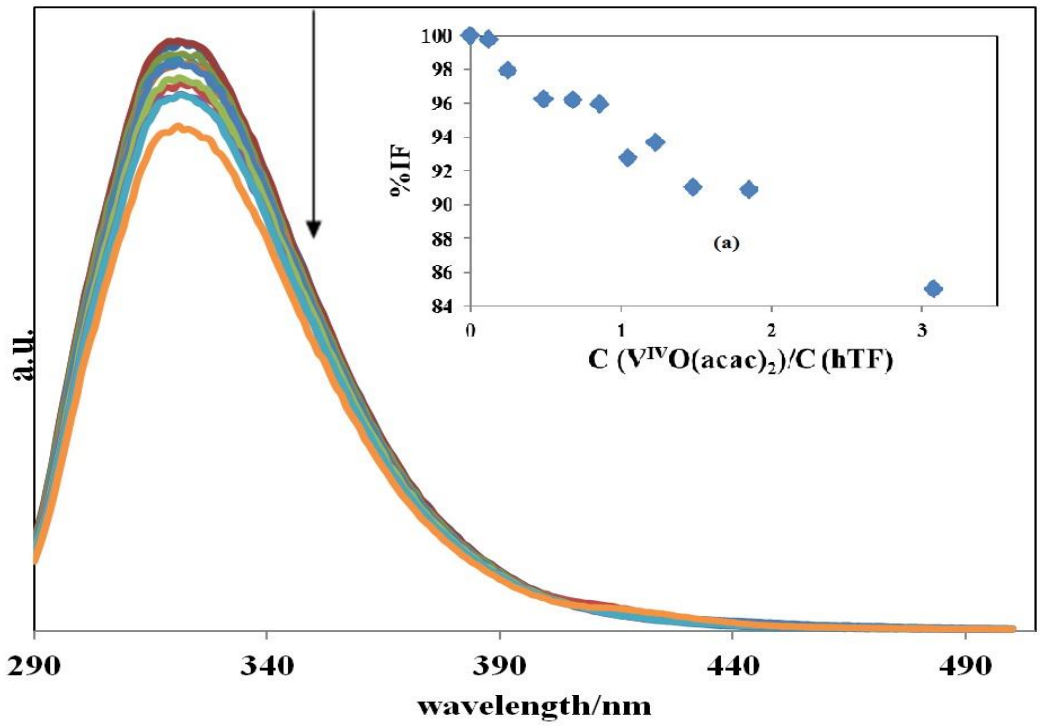

Figure 46. Fluorescence emission spectra measured for the hTF-$V^{IV}O(acac)_2$ solution. The hTF concentration used was 1.02×10^{-6} M and that of $V^{IV}O(acac)_2$ was stepwise increased from 0 to 3.09×10^{-6} M (from hTF: $V^{IV}O(acac)_2$ ratios of 1:0 to 1:3.08). Other conditions: T=298 K; pH=7.4; λ_{ex}=280 nm. The arrow shows $V^{IV}O(acac)_2$ concentration increase. (a) % of fluorescence intensity decrease versus $V^{IV}O(acac)_2$:hTF ratio.

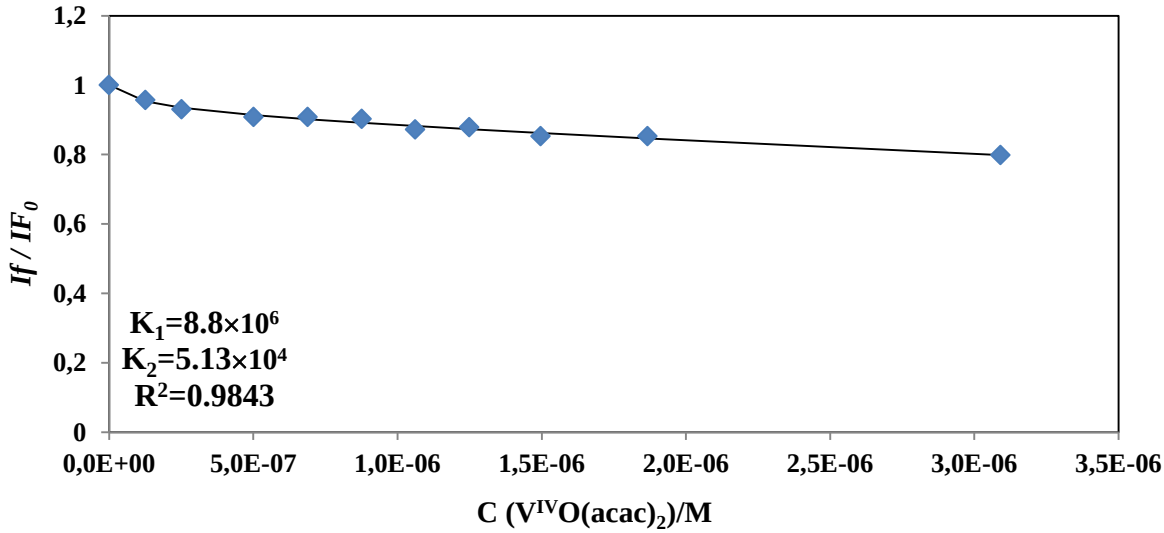

Figure 47. Stern-Volmer plot: corrected relative fluorescence intensity of the hTF-$V^{IV}O(acac)_2$ solution (data from Figure 46) vs. concentration of $V^{IV}O(acac)_2$. *If* and IF_0 are the fluorescence intensities at the maximum emission wavelength λ_{em}=322 at the concentration of the complex in a sample and in the absence of the complex respectively.The trendline equation is $y=(0.078/(1+8.8\times10^6\cdot x))+(0.922/(1+5.13\times10^4\cdot x))$.

Figure 48 depicts fluorescence emission spectra measured for the hTF-$V^{IV}O(acac)_2$ solution (*experiment 4.7.*) using λ_{ex}=295 nm.$V^{IV}O(acac)_2$ is close enough to the tryptophan residues to produce some concentration-dependent quenching effect which is quite small.[125] Addition of the highest concentration of $V^{IV}O(acac)_2$ (ratio 1:3.08) causes a decrease in the fluorescence intensity of 7.22%.

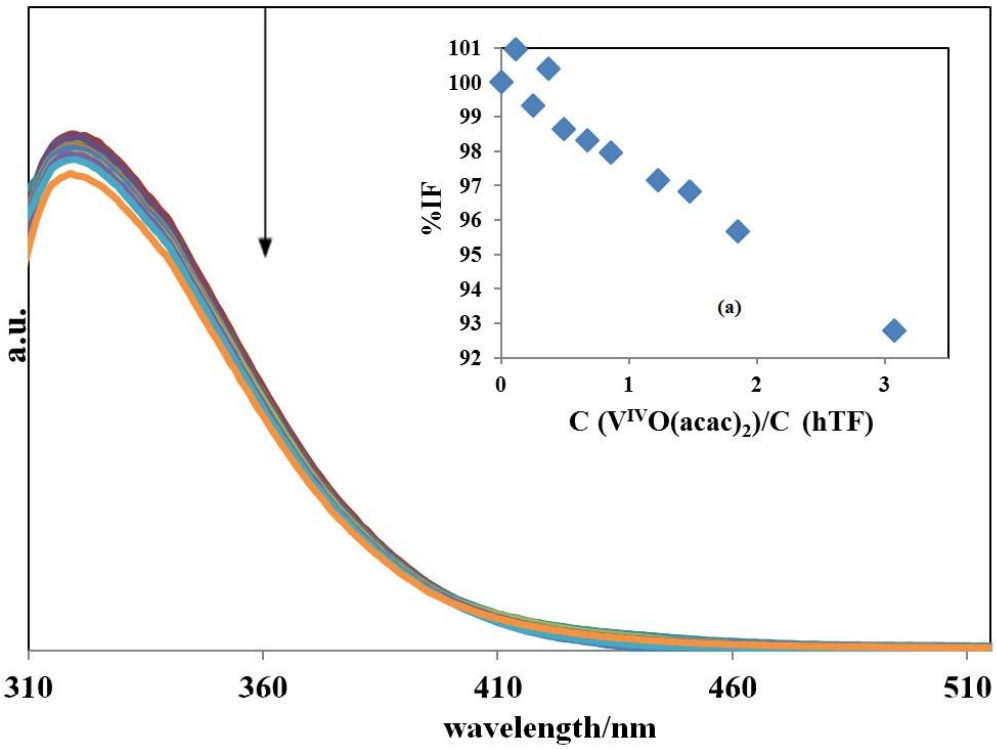

Figure 48. Fluorescence emission spectra measured for the hTF-$V^{IV}O(acac)_2$ solution. The hTF concentration used was 1.02×10^{-6} M and that of $V^{IV}O(acac)_2$ was stepwise increased from 0 to 3.09 $\times10^{-6}$ M (from hTF: $V^{IV}O(acac)_2$ ratios of 1:0 to 1:3.08). Other conditions: T=298 K; pH=7.4; λ_{ex}=295 nm. The arrow shows $V^{IV}O(acac)_2$ concentration increase. (a) % of fluorescence intensity decrease versus $V^{IV}O(acac)_2$:hTF ratio.

Figure 49 depicts corrected relative fluorescence intensity of the hTF-$V^{IV}O(acac)_2$ solution measured using λ_{ex}=295 nm. The Stern-Volmer analysis did not give a good fitting to the data obtained as the dependence is not linear. Since a hyperbolic behaviour is observed the following equation was applied: $y=(xa/(1+K_1 \cdot x))+(xc/(1+K_2 \cdot x))$ where *xa* an *xc* are the molar fractions of two different populations of fluorophores with different quenching rate constants K_1 and K_2. The biphasic dependence suggests that one population of fluorophores is more accessible to the quencher than the other, hence, there is more than one independent binding site, and hTF may be quenched by both quenching mechanisms (static and dynamic) stimultaneously.[125] The quenching rate constants obtained are $K_1=7.1\times10^6$ and $K_2=2.4\times10^4$. The respective fractions expressed in % are 7 and 93.

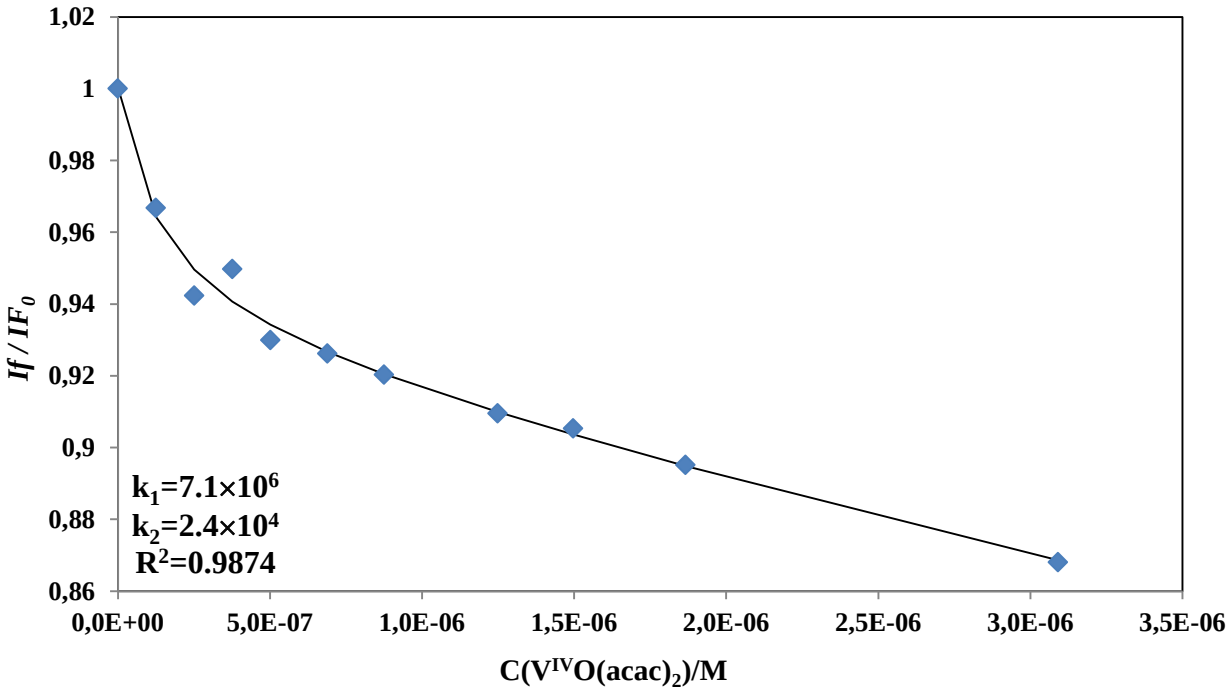

Figure 49. Corrected relative fluorescence intensity of the hTF-$V^{IV}O(acac)_2$ solution (data from Figure 48) vs. concentration of $V^{IV}O(acac)_2$. *If* and IF_0 are the fluorescence intensities at the maximum emission wavelength λ_{em}=322 at the concentration of the complex in a sample and in the absence of the complex respectively. The trendline equation is $y=(0.07/(1+7.1\times10^6\cdot x))+(0.93/(1+2.4\times10^4\cdot x))$.

Among all the systems analyzed which have 2 constants (i.e. two quenching mechanisms), one constant (K_1) is a high rate constant, which corresponds to less than 10% of the quenchers (the corresponding binding site is closer to the Trp residues, but not easily accessible[125]); the other constant (K_2) corresponds to ~90% of the quenchers, and is used in this work to compare all the systems. Stern-Volmer dynamic quenching constants and quenching rate constants (K_2) are presented in the Table 8.

Analysis of the fluorescence data shows that V^{IV} binds to hTF at two distinct sites (with two different binding constants) for all systems except hTF-$V^{IV}O$(oda)(phen) whose data is not enough to make such conclusion. Depending on the hTF conformation each binding site can be more or less accessible to the complex (quencher). One of the sites can be deeply buried in the hTF hydrophobic cavity and thus be inaccessible for the quencher. Basing on the comparison of the quenching constants, quenching capacity increases in the following order (λ_{ex}=280 nm): $V^{IV}O(oda)(H_2O)_2$ < $V^{IV}O$(oda)(phen) < $V^{IV}O(acac)_2$ < $V^{IV}O$(oda)(bipy); (λ_{ex}=295 nm): $V^{IV}O(acac)_2$ < $V^{IV}O$(oda)(bipy) which allows to suggest that $V^{IV}O$(oda)(bipy) has the highest binding strength to hTF and the highest ability to lower the electronic density of the hTF hydrophobic cavity. [125]

Table 8. Stern-Volmer dynamic quenching constants (K_{sv}) and quenching rate constants (K_2) obtained for hTF- $V^{IV}O(oda)(H_2O)_2$, $V^{IV}O(oda)(bipy)$, $V^{IV}O(oda)(phen)$ and $V^{IV}O(acac)_2$ systems.

System	Constants at λ_{ex}=280 nm	Constants at λ_{ex}=295 nm
hTF- $V^{IV}O(oda)(H_2O)_2$	$K_2=1.93\times10^4$	-
hTF-$V^{IV}O(oda)(bipy)$	$K_{sv}=5.47x10^4$	$K_2=1.55\times10^5$
hTF-$V^{IV}O(oda)(phen)$	$K_{sv}=3.71\times10^4$	-
hTF- $V^{IV}O(acac)_2$	$K_2=5.13\times10^4$	$K_2=2.4\times10^4$

The analysis of the data obtained from the *experiment 4.9.* with hTF-$V^{IV}O(oda)(phen)$ system at 25, 30, 35, 40º C (figures are not presented) showed that in the uncorrected data the quenching rate constant decreases with increasing temperature, which supports a static quenching.[125]

4.3.0. Studies of the interaction of the complexes with HSA.

4.3.1. Studies by circular dichroism (CD). Background.

There are several possible binding sites, and vanadium may bind to them with different strength. There is a variety species possible to be formed with the each addition of one mol equivalent of $V^{IV}O^{2+}$ complexes. CD bands in the visible range can be seen only when there is coordination between the blood serum protein and vanadium; only when this happens the protein may effectively transfers chirality from the chiral centers to the V^{IV} center. The more effective is the chirality transfer, the higher the CD bands intensities. In the CD in the visible range we may mainly measure d-d electronic transitions of $(V^{IV}O^{2+})_n$–protein complexes. The final CD spectrum recorded is the sum of CD signals of all the complexes formed in one particular system.[96]

Till now there are no publications on the binding of VO-oda complexes to HSA. There are studies of binding of $VO(acac)_2$ to HSA.[98,118] Garriba *et al.*, based on measuring EPR spetra of solutions containing $VO(acac)_2$ and HSA state that there is no binding. [98] On the contrary, Makinen *et al.* [118] consider that such binding takes place and is relevanl for te therapeutic properties of $VO(acac)_2$, as they state that it is HSA that transports the complex to the cells.

4.3.1.1. The CD spectra of HSA-$V^{IV}O$-oda complexes.

The Figure 50 depicts the changes in the CD spectra of solutions containing HSA and 0.26 - 5.05 mol equivalents of $V^{IV}O(oda)(bipy)$ (*experiment 2.3.*).

The solution of HSA by itself produces no CD spectra in the 330-800 nm range so it was taken as a baseline in Figure 50. After addition of 0.26 mol equivalents of $V^{IV}O(oda)(bipy)$

the spectrum changes very slightly, a negative band being observed. Then, the broad negative band develops further up to addition of 1.53 mol equivalents of $V^{IV}O$(oda)(bipy). Upon addition of 2 or higher mol equivalents of $V^{IV}O$(oda)(bipy) significant changes are observed as broad positive bands form with λ_{max} at 435-680 nm and 680-800 nm.

The CD spectra of molar ratios higher than 2.5 do not follow a clear trend. The 50 mm quatz cell is not easy to use, and it is possible that small bubbles might interfere with the measurements. However, globally broad positive bands are formed in the range 435-800 nm, and their intensity tends to increase with the amount of complex added. From these CD spectra no prediction can be made regarding the binding sites of the complex at the HSA protein.

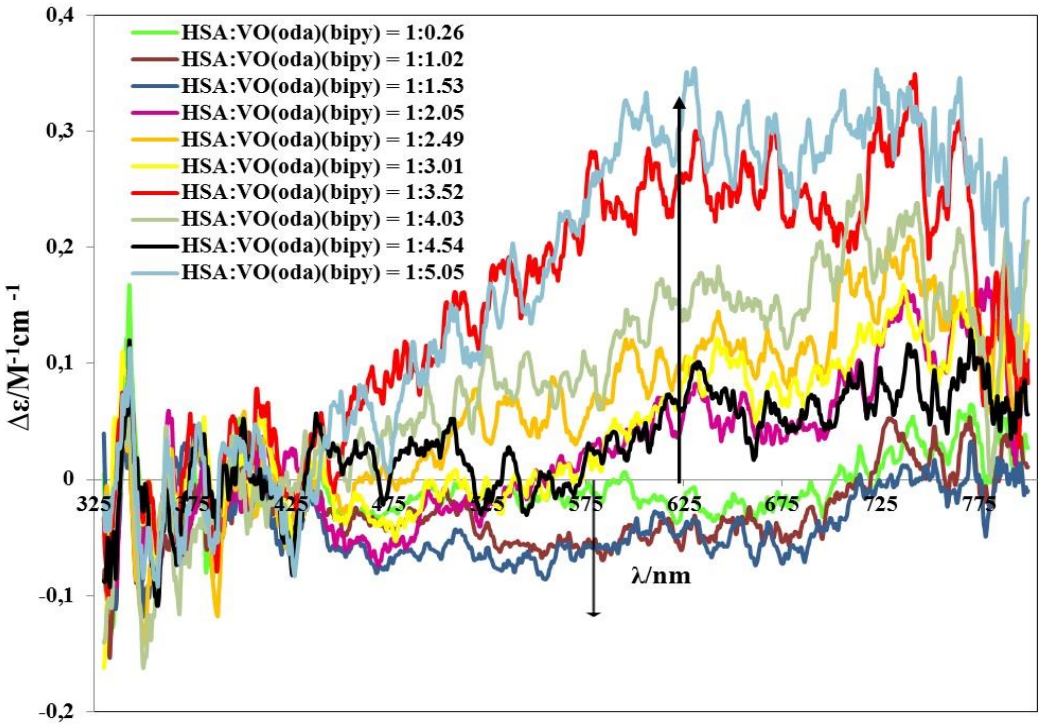

Figure 50. CD spectra of solutions containing HSA (5.37×10^{-4} M) in PBS upon stepwise additions of $V^{IV}O$(oda)(bipy) (4.8×10^{-2} M)) in DMSO. Maximum % of DMSO added was 5.4; cell path length was 50 mm.

4.3.1.2. The CD spectra of solutions containing HSA and $V^{IV}O(acac)_2$.

Figure 51 depicts the changes in the CD spectra of solution of HSA upon addition of 0.51 – 5 mol equivalents of $V^{IV}O(acac)_2$ (*experiment 2.6.*). Addition of $V^{IV}O(acac)_2$ of up to a ratio 5 to a HSA solution does not yield any significant change in the CD spectra. All the spectra measured almost coincide. Therefore, the conclusions are that either (i) $V^{IV}O(acac)_2$ does not bind to HSA or (ii) in the CD spectra in this particular region the binding cannot be detected.

This also means that no bond is formed between chiral donors of HSA to V^{IV} so that no ICD is measuted in the visible range.

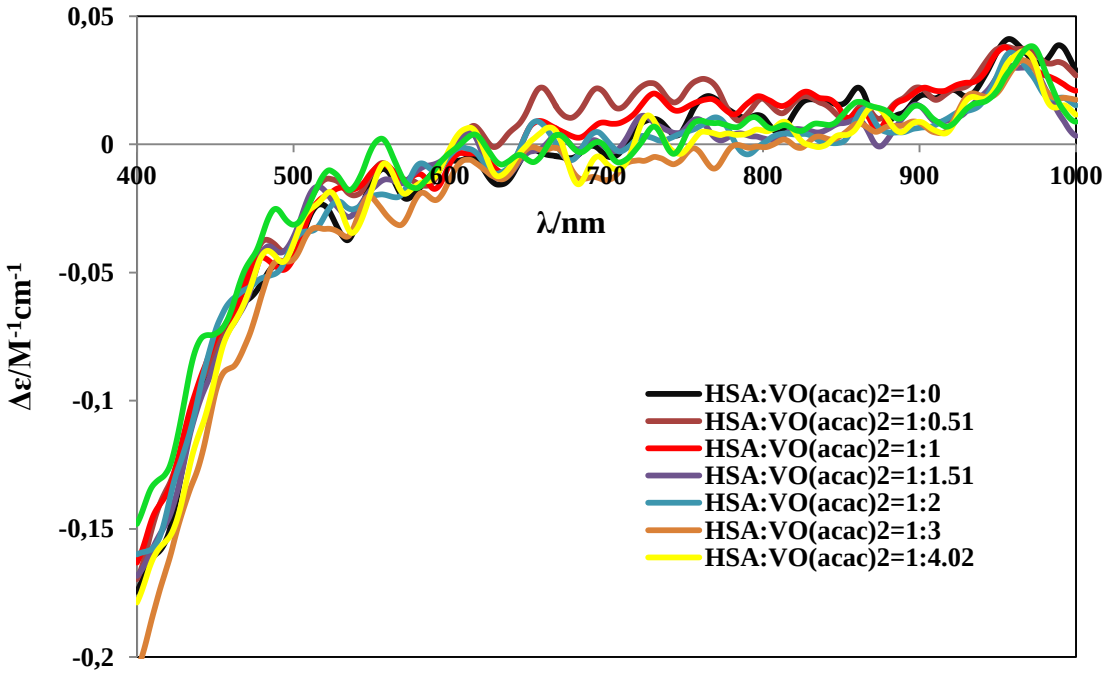

Figure 51. CD spectra of a solution containing HSA (6.02×10^{-4} M) in PBS and after stepwise addition of $V^{IV}O(acac)_2$ (3.64×10^{-2} M) in DMSO. Maximum % of DMSO added was 6.54. The cell path length is 50 mm.

4.3.2. Studies by EPR. The EPR spectra of solutions containing HSA and $V^{IV}O(acac)_2$.

Figure 52 depicts the X-band EPR spectra of the solutions containing HSA in PBS and $V^{IV}O(acac)_2$ in DMSO (*experiment 3.7.*) and of the solution containing $V^{IV}O(acac)_2$ in MeOH. The X-band EPR spectra of solutions containing HSA and $V^{IV}O^{2+}$ (ratios 1:1 and 1:4.6) are included for comparison. The series of spectra being analyzed do not superimpose with the spectrum of solution of $V^{IV}O(acac)_2$ in MeOH. This probably means that (i) V^{IV} of $V^{IV}O(acac)_2$ binds to HSA (although the solvents used differ). Moreover, it is clear that they do not superimpose with the spectra of solutions of HSA and $V^{IV}OSO_4$ (ratios 1:1 and 1:4.6), even though the last two spectra are not well resolved in the high field of the parallel region. This might be an indication that (ii) $V^{IV}O(acac)_2$ binds to HSA with at least one $acac^-$ ligand.

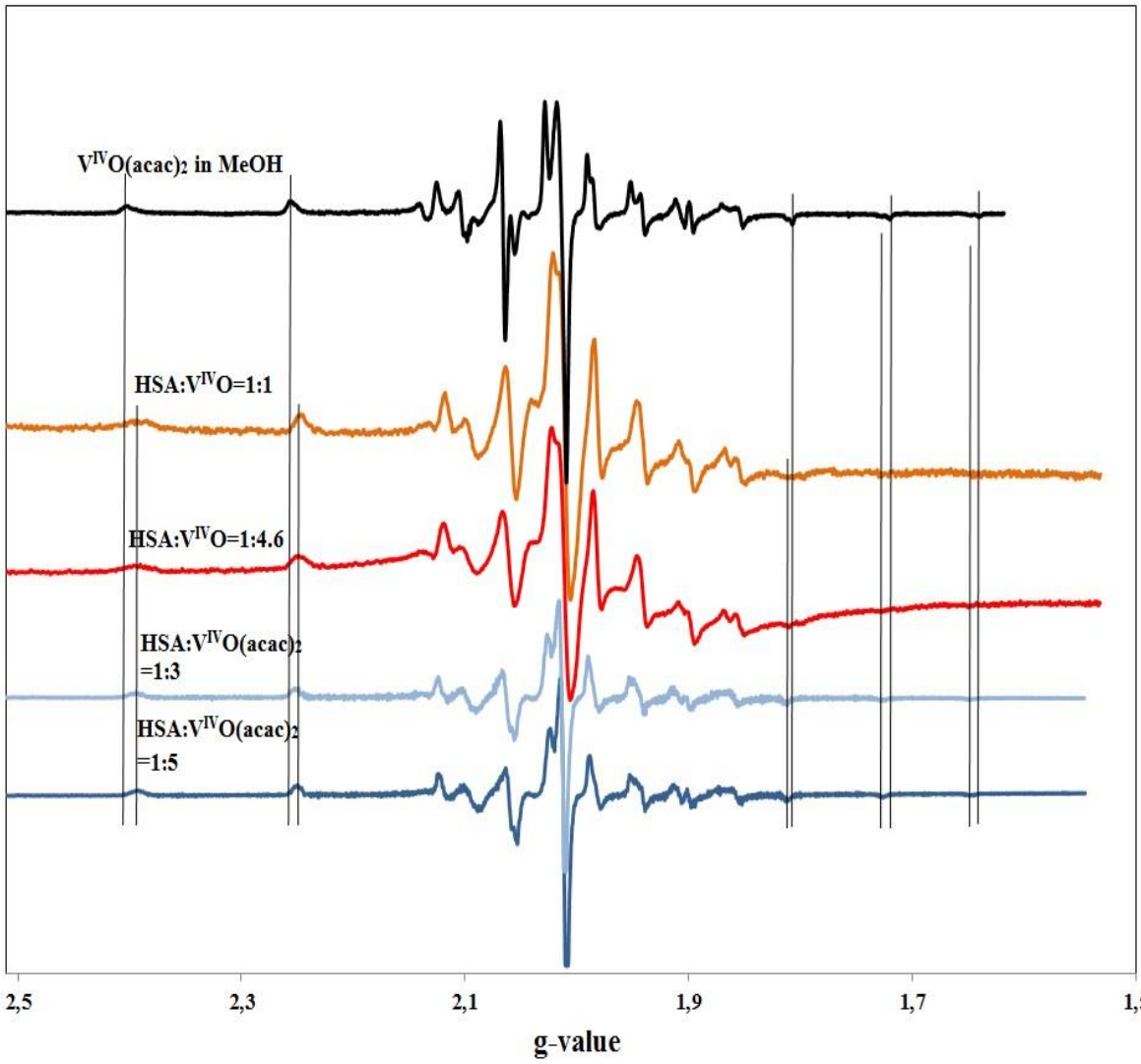

Figure 52 X-band EPR spectra of solutions containing HSA (5.73×10^{-4} M, 5.56×10^{-4} M) in PBS and $V^{IV}O(acac)_2$ (1.72×10^{-3} M, 2.78×10^{-3} M) in DMSO respectively. The X-band EPR spectra of the solution containing $V^{IV}O(acac)_2$ in MeOH, solutions containing HSA (6.5×10^{-4} M) and $V^{IV}OSO_4$ ($C=C_{HSA}$ and $C= C_{HSA}\times4.6$) in HEPES-S buffer are included for comparison. Maximum % of DMSO added was 6.54; T=77 K.

Figure 53 depicts the amplification of the low and high field ranges of the X-band EPR spectra presented in the Figure 52. Spin Hamiltonian parameters (g_x, g_y, g_z, A_x, A_y and A_z) of the samples being analyzed, the sample of $V^{IV}O(acac)_2$ in MeOH and of samples containing different $V^{IV}O$-HSA species reported by different authors are presented in the Table 9. It is clear that the peaks in the parallel region in both low and high field ranges of the samples being analyzed do not superimpose with the peaks of the the spectra of solutions of $V^{IV}O(acac)_2$ in MeOH, HSA:$V^{IV}O^{2+}$=1:1 and HSA:$V^{IV}O^{2+}$=1:4.6; this corroborates conclusions (i) and (ii). However, it contradicts to the assumption (i) made from CD analysis

of this system (*experiment 2.6.*) and stating that $V^{IV}O(acac)_2$ does not bind to HSA, and also to the previous findings stating that such binding does not occur made by Garriba *et. al.* [98]

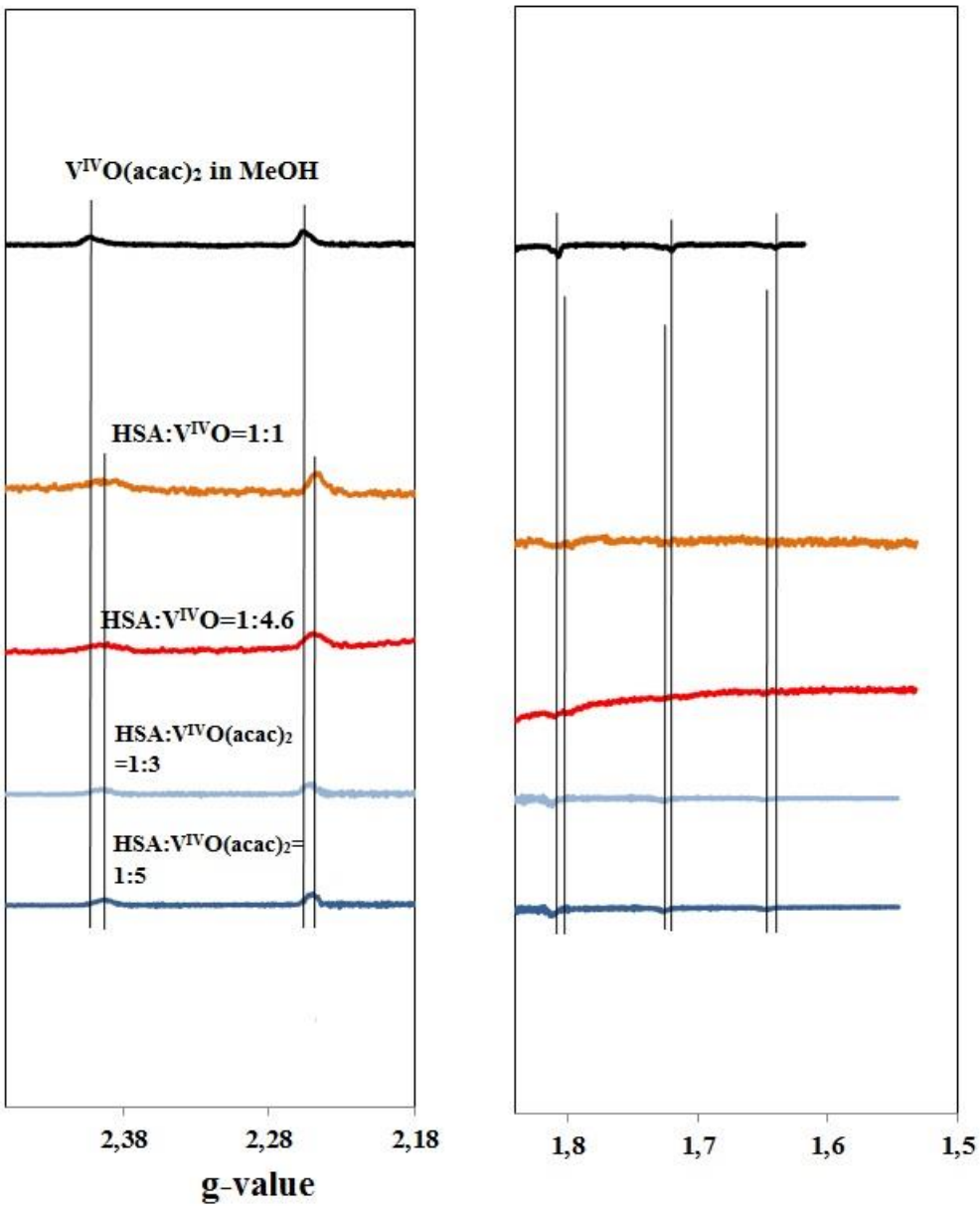

Figure 53. Amplification of the low and high field ranges of the X-band EPR spectra of solutions containing HSA (5.73×10^{-4} M, 5.56×10^{-4} M) in PBS and $V^{IV}O(acac)_2$ (1.72×10^{-3} M, 2.78×10^{-3} M) in DMSO respectively. Amplification of the X-band EPR spectra of the solution containing $V^{IV}O(acac)_2$ in MeOH, solutions containing HSA (6.5×10^{-4} M) and $V^{IV}OSO_4$ ($C=C_{HSA}$ and $C= C_{HSA}\times4.6$) in HEPES-S buffer are included for comparison. Maximum % of DMSO added was 6.54; T=77 K.

Table 9. Spin Hamiltonian parameters (g_x, g_y, g_z, A_x, A_y and A_z) of samples for HSA-$V^{IV}O(acac)_2$ system and for $V^{IV}O(acac)_2$ in MeOH, obtained by simulation of the experimental EPR spectra with the computer program of Rockenbauer and Korez[116], and those reported by other authors for different $V^{IV}O$–HSA species.

System		**g_x, g_y**	**g_z**	**A_x, A_y ($\times 10^4$ cm^{-1})**	**A_z ($\times 10^4$ cm^{-1})**
$V^{IV}O(acac)_2$ in MeOH		1.984	1.954	60.8	171.2
$V^{IV}O$–HSA VBS1	ref[127]		1.9265±0.0005		166.50±0.50
	ref[128]		1.939±0.001		172.8±0.5
	ref[113]		1.946		164.6
$V^{IV}O$–HSA VBS2	ref[127]		1.9355±0.0005		164.50±0.50
	ref[128]		1.938±0.001		177.1±0.5
	ref[113]		1.947		171.2
Multinuclear species $(V^{IV}O)_n$–^{m}HSA	ref[98]		1.947		164.6
Dinuclear species $(V^{IV}O)_2$–^{d}HSA	ref[98]		1.981		80
HSA:$V^{IV}O(acac)_2$=1:3		1.986	1.958	58.4	169.4
HSA:$V^{IV}O(acac)_2$=1:5		1.985	1.959	58.0	169.2

The g_z values obtained in this work for all the samples HSA:$V^{IV}O(acac)_2$ are higher than those obtained for $V^{IV}O(acac)_2$ in MeOH and for all the $V^{IV}O$–HSA species. A_z values obtained in this work for the same samples differ from all the A_z values obtained for $V^{IV}O(acac)_2$ in MeOH and for all the $V^{IV}O$–HSA species. This fact corroborates the conclusions (i) and (ii) and contradicts to the assumption (i) made from CD analysis of this system (*experiment 2.6.*) and stating that $V^{IV}O(acac)_2$ does not bind to HSA, and also to the previous findings that such binding does not occur made by Garriba *et. al.* [98]

4.3.3. Studies by fluorescence spectroscopy. Background.

Three main aromatic amino acids contribute to the HSA fluorescence: phenylalanine, tyrosine and tryptophan. But, as it was explained previously for hTF, the intrinsic fluorescence comes almost completely from tryptophan alone. HSA has 1 tryptophan residue (Trp-214 located in subdomain IIA), 18 tyrosine residues and 31 phenilalanine residues.[79] Noteworthy, this single Trp-214 is located in close environment of MBS (Asn-99, His-67, Asp-249, His-247) which is vanadium weak binding site (VBS2).[79]

4.3.3.1. The fluorescence spectra of HSA-$V^{IV}O$-oda complexes.

Figure 54 depicts fluorescence emission spectra of the HSA -$V^{IV}O(oda)(H_2O)_2$ system (*experiment 4.2.*) measured using λ_{ex}=280 nm. HSA demonstrates strong fluorescence emission with λ_{max} at 330 nm. As the complex concentration increases HSA fluorescence decrease is observed which means that the fluorescence quenching is concentration-dependent and that $V^{IV}O(oda)(H_2O)_2$ is close enough to the tryptophan and/or tyrosine residues. Hovewer, the quenching effect is rather small. Addition of the highest concentration of $V^{IV}O(oda)(H_2O)_2$ (ratio 1:18.86) causes a decrease in the fluorescence intensity of ~12.9 %.

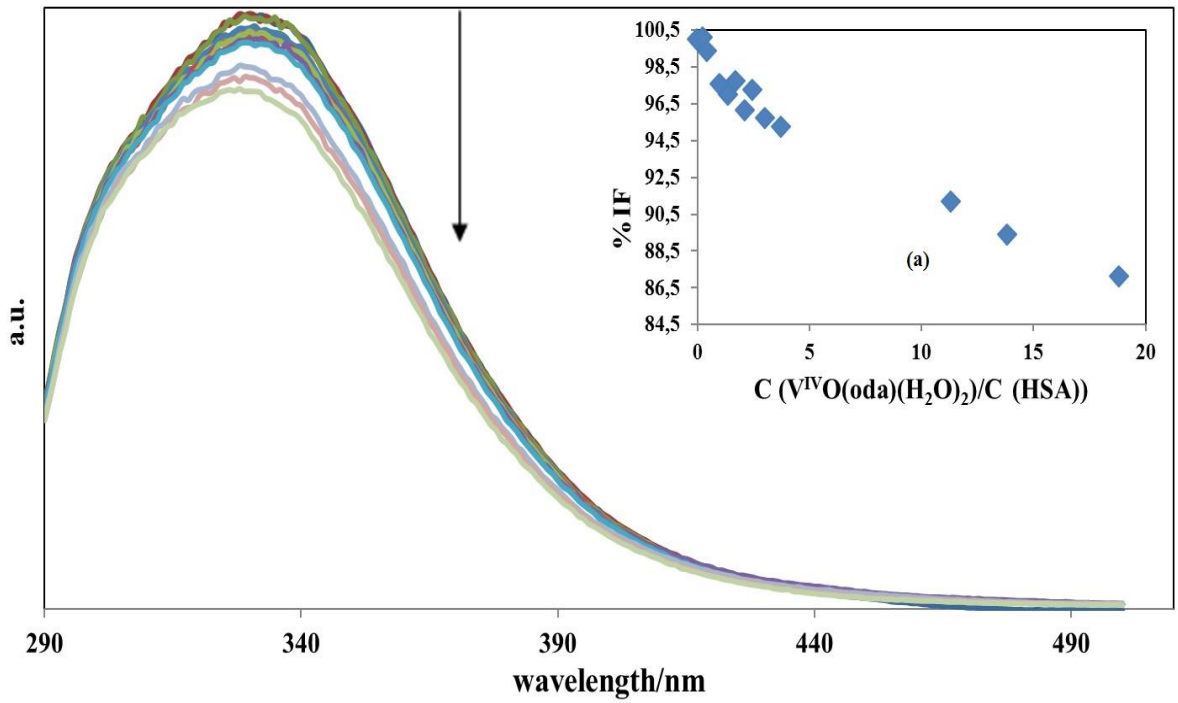

Figure 54. Fluorescence emission measured for the HSA-$V^{IV}O(oda)(H_2O)_2$ solution. The HSA concentration used was 2.6×10^{-6} M and that of $V^{IV}O(oda)(H_2O)_2$ was stepwise increased from 0 to 4.66×10^{-5} M (from HSA:$V^{IV}O(oda)(H_2O)_2$ ratios of 1:0 to 1:18.86). Other conditions: T=298 K; pH=7.4; max % of MeOH added 4.76; λ_{ex}=280 nm. The arrow shows $V^{IV}O(oda)(H_2O)_2$ concentration increase. (a) % of fluorescence intensity decrease versus $V^{IV}O(oda)(H_2O)_2$:HSA ratio.

Figure 55 depicts corrected relative fluorescence intensity of the HSA-$V^{IV}O(oda)(H_2O)_2$ solution at λ_{ex}=280 nm. The Stern-Volmer analysis gave an adequate fitting to the data obtained as the dependence is linear. This means that in the given conditions there is one type of V^{IV} binding to HSA with one Stern-Volmer dynamic quenching constant as quenching is mainly due to dynamic process, dominated by diffusion.[125] The Stern-Volmer dynamic quenching constant from the equation obtained (a slope) is $K_{sv}=2.5\times10^3$.

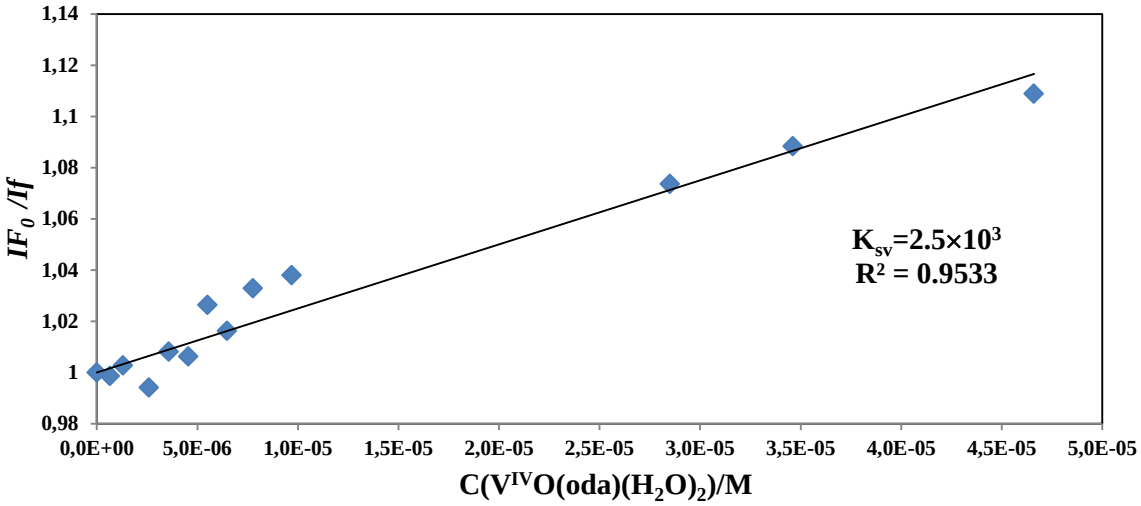

Figure 55. Stern-Volmer plot: corrected relative fluorescence intensity of the HSA-$V^{IV}O(oda)(H_2O)_2$ solution (data from Figure 54) vs. concentration of $V^{IV}O(oda)(H_2O)_2$. *If* and IF_0 are the fluorescence intensities at the maximum emission wavelength λ_{em}=330 at the concentration of the complex in a sample and in the absence of the complex respectively. The trendline equation is $y= 2.5\times10^3 + 1$.

Figure 56 depicts fluorescence emission spectra of the HSA-$V^{IV}O(oda)(bipy)$ solution (*experiment 4.4.*) measured using λ_{ex}=280 nm. As the complex concentration increases the HSA fluorescence decrease is observed which means that the fluorescence quenching is concentration-dependent and that $V^{IV}O(oda)(bipy)$ is close enough to the tryptophan and/or tyrosine residues. Hovewer, the quenching effect is rather small, but more important than that for $V^{IV}O(oda)(H_2O)_2$. Addition of the highest concentration of $V^{IV}O(oda)(bipy)$ (ratio of 1:1.81) causes a decrease in the fluorescence intensity of ~24%.

Figure 57 depicts corrected relative fluorescence intensity corrected with the UV-Vis absorption data of the HSA-$V^{IV}O(oda)(bipy)$ system at λ_{ex}=280 nm. The Stern-Volmer analysis did not give a good fitting to the data obtained as the dependence is not linear. Since a hyperbolic behaviour is observed the following equation was applied: $y=(xa/(1+K_1\cdot x))+(xc/(1+K_2\cdot x))$ where *xa* and *xc* are the molar fractions of two different populations of fluorophores with different quenching rate constants K_1 and K_2.

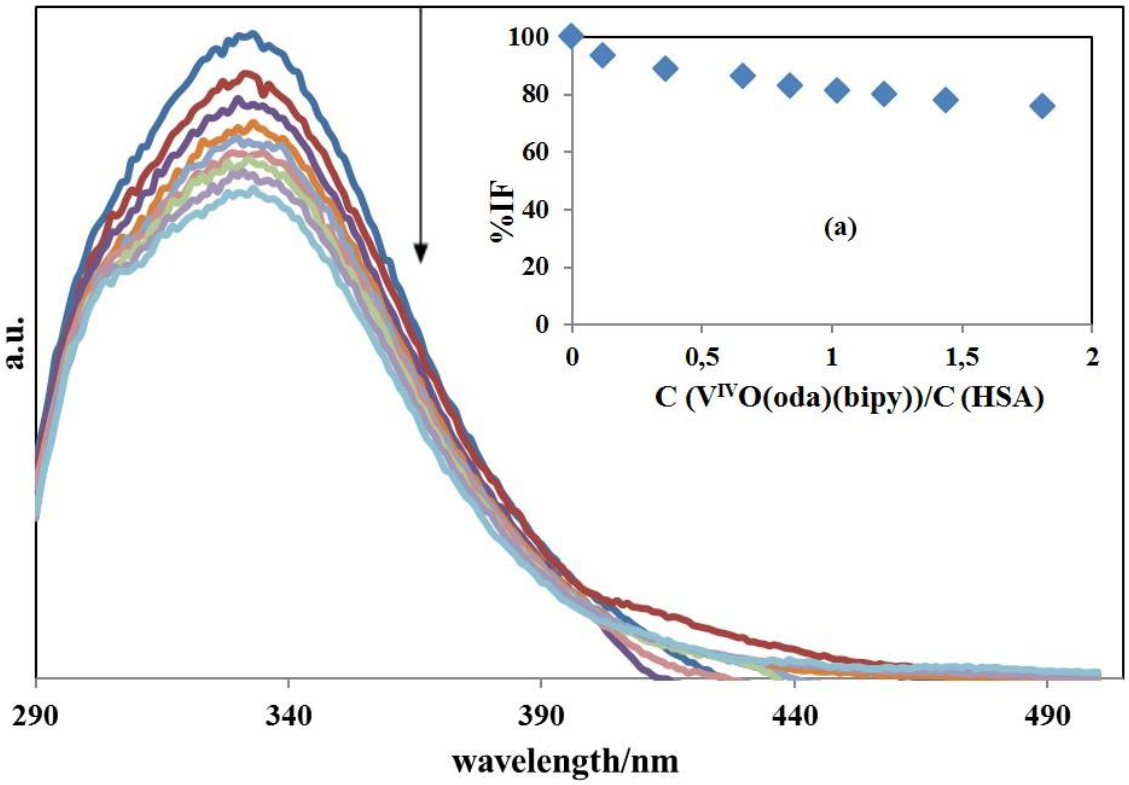

Figure 56. Fluorescence emission spectra measured for the HSA-$V^{IV}O$(oda)(bipy) solution. The HSA concentration was 1.03×10^{-6} M and that of $V^{IV}O$(oda)(bipy) was stepwise increased from 0 to 1.84×10^{-6} M (from HSA: $V^{IV}O$(oda)(bipy) ratios of 1:0 to 1:1.81). Other conditions: T=298 K; pH=7.4; max % of DMSO added 0.99; λ_{ex}=280 nm. The arrow shows $V^{IV}O$(oda)(bipy) concentration increase. (a) % of fluorescence intensity decrease versus $V^{IV}O$(oda)(bipy):HSA ratio.

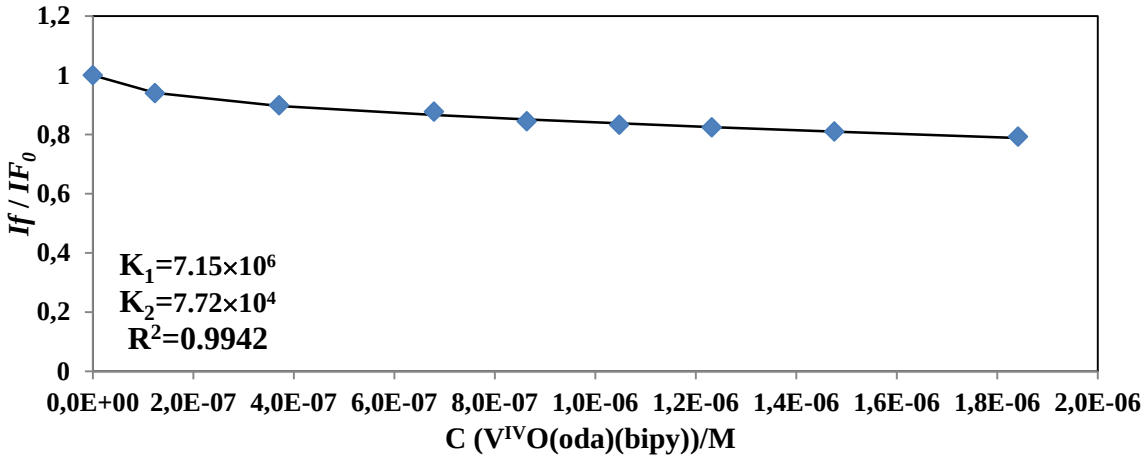

Figure 57. Corrected relative fluorescence of the HSA-$V^{IV}O$(oda)(bipy) solution (data from Figure 56) vs. concentration of $V^{IV}O$(oda)(bipy). *If* and IF_0 are the fluorescence intensities at the maximum emission wavelength λ_{em}=333 at the concentration of the complex in a sample and in the absence of the complex respectively. The trendline equation is $y=(0.108/(1+7.15\times10^{6}\cdot x))+(0.892/(1+7.72\times10^{4}\cdot x))$.

The biphasic dependence suggests that one population of fluorophores is more accessible to the quencher than the other, hence, there is more than one binding types, and HSA may be quenched by both quenching mechanisms (static and dynamic) stimultaneously.[125] The quenching rate constants obtained are $K_1=7.15\times10^6$ and $K_2=7.72\times10^4$. The corresponding fractions expressed in % are 10.8 and 89.2.

Figure 58 depicts fluorescence emission spectra of the HSA-$V^{IV}O$(oda)(bipy) solution (*experiment 4.4.*) at λ_{ex}=295 nm. HSA demonstrates strong fluorescence emission with λ_{max} at 339 nm. As the complex concentration increases the HSA fluorescence depicts a quite significant decrease which means that the fluorescence quenching is concentration-dependent and that $V^{IV}O$(oda)(bipy) is close enough to the tryptophan residue. The intensity decreases siglificantly up to the ratio 3, and then changes slightly which possibly means that after this ratio HSA binding sites close to Trp residue become saturated by the complex so this Trp is not much affected by further binding. A remarkable red shift of the emission spectra towards longer wavelength is also observed which means that tryptophan residue becomes surrounded with more hydrophilic media during binding process, which implies more open HSA conformation.[125]Addition of the highest concentration of $V^{IV}O$(oda)(bipy) (ratio 1:9.03) causes a decrease in the fluorescence intensity of ~68 %.

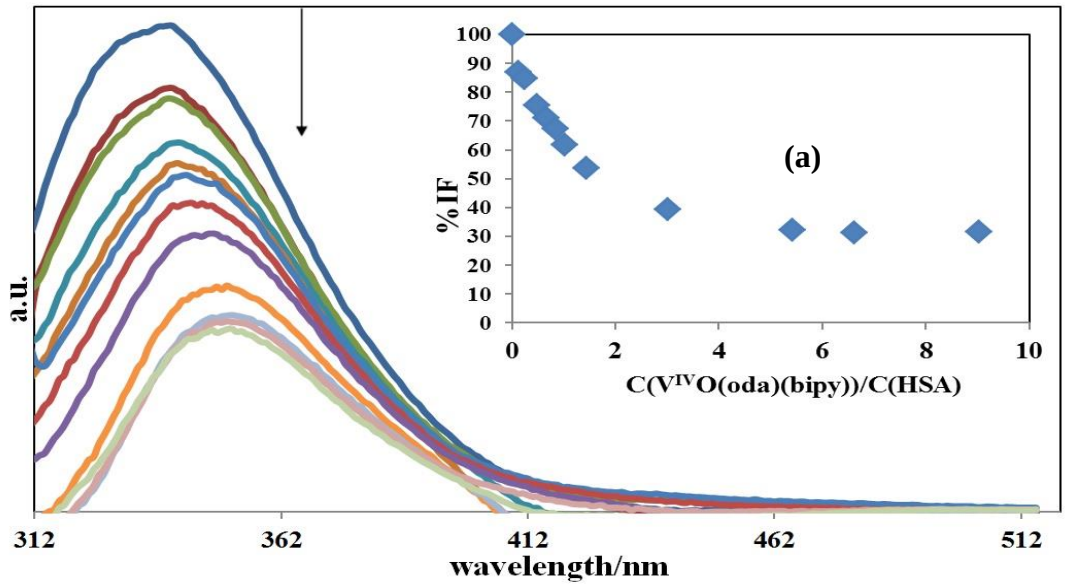

Figure 58. Fluorescence emission spectra measured for the HSA-$V^{IV}O$(oda)(bipy) solution. The HSA concentration used was 1.03×10^{-6} M and that of $V^{IV}O$(oda)(bipy) was stepwise increased from 0 to 8.86×10^{-6} M (from HSA:$V^{IV}O$(oda)(bipy) ratios of 1:0 to 1:9.03). Other conditions: T=298 K; pH=7.4; max % of DMSO added 4.76; λ_{ex}=295 nm. The arrow shows $V^{IV}O$(oda)(bipy) concentration increase. (a) % of fluorescence intensity decrease versus $V^{IV}O$(oda)(bipy):HSA ratio.

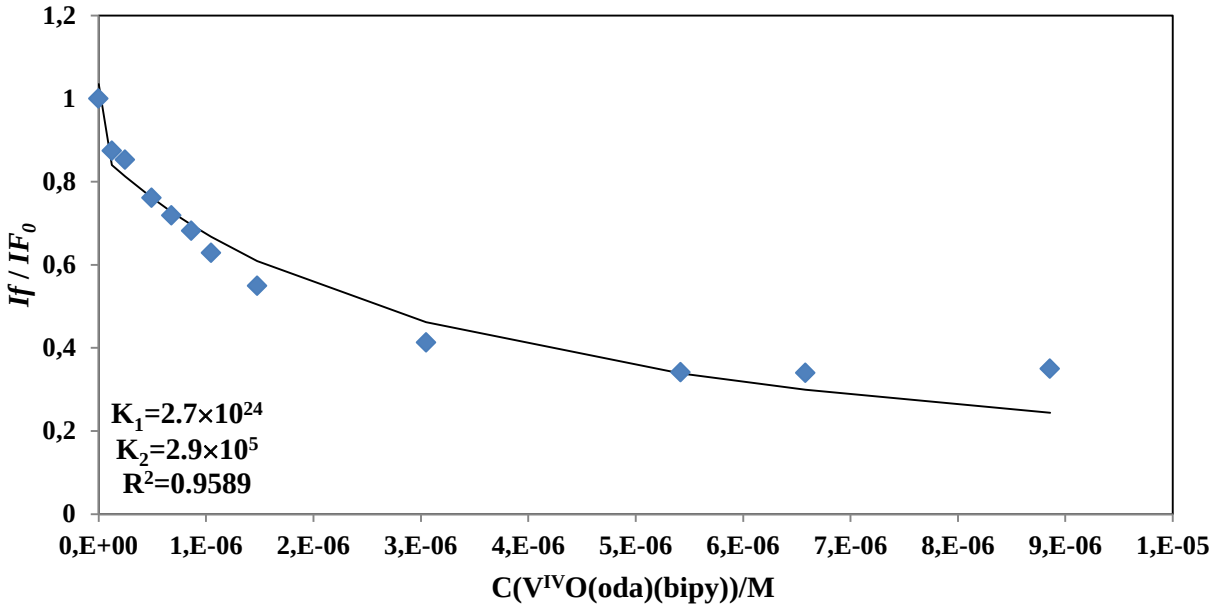

Figure 59. Corrected relative fluorescence of the HSA-$V^{IV}O$(oda)(bipy) solution (data from Figure 58) vs. concentration of $V^{IV}O$(oda)(bipy). *If* and IF_0 are the fluorescence intensities at the maximum emission wavelength λ_{em}=339 at the concentration of the complex in a sample and in the absence of the complex respectively. The trendline equation is $y=(0.164/(1+2.7\times10^{24}\cdot x))+(0.87/(1+2.9\times10^{5}\cdot x))$.

Figure 59 depicts corrected relative fluorescence intensity of the HSA-$V^{IV}O$(oda)(bipy) system at λ_{ex}=295 nm. The Stern-Volmer analysis did not give a good fitting to the data obtained as the dependence is not linear. Since a hyperbolic behaviour is observed the following equation was applied: $y=(xa/(1+k_1\cdot x))+(xc/(1+k_2\cdot x))$ where *xa* and *xc* are the molar fractions of two different populations of fluorophores with different quenching rate constants k_1 and k_2. The biphasic dependence suggests that one population of fluorophores is more accessible to the quencher than the other, hence, there is more than one binding types, and HSA may be quenched by both quenching mechanisms (static and dynamic) stimultaneously.[125] It is clear from Figure 59 that the function gains hyperbolic behaviour from the HSA:$V^{IV}O$(oda)(bipy) ratio of 1:1.44; this may mean start of binding to VBS2, e.g. MBS, as MBS can bind more than one mol equivalent of V^{IV}.[79] The quenching rate constants obtained are $K_1=2.7\times10^{24}$ and $K_2=2.9\times10^{5}$. The corresponding fractions expressed in % are 16.4 and 87.

Figure 60 depicts fluorescence emission spectra of the HSA-$V^{IV}O$(oda)(phen) solution (*experiment 4.6.*) measured using λ_{ex}=280 nm. As the complex concentration increases the HSA fluorescence decreases, this means that the fluorescence quenching is concentration-dependent and that $V^{IV}O$(oda)(phen) is close enough to the tryptophan and/or tyrosine

residues.[125] Hovewer, the quenching effect rather small. Addition of the highest concentration of $V^{IV}O$(oda)(phen) (ratio 1:2.97) causes a decrease in the fluorescence intensity of ~19.4%.

Figure 61 depicts corrected relative fluorescence intensity of the HSA-$V^{IV}O$(oda)(phen) solution measured using λ_{ex}=280 nm. The Stern-Volmer analysis gave an adequate fitting to the data obtained as the dependence is linear. This means that in the given conditions there is one type of V^{IV} binding to HSA with one Stern-Volmer dynamic quenching constant as quenching is mainly due to dynamic process, dominated by diffusion.[125] The Stern-Volmer dynamic quenching constant from the equation obtained (the slope), $K_{sv}=1.35\times10^4$.

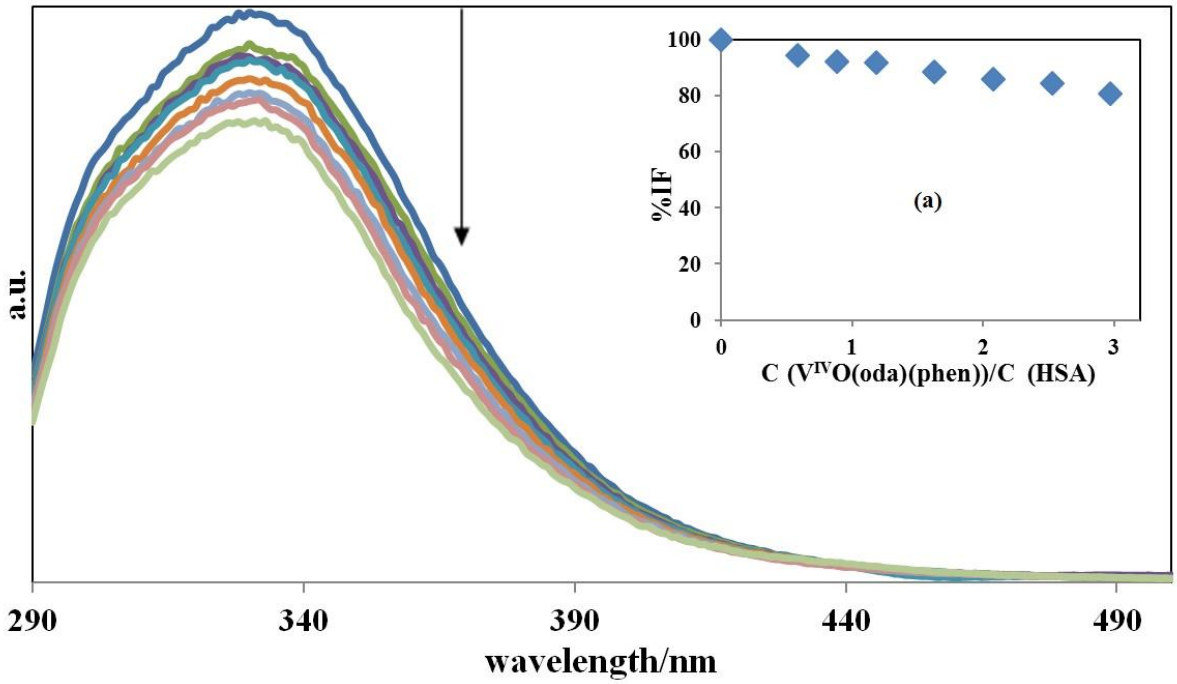

Figure 60. Fluorescence emission spectra measured for the HSA-$V^{IV}O$(oda)(phen) solution. The HSA concentration used was 2.55×10^{-6} M and that of $V^{IV}O$(oda)(phen) was stepwise increased from 0 to 7.53×10^{-6} M (from HSA: $V^{IV}O$(oda)(phen) ratios of 1:0 to 1:2.97). Other conditions: T=298 K; pH=7.4; max % of DMSO added 0.66; λ_{ex}=280 nm. The arrow shows $V^{IV}O$(oda)(phen) concentration increase. (a) % of fluorescence intensity decrease versus $V^{IV}O$(oda)(phen):HSA ratio.

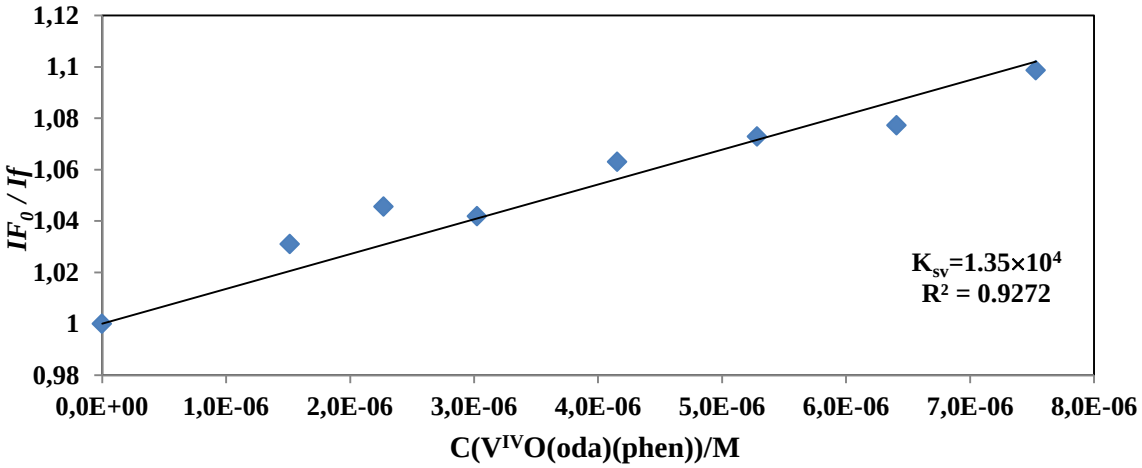

Figure 61. Stern-Volmer plot: corrected relative fluorescence intensity of the HSA-$V^{IV}O$(oda)(phen) solution (data from Figure 60) vs. concentration of $V^{IV}O$(oda)(phen). *If* and IF_0 are the fluorescence intensities at the maximum emission wavelength λ_{em}=330 at the concentration of the complex in a sample and in the absence of the complex respectively. The trendline equation is $y=1.35\times10^4 \cdot x+1$.

4.3.3.2. The fluorescence spectra of solutions containing HSA and $V^{IV}O(acac)_2$.

Figure 62 depicts fluorescence emission spectra of the HSA-$V^{IV}O(acac)_2$ solution (*experiment 4.8.*) measured using λ_{ex}=280 nm. As the complex concentration increases the HSA fluorescence noticeable decrease is observed which means that the fluorescence quenching is concentration-dependent and that $V^{IV}O(acac)_2$ is close enough to the tryptophan and/or tyrosine residues.[125] A slight blue shift of the emission spectra towards shorter wavelength is also observed which means that tryptophan and/or tyrosine residues become surrounded with more hydrophobic media during binding process, which implies more closed HSA conformation.[125]Addition of the highest concentration of $V^{IV}O(acac)_2$ (ratio 1:19.33) causes a decrease in the fluorescence intensity of ~31.5 %.

Figure 63 depicts corrected relative fluorescence intensity of the HSA-$V^{IV}O(acac)_2$ solution measured using λ_{ex}=280 nm. The Stern-Volmer analysis gave an adequate fitting to the data obtained as the dependence is linear. This means that in the given conditions there is one type of V^{IV} binding to HSA with one Stern-Volmer dynamic quenching constant as quenching is mainly due to dynamic process, dominated by diffusion.[125] The Stern-Volmer dynamic quenching constant from the equation obtained (the slope) is $K_{sv}=2.5\times10^4$.

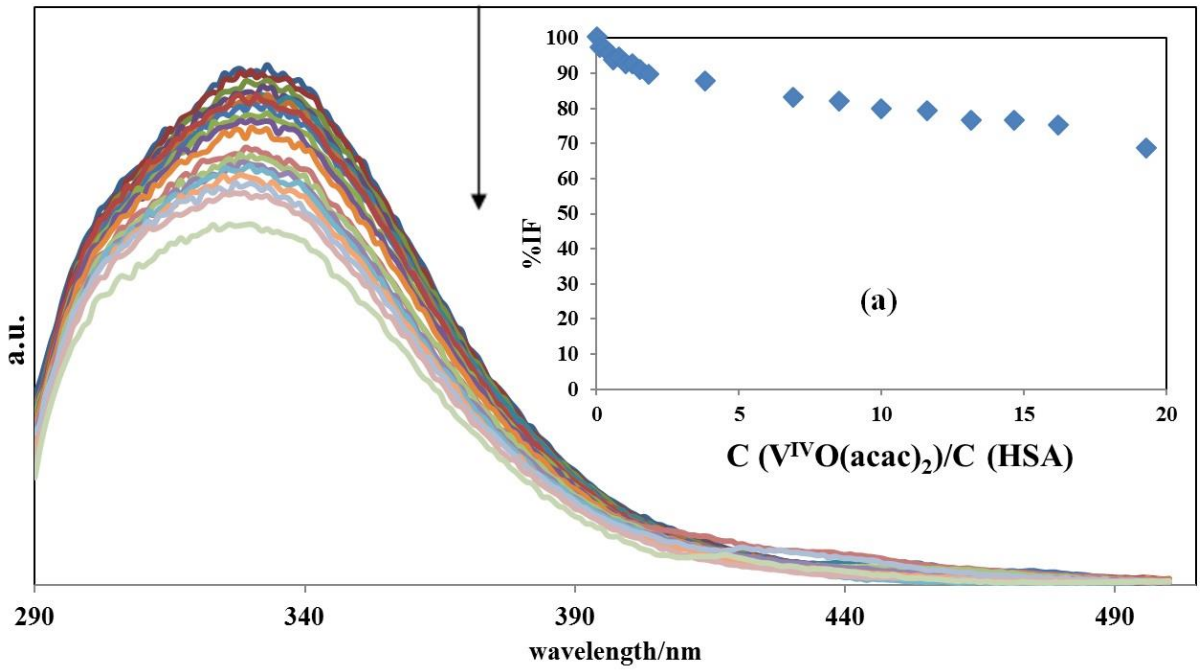

Figure 62. Fluorescence emission spectra measured for the HSA-$V^{IV}O(acac)_2$ solution. The HSA concentration used was 1.008×10^{-6} M and that of $V^{IV}O(acac)_2$ was stepwise increased from 0 to 1.8×10^{-5} M (from HSA: $V^{IV}O(acac)_2$ ratios of 1:0 to 1:19.33). Other conditions: T=298 K; pH=7.4; λ_{ex}=280 nm. The arrow shows $V^{IV}O(acac)_2$ concentration increase. (a) % of fluorescence intensity decrease versus $V^{IV}O(acac)_2$:HSA ratio.

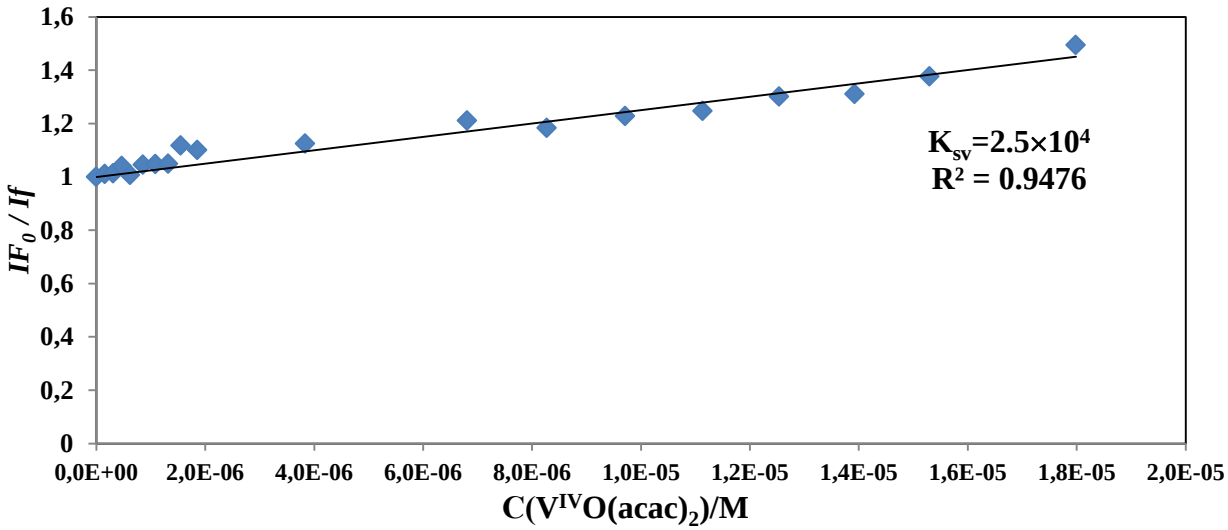

Figure 63. Stern-Volmer plot: corrected relative fluorescence intensity of the HSA-$V^{IV}O(acac)_2$ solution (data from Figure 62) vs. concentration of $V^{IV}O(acac)_2$. *If* and IF_0 are the fluorescence intensities at the maximum emission wavelength λ_{em}=333 at the concentration of the complex in a sample and in the absence of the complex respectively. The trendline equation is $y=2.5\times10^4 x+1$.

Figure 64 depicts fluorescence emission spectra of the HSA-$V^{IV}O(acac)_2$ solution (*experiment 4.8.*) measured using λ_{ex}=295 nm. As the complex concentration increases the

fluorescence decreases, which means that the fluorescence quenching is concentration-dependent and that $V^{IV}O(acac)_2$ is close enough to the tryptophan residue.[125] Hovewer, the quenching effect is not strong. Addition of the highest concentration of $V^{IV}O(acac)_2$ (ratio 1:16.24) causes a decrease in the fluorescence intensity of ~24.4%.

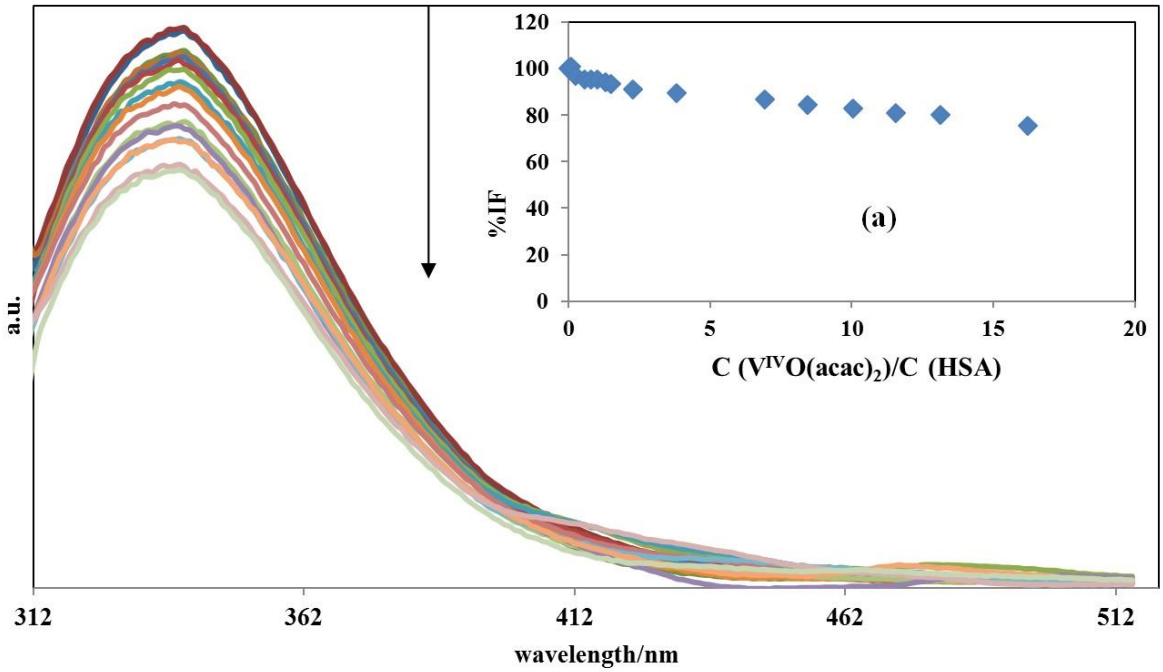

Figure 64. Fluorescence emission spectra measured for the HSA - $V^{IV}O(acac)_2$ solution. The HSA concentration used was 1.03×10^{-6} M and that of $V^{IV}O(acac)_2$ was stepwise increased from 0 to 1.53×10^{-5} M (from HSA: $V^{IV}O(acac)_2$ ratios of 1:0 to 1:16.24). Other conditions: T=298 K; pH=7.4; λ_{ex}=295 nm. The arrow shows $V^{IV}O(acac)_2$ concentration increase. (a) % of fluorescence intensity decrease versus $V^{IV}O(acac)_2$:HSA ratio.

Figure 65 depicts corrected relative fluorescence intensity of the HSA-$V^{IV}O(acac)_2$ solution measured using λ_{ex}=295 nm. The Stern-Volmer analysis did not give a good fitting to the data obtained as the dependence is not linear. Since a hyperbolic behaviour of the function was observed the following equation was applied: $y=(xa/(1+k_1\cdot x))+(xc/(1+k_2\cdot x))$ where *xa* and *xc* are the molar fractions of two different populations of fluorophores with different quenching rate constants k_1 and k_2. The biphasic dependence suggests that one population of fluorophores is accessible to the quencher while the other not, hence, there is more than one type of binding, and HSA may be quenched by both quenching mechanisms (static and dynamic) stimultaneously.[125] The quenching rate constants obtained are $k_1=3.31\times10^5$ and $k_2=4.6\times10^3$. The corresponding fractions expressed in % are 20.5 and 79.6.

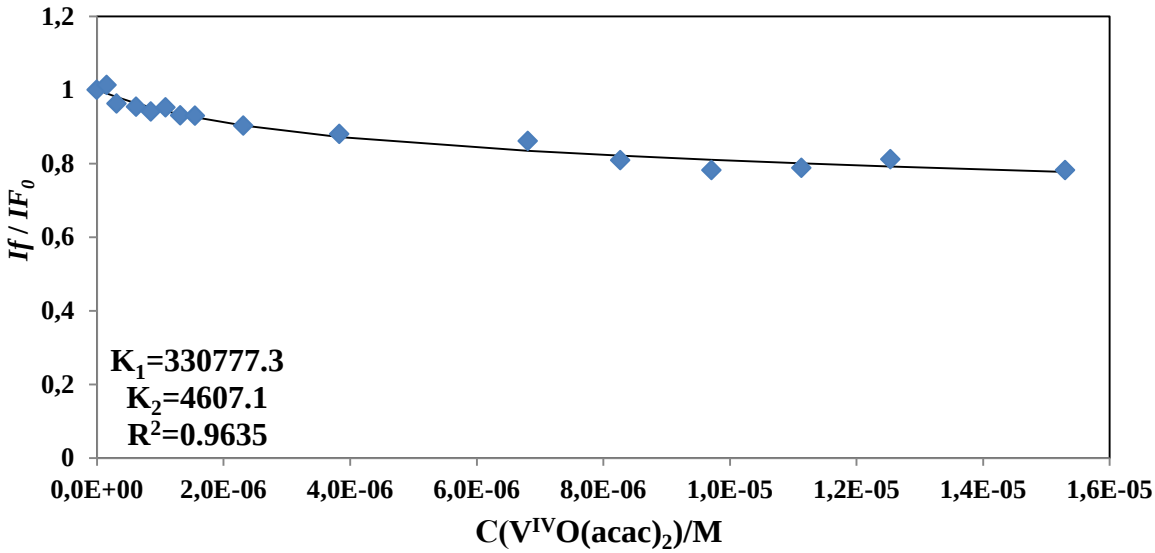

Figure 65. Corrected relative fluorescence of the HSA-$V^{IV}O(acac)_2$ solution (data from Figure 64) vs. concentration of $V^{IV}O(acac)_2$. T=298 K; pH=7.4, λ_{ex}=295 nm. *If* and IF_0 are the fluorescence intensities at the maximum emission wavelength λ_{em}=340 at the concentration of the complex in a sample and in the absence of the complex respectively. The trendline equation is $y=(0.205/(1+3.31\times10^{5}\cdot x))+(0.796/(1+4.6\times10^{3}\cdot x))$.

Among all the systems analyzed which have 2 constants (i.e. two types of binding), one constant (K_1) is a high rate constant, which corresponds to less than 10% of the quenchers (the corresponding binding site is closer to the Trp residues, but not easily accessible[125]); the other constant (K_2) corresponds to ~ 90% of the quenchers, and is used in this work to compare all the systems. Stern-Volmer dynamic quenching constants and quenching rate constants (K_2) are presented in the Table 10.

Table 10. Stern-Volmer dynamic quenching constants (K_{sv}) and quenching rate constants (K_2) obtained for HSA - $V^{IV}O(oda)(H_2O)_2$, $V^{IV}O(oda)(bipy)$, $V^{IV}O(oda)(phen)$ and $V^{IV}O(acac)_2$ systems.

System	Constants at λ_{ex}=280 nm	Constants at λ_{ex}=295 nm
HSA-$V^{IV}O(oda)(H_2O)_2$	$K_{sv}=2.5\times10^{3}$	-
HSA-$V^{IV}O(oda)(bipy)$	$K_2=7.72\times10^{4}$	$K_2=2.9\times10^{5}$
HSA-$V^{IV}O(oda)(phen)$	$K_{sv}=1.35\times10^{4}$	-
HSA-$V^{IV}O(acac)_2$	$K_{sv}=2.5\times10^{4}$	$K_2=4.6\times10^{3}$

Analysis of data of all the complex-HSA systems shows that tryptophan and/or tyrosine residues are not equally accessible to the complexes studied and the binding types vary with different complexes and both excitation wavelengths. $V^{IV}O(oda)(H_2O)_2$ appears to bind to HSA by one binding type (basing on the information obtained at λ_{ex}=280 nm) even thought

the last complex:protein ratio was very high (18.86) and to quench the fluorescence predominantly by one mechanism. $V^{IV}O$(oda)(bipy) appears to bind by more than one binding type and to quench the fluorescence by two mechanisms simultaneously.[125] Moreover, binding of $V^{IV}O$(oda)(bipy) to HSA is characterized by the strong red shift observed at λ_{ex}=295 nm.

Basing on the information obtained at λ_{ex}=280 nm $V^{IV}O(acac)_2$ appears to bind only by one binding type and to quench the fluorescence predominantly by one mechanism. At this excitation wavelength binding of $V^{IV}O(acac)_2$ to HSA is characterized by the slight blue shift.

Basing on the information obtained at λ_{ex}=295 nm $V^{IV}O(acac)_2$ appears to bind by more than one binding type and to quench the fluorescence by two mechanisms simultaneously, this meaning that Trp residue is more affected during binding process. Basing on the comparison of the quenching constants, quenching capacity increases in the following order (λ_{ex}=280 nm): $V^{IV}O(oda)(H_2O)_2$ < $V^{IV}O$(oda)(phen) < $V^{IV}O(acac)_2$ < $V^{IV}O$(oda)(bipy); (λ_{ex}=295 nm): $V^{IV}O(acac)_2$ < $V^{IV}O$(oda)(bipy) which allows to suggest that $V^{IV}O$(oda)(bipy) has the highest binding strength to HSA and the highest ability to lower the electronic density of the HSA hydrophobic cavity.[125] Moreover, these results are the same as those obtained for hTF-systems.

4.4.0. CONCLUSIONS

4.4.1. Conclusions about each system analyzed.

1. $V^{IV}O(oda)(H_2O)_2$ stability studies. The solution of $V^{IV}O(oda)(H_2O)_2$ was reasonably stable at least for ~60 minutes. After this period of time the absorption decreases with time, but the λ_{max} of the bands remains the same. The possible reasons for this are progressive hydrolysis and oxidation of V^{IV} to V^{V} species.

2. hTF - $V^{IV}O(oda)(H_2O)_2$ system.

Results of CD analysis showed that $V^{IV}O(oda)(H_2O)_2$ binds to hTF with at least one ligand kept in the coordination sphere. The spectra measured do not allow concluding if hTF only binds 2 mole equivalents of the $V^{IV}O(oda)(H_2O)_2$ (at the Fe^{III} binding sites) or if additional binding occurs also at surface His groups. Results of EPR analysis corroborate the results obtained from the CD spectra.

Results of fluorescence analysis at λ_{ex}=280 nm showed that $V^{IV}O(oda)(H_2O)_2$ partly causes concentration-dependent quenching of hTF fluorescence (addition of 3.46 mol equivalents of $V^{IV}O(oda)(H_2O)_2$ decreases the fluorescence intensity by ~ 21 %). Stern-Volmer analysis did not give a good fitting to the data. Hyperbolic adjustment of quenching constants gave $K_1 = 6.89\times10^5$ and $K_2 = 1.93\times10^4$ (quenching with fractions of 8.9 % and 91 %). These results are in agreement with the CD and EPR results.

3. hTF - $V^{IV}O(oda)(bipy)$ system.

Results of CD spectra indicate that $V^{IV}O(oda)(bipy)$ binds to hTF with at least one ligand. For samples of $V^{IV}O(oda)(bipy)$ and hTF that passed through size exclusion columns, the analysis of vanadium confirmed the possibility of binding V in molar ratios up to 4. Therefore, binding probably takes place both at the iron binding sites and at additional sites (possibly also at surface His groups).

The EPR results agree with the possibility of binding of $V^{IV}O^{2+}$ to hTF in a form that includes the two ligands.

Results of fluorescence analysis at λ_{ex}=280 nm showed that $V^{IV}O(oda)(bipy)$ yields a weak concentration-dependent quenching of hTF fluorescence (addition of 3.26 mol equivalents of $V^{IV}O(oda)(bipy)$ decreases fluorescence intensity by ~ 18 %). Stern-Volmer analysis gave a dynamic quenching constant K_{sv}=5.47x10^4. Results of fluorescence analysis at λ_{ex}=295 nm showed an apparently different information. $V^{IV}O(oda)(bipy)$ partly causes concentration-dependent quenching of hTF fluorescence which is stronger than at λ_{ex}=280 nm (addition of

1.96 mol equivalents of $V^{IV}O$(oda)(bipy) decreases the fluorescence intensity by ~31.2 %). Stern-Volmer analysis did not give a good fitting to the data. Hyperbolic adjustment of quenching constants gave $K_1 = 6.11\times10^6$ and $K_2 = 1.55\times10^5$ (quenching with fractions of 9.2 % and 91 %). The results of fluorescence analysis are in agreement with CD and EPR results.

4. hTF - $V^{IV}O$(oda)(phen) system.

Results of CD analysis showed that $V^{IV}O$(oda)(phen) binds to hTF in some way retaining both ligands in the binding process.

Results of EPR analysis showed that $V^{IV}O$(oda)(phen) binds to hTF probably with phen equatorially. However, the binding does not correspond simply to that of $V^{IV}O$(phen), but seems to involve $V^{IV}O$(oda)(phen), possibly with oda partly hydrolysed. EPR of solutions containing ratios of hTF:$V^{IV}O$:phen of 1:3:3 1:3:5 superimpose those of $V^{IV}O$(oda)(phen) + hTF, but the CD spectra differ.

Results of fluorescence analysis at λ_{ex}=280 nm showed that $V^{IV}O$(oda)(phen) causes some concentration-dependent quenching of hTF fluorescence (addition of 1.28 mol equivalents of $V^{IV}O$(oda)(phen) decreases the fluorescence intensity by ~16 %). Stern-Volmer analysis gave a dynamic quenching constant $K_{sv}=3.71\times10^4$. Results of fluorescence analysis at λ_{ex}=280 and 295 nm at 25, 30, 35, 40º C showed that in the uncorrected data the quenching rate constant decreases with increasing temperature, which supports a static quenching.

5. hTF - $V^{IV}O(acac)_2$ system.

Results of CD analysis showed that $V^{IV}O(acac)_2$ binds hTF with at least one $acac^-$ ligand, contradicting previous reports that such binding does not occur. [117,118] The same conclusion was confirmed by results of CD analysis in the experiment with PD-10 columns. $V^{IV}O$-complexes responsible for the CD spectra measured at $V^{IV}O(acac)_2$:hTF ratios up to ca. 2 are bound at the Fe^{III} binding sites of hTF. For higher ratios binding also takes place at other sites.

Results of EPR analysis suggest that $V^{IV}O(acac)_2$ binds to hTF with at least one $acac^-$ ligand, confirming the results of CD analysis.

Results of fluorescence analysis at λ_{ex}=280 nm showed that $V^{IV}O(acac)_2$ causes some concentration-dependent quenching of hTF fluorescence (addition of 3.08 mol equivalents of $V^{IV}O(acac)_2$ decreases the fluorescence intensity by ~15 %), but the quenching effect is weak. Stern-Volmer analysis did not give a good fitting to the data. Hyperbolic adjustment of quenching constants gave $K_1=8.8\times10^6$ and $K_2=5.13\times10^4$ (quenching with fractions of 7.8 %

and 92.2 %). These results are in agreement with the CD and EPR results. Results of fluorescence analysis at λ_{ex}=295 nm showed quite small $V^{IV}O(acac)_2$ quenching effect (addition of 3.08 mol equivalents of $V^{IV}O(acac)_2$ decreases the fluorescence intensity by ~ 7.22 %). Hyperbolic adjustment of quenching constants gave $K_1 = 7.1\times10^6$ and $K_2 = 2.4\times10^4$ (quenching with fractions of 7 % and 93 %).

6. HSA - $V^{IV}O(oda)(H_2O)_2$ system.

Results of fluorescence analysis at λ_{ex}=280 nm showed that $V^{IV}O(oda)(H_2O)_2$ partly causes concentration-dependent quenching of HSA fluorescence (addition of 18.86 mol equivalents of $V^{IV}O(oda)(H_2O)_2$ decreases the fluorescence intensity by ~ 12.9 %), but the quenching effect is quite weak. Stern-Volmer analysis gave dynamic quenching constant $K_{sv}=2.5\times10^3$.

7. HSA -$V^{IV}O(oda)(bipy)$ system.

From the results of CD analysis it can be concluded that $V^{IV}O(oda)(bipy)$ binds to HSA. However, no prediction can be made regarding the binding sites of $V^{IV}O(oda)(bipy)$ at the HSA.

Results of fluorescence analysis at λ_{ex}=280 nm showed that $V^{IV}O(oda)(bipy)$ causes concentration-dependent quenching of HSA fluorescence (addition of 1.81 mol equivalents of $V^{IV}O(oda)(bipy)$ decreases the fluorescence intensity by ~ 24 %). Stern-Volmer analysis did not give a good fitting to the data. Hyperbolic adjustment of quenching constants gave $K_1=7.15\times10^6$ and $K_2=7.72\times10^4$ (quenching with fractions of 10.8% and 89.16 %). Results of fluorescence analysis at λ_{ex}=295 nm showed that $V^{IV}O(oda)(bipy)$ causes a significant concentration-dependent quenching of HSA fluorescence (addition of 9.03 mol equivalents of $V^{IV}O(oda)(bipy)$ decreases the fluorescence intensity by ~ 68 %). A quite significant red shift of the emission spectra towards longer wavelength is also observed which means that tryptophan residue becomes surrounded with more hydrophilic media during binding process, which implies more open HSA conformation. Stern-Volmer analysis did not give a good fitting to the data. Hyperbolic adjustment of quenching constants gave $K_1=2.7\times10^{24}$ and $K_2=2.9\times10^5$ (quenching with fractions of 16.4 % and 87 %). These results are compatible with the CD data obtained.

8. HSA-$V^{IV}O(oda)(phen)$ system.

Results of fluorescence analysis at λ_{ex}=280 nm showed that $V^{IV}O(oda)(phen)$ partly causes small concentration-dependent quenching of HSA fluorescence (addition of 2.97 mol

equivalents of $V^{IV}O(oda)(phen)$ decreases the fluorescence intensity by ~ 19.4 %). Stern-Volmer analysis gave dynamic quenching constant $K_{sv}=1.35\times10^4$.

9. HSA - $V^{IV}O(acac)_2$ system.

The results of CD analysis showed that that either $V^{IV}O(acac)_2$ does not bind to HSA or in the CD spectra in the range analyzed the binding cannot be detected. If binding takes place, it does not give rise to significant Δε values and may take place at imidazole groups of surface His residues (or non-covalent binding).

Results of EPR analysis suggests that $V^{IV}O(acac)_2$ binds to HSA with at least one $acac^-$ ligand.

Results of fluorescence analysis at λ_{ex}=280 nm showed that $V^{IV}O(acac)_2$ causes a small concentration-dependent quenching of HSA fluorescence (addition of 19. 3 mol equivalents of $V^{IV}O(acac)_2$ decreases the fluorescence intensity by only ~31.5 %). A slight blue shift of the emission spectra towards shorter wavelength is also observed, which means that tryptophan and/or tyrosine residues become surrounded with more hydrophobic media during binding process, which implies more "closed" HSA conformation. However, it should be noted that relatively high ratios of complex were used. Stern-Volmer analysis gave dynamic quenching constant $K_{sv}=2.5\times10^4$. Results of fluorescence analysis at λ_{ex}=295 nm showed that $V^{IV}O(acac)_2$ also causes a small concentration-dependent quenching of HSA fluorescence (addition of 16.2 mol equivalents of $V^{IV}O(acac)_2$ decreases the fluorescence intensity by only ~ 24.4 %). Stern-Volmer analysis did not give a good fitting to the data. Hyperbolic adjustment of quenching constants gave $K_1 = 3.31\times10^5$ and $K_2 = 4.6\times10^3$ (quenching with fractions of 20.5 % and 79.6 %).

Globally the data do not confirm that the binding involves coordination of V^{IV} of $V^{IV}O(acac)_2$ to donor atoms of HSA.

4.4.2. General conclusions

1. The CD and EPR analyses showed that all the complexes analyzed bind to hTF and HSA with at least one ligand (except HSA - $V^{IV}O(acac)_2$ system where binding is not confirmed).

2. The complexes studied are able to quench the fluorescence of both hTF and HSA at both excitement wavelengths 280 and 295 nm, but in most cases this quenching is not very effective. The main trend of quenching for most of the complex-protein systems supports the existence of more than one binding site on hTF and HSA.

3. Based on the comparison of the quenching constants in hTF-complex systems, quenching capacity increases in the following order (λ_{ex}=280 nm): $V^{IV}O(oda)(H_2O)_2$ < $V^{IV}O(oda)(phen)$ < $V^{IV}O(acac)_2$ < $V^{IV}O(oda)(bipy)$; (λ_{ex}=295 nm): $V^{IV}O(acac)_2$ < $V^{IV}O(oda)(bipy)$ which allows to suggest that $V^{IV}O(oda)(bipy)$ has the highest binding strength to hTF and the highest ability to lower the electronic density of the hTF hydrophobic cavity. The same order is obtained for HSA-complex systems.

4. **$V^{IV}O(acac)_2$:**

- $VO(acac)_2$ binds to hTF;
- The $V^{IV}O$ content found by ICP in desalted samples goes up to $V^{IV}O$:hTF ratio of 3:1**;**
- The data obtained do not confirm the binding of V^{IV} of $V^{IV}O(acac)_2$ to HSA.

$V^{IV}O$-oda complexes:

- All $V^{IV}O$-oda complexes bind to hTF;
- The V^{IV} of $V^{IV}O(oda)(bipy)$ and $V^{IV}(oda)(phen)$ bind to HSA;
- The $V^{IV}O$ content found by ICP in desalted samples containing $V^{IV}O(oda)(bipy)$ goes up to $V^{IV}O$:hTF ratio of 4:1.

5.0. FUTURE PERSPECTIVES

This work has led to relevant conclusions about the interaction of $V^{IV}O(oda)(H_2O)_2$, $V^{IV}O(oda)(bipy)$, $V^{IV}O(oda)(phen)$ and $V^{IV}O(acac)_2$ with hTF and HSA, but further CD and EPR studies are recommended to carry out with the studied complexes and HSA to better understand their interaction with HSA.

hTF-$V^{IV}O(oda)(phen)$ system behaved somewhat strangely in this work, especially in fluorescence studies (probably, due to the relatively high fluorescence of $V^{IV}O(oda)(phen)$ complex). Therefore, further studies to better understand the tendency of binding in this system are recommended.

To further understand the systems, studies are recommended with complexes $V^{IV}O(tda)(H_2O)_2$, $V^{IV}O(tda)(bipy)$, $V^{IV}O(tda)(phen)$ (tda – thiodiacetic acid); it was not possible to synthesize with adequate purity in this work.

6.0. REFERENCES

(1) D. Rehder, J. Wiley & Sons Ltd, *Bioinorganic Vanadium Chemistry,* Department Chemie, Universität Hamburg, Germany, Copyright © **2008**, West Sussex PO19 8SQ, England.

(2) H. Yasui, Y. Adachi, A. Katoh and H. Sakurai, *J. Biol. Inorg. Chem*;**2007**, 12, 843–853.

(3) H. Sakurai, K. Fujii, H. Watanabe and H. Tamura, *Biochem. Biophys. Res. Commun*. **1995**, 214, 1095–1101.

(4) O.J. D'Cruz, Y. Dong and F. M. Uckun, *Biochem. Biophys. Res. Commun*. **2003**, 302,253–264.

(5) S. Y. Wong, R. W.-Y. Sun, N. P.-Y. Chung, C.-L. Lin and C.-M., *Chem. Commun*. **2005**, 3544–3546.

(6) J. C. Pessoa, S. Etcheverry, D. Gambino *Review. Vanadium compounds in medicine*. **2014**

(7) B. Lyonnet, X. Martz and E. Martin, *La Presse Medicale*. **1899**, 32, 191–192

(8) S. David, V. Barros, C. Cruz and R. Delgado, *FEMS Microbiol. Lett*. **2005**, 251, 119–124.

(9) A. Maitiand S. Ghosh, *J. Inorg. Biochem.***1989**, 36, 131–139.

(10) G. Elberg, J. Liand Y. Shechter, Part 2: *Health Effects (J. O. Nriagu, Ed.), John Wiley & Sons*, Inc., New York. **1998**, Ch. 14.

(11) S. Shigeta, S. Mon, T. Yamase, N. Yamamoto and N. Yamamoto, *Biomed. Pharmacother*. **2006**, 60, 211–219.

(12) D. Gambino, *Coord. Chem. Rev*. October **2011**, Volume 255, Issues 19–20, 2193–2203.

(13) N. Sharma, Himachal Pradesh University, *J. Coord. Chem.* **2010**; 63:176-184.

(14) D'Cruz, P. Ghoshand Fatih M., Wayne Hughes Institute, *Biol. Reprod.*, **1998**, 1515-1526.

(15) D'Cruz OJ, Phalguni Ghosh, and Fatih M.Uckun, *Mol. Hum. Reprod.* vol.4 no.7,**1998**, 683–693.

(16) D'Cruz OJ, Dong Y, Uckun F.M., *Biochem. Biophys. Res. Commun.* **2003**,302 (2):253-64.

(17) P. Ghosh, O. J. D'Cruz, D. D. DuMez, J. Peitersen and F. M. Uckun, J. *Inorg. Biochem*. **1999**, 75, 135–143.

(18) O. J. D'Cruz, B. Waurzyniak and F. M. Uckun, *Toxicology.* **2002**, 170,31–43.

(19) J.H. McNeill, V.G. Yuen, H.R. Hoveyda, C. Orvig, *J. Med. Chem*. **1992**, 35, 1489–1491.

(20) Y.Shechter, A.Shisheva, R.Lazar, J.Libman, A.Shanzer, *Biochem*. **1992,** 31, 2063–2068.

(21) E.J. Underwood, Trace Elements in Human and Animal Nutrition, *Academic Press*, New York, **1977**.

(22) K.H. Thompson, B.D. Liboiron, Y. Sun, K.D. Bellman, I.A. Setyawati, B.O. Patrick, V.Karunaratne, G. Rawji, J. Wheeler, K. Sutton, S. Bhanot, C. Cassidy, J.H. McNeill, V.G.Yuen, C. Orvig, *J. Biol. Inorg. Chem.***2003**, 8, 66–74.

(23) I.E. Leon, A.L. Di Virgilio, V. Porro, C.I. Muglia, L.G. Naso, P.A. Williams, M. Bollati-Fogolin, S.B. Etcheverry, *Dalton Trans.*. **2013**, 42, 11868 -11880.

(24) J. Rivadeneira, D.A. Barrio, S.B. Etcheverry, E.J. Baran, *Biol. Trace Elem. Res*. **2007**, 118,159-166.

(25) I.E. Leon, S.B. Etcheverry, B.S. Parajon-Costa, E.J. Baran, *Biol. Trace Elem. Res.* **2012**, 147, 403-407.

(26) I.E. Leon, N. Butenko, A.L. Di Virgilio, C.I. Muglia, E.J. Baran, I. Cavaco, S.B. Etcheverry, *J. Inorg. Biochem.***2014**, 134, 106–117.

(27) M. Yodoshi, M. Odoko, N. Okabe, *Chem. Pharm. Bull.***2007**, 55, 853-860.

(28) E. E. Hamilton, P. E. Fanwick and J. J. Wilker, *J. Am. Chem. Soc*. **2006**, 128, 3388–3395.

(29) E. E. Hamilton and J. J. Wilker, *Angew. Chem. Int. Ed*. **2004**, 43, 3290–3292.

(30) A. M. Evangelou, *Crit. Rev. Oncol./Hematol*. **2002**, 42, 249–265.
(31) A.M. Cortizo, S.B. Etcheverry, *Mol. Cell. Biochem.* **1995**, 145, 97–102.
(32) V.C. Sálice, A.M. Cortizo, C.L. Gómez Dumm, S.B. Etcheverry, *Mol. Cell. Biochem*. **1999**, 198, 119–128.
(33) S.B. Etcheverry, E.G. Ferrer, L. Naso, J. Rivadeneira, V. Salinas, P.A.M.Williams, J. *Biol. Inorg. Chem.***2008**, 13, 435–447.
(34) I. Goldwaser, S. Qian, E. Gershonov, M. Fridkin, Y. Shechter, *Mol. Pharmacol*. **2000**, 58, 738–746.
(35) W. Dabros, A. Kordowiak, *Folia Histochem. Cytobiol.***2007**, 45, 239–244.
(36) M.N. Islam, A.A. Kumbhar, A.S. Kumbhar, M. Zeller, R.J. Butcher, M.B. Dusane, B.N.Joshi, *Inorg. Chem*. **2010**, 49, 8237–8246.
(37) M.S. Molinuevo, D. A. Barrio, A. M. Cortizo, S. B. Etcheverry, *Cancer Chemother. Pharmacol.*. **2003**, 53: 163–172.
(38) I.E. León, A.L. Di Virgilio, D.A. Barrio, G. Arrambide, D. Gambino, S.B. *Etcheverry, Metallomics* **2012**, 4, 1287–1316.
(39) X. Shi, H. Jiang, Y. Mao, J. Ye, U. Saffiotti, *Toxicology*.**1996**, 106, 27–38
(40) A. Sreedhara, N. Susa, A. Patwardhan, C. P. Rao., *Biochem. Biophys. Res. Commun***. 1996,** 224,115-120.
(41) Rang, H.P.; Dale, M.M.; Flower, R.*J. Rang and Dale's Pharmacology; 6th ed.*; *Churchill Livingstone*. **2007**.
(42) S.B. Etcheverry and A.M. Cortizo, *American Chemical Society*. **2009** Copyright © 1998, 270–276.
(43) S. Mehtab, G. Goncalves, S. Roy, A.L. Tomaz, T. Santos-Silva, M.F. Santos, M.J. Romão, T. Jakusch, T. Kiss, J.C. Pessoa, *J. Inorg. Biochem.***2013**, 121, 187–195.
(44) B.L. Rai, Z. D. Liu, D. Y. Liu, S. L. Lu, R. C. Hider, *Eur. J. Med. Chem*. **1999**, 34, 475-485.
(45) W.R. Harris, B. Yang, S. Abdollahi, Y. Hamada, *J. Inorg. Biochem.***1999**, 76, 231-242.
(46) D.C. Crans, S.S. Amin, A.D. Keramidas, in: J. O. Nriagu, *Wiley*. **1988**.
(47) P.J. Stankiewicz, A.S. Tracey, *Met. Ions Biol. Syst*. **1995**, 31, 249-286.
(48) D. Rehder, *Future Med. Chem*. **2012**, 4, 1823.
(49) B. Venugopal and T.C. Luckey, *Plenum*, New York, **1978**.
(50) J. Edel, E. Sabbioni, Biol. *Trace Element Res*. **1989**, 3, 265-275.
(51) A.R. Byrne, L. Kosta, Sci. *Total Environ*. **1978**, 1017-1030.
(52) B.R. Nechay, L.B. Nanningaand P.S.E. Nechay, Fed. *Proc*. **1986**, 5123-5132.
(53) J.J. Mongold, G.H. Cros, L. Vian, A. TEP, S. Ramanadham, G. S1ou, J. Diaz, J.H. Mcneill and J. J. Serrano, Pharmacol. *Toxicol*. **1990**, 6, 7192-198.
(54) Rodney J. French and Peter J.H. Jones, *Life Sciences*. **1992**, 52, 339-346.
(55) Thompson K.H., Lichter J, LeBel C, Scaife MC, McNeill JH, Orvig C. *J. Inorg. Biochem.* **2009**, 103, 554-558.
(56) World Health Organization (W.H.O.), *Vanadium: Environmental Health Criteria.* **1988**, 8, 46-47.
(57) B.V. Venkataramanand, S. Sudha Asian *J. Exp. Sci*. **2005**, 19 (2), 127-134.
(58) Debbie C. Crans and Alan S. Tracey. *In Vanadium Compounds*; Tracey A., et al. 1998, 1-29.

(59) http://www.chemspider.com/Chemical-Structure.5361637.html, Lastly accessed 26.03.2015
(60) http://en.wikipedia.org/wiki/File:Acetylacetone_keto-enol_equilibrium.png, Lastly accessed 26.03.2015.
(61) W. Caminati, J.-U. Grabow J. Am. Chem. Soc, **2006**, 128,854–857.
(62) Kimberly A. Manbeck, Nicholas C. Boaz, Nathaniel C. Bair, Allix M. S. Sanders, and Anderson L. Marsh, J. Chem. Educ. **2011**, 10, 1444–1445.
(63) Z. Yoshida, H. Ogoshi, T. Tokumitsu, *Tetrahedron*.**1970**, 26, 5691–5697.
(64) http://en.wikipedia.org/wiki/Bipyridine, Lastly accessed **26.03.2015**.
(65) https://www.angelo.edu/faculty/kboudrea/molecule_gallery/04_aromatics/00_aromatics.htm, Lastly accessed **26.03.2015**.
(66) D. Rıo, A. Galindo, J. Tejedo , F. J. Bedoya , A. Ienco , C. Mealli, *Inorg. Chem. Commun.* **2000**, 3, 32–34.
(67) I. E. León, S. B. Etcheverry, B. S. Parajón-Costa, and E. J. Baran. J. *Mex. Chem. Soc*. **2013**, 57(3), 175-179.
(68) I. E. León, S. B. Etcheverry, B.S. Parajón-Costa, E. J. Baran, *Biol Trace Elem Res*. **2012**, 147, 403–407.
(69) E. V. Fedorova, V. B. Rybakov, V. M. Senyavin, A. V. Anisimov, and L. A. Aslanov. *Crystallogr. Rep*. **2005**, 50 (2), 224–229.
(70) David A. Evans, *Angew. Chem. Int*. **2014**, 53, 99.
40 – 11145.
(71) J. C. Pessoa, I. Correia, G. Gonçalves and I. Tomaz , J. Argent. Chem. Soc., 97 (1), **2009**, 151-165.
(72) A.L. Di Virgilio, J. Rivadeneira, C.I. Muglia, M.A. Reigosa, N. Butenko, I. Cavaco, S.B.Etcheverry, *BioMetals*. **2011**, 24 (6), 1153-1168.
(73) J. Rivadeneira, D.A Barrio, S.B Etcheverry, E.J Baran, *Biol. Trace Elem. Res*. **2007**, Volume 118, 159-166.
(74) Rivadeneira J, Di Virgilio A.L., Barrio D.A., Muglia C.I, Bruzzone L, Etcheverry S.B. *Med Chem*. **2010**, 6(1), 9-23.
(75) D. L. Nelson, M. M. Cox. *The principles of biochemistry. Fifth edition***. 2008** by W. H. Freeman and Company, 1302.
(76) N. Butenko, A. I. Tomaz, O. Nouri, E. Escribano, V. Moreno, S. Gama,V. Ribeiro, J. P. Telo, J. C. Pesssoa, I. Cavaco, *J. Inorg. Biochem.***2009**,103, 622–632.
(77) T. Peters, Jr, *All About Albumin. Biochemistry, Genetics, and Medical Applications. Elsevier*, **1995**.
(78) G. Colmenarejo. *Med Res Rev, Wiley*.**2003** Vol. 23, No. 3, 275-301.
(79) I. Correia, T. Jakusch, E. Cobbinna, S. Mehtab, I. Tomaz, N. V. Nagy, A. Rockenbauer, J. C. Pessoa, T. Kiss, D. Trans. 41, **2012**, 6477-6487.
(80) http://pubs.rsc.org/en/content/articlelanding/2009/ob/b911605b#!divAbstract, Lastly accessed **04.04.2015**.
(81) M. C. Chung, *Biochemical Education*, Vol.12 (4) **1984**, 146-154.
(82) Martel P., Kim, S M and Powell, B M., *Biophys.* J 31, **1980**, 371-380.
(83) R. T. MacGillivray, E. Mendez, S. K. Sinha, M. R. Sutton, J. Lineback-Zins, and K. Brew. *Proc Natl Acad Sci U S A*,**1982,** 79(8), 2504–2508.

(84) Spik G., Bayard B., Fournet B., Strecker G., Bouquelet S., Montreuil *J. FEBS Lett*. **1975**, 50, 296–299.
(85) Dorland L.; Haverkamp J.; Schut B. L.; Vliegenthart J.; Spik G.; Strecker G.; Fournet B.; Montreuil *J. FEBS Lett.* **1977**, 77, 15-20.
(86) Wong K-L.; Regoeczi E. Int. *J. Pept. Protein Res*. **1977**, 9, 241-248.
(87) Putman F. W., *Academic Press*, 1, 1975, 265-315.
(88) Hemmaplardh D. and Morgan E. H, *Biochim Biophys Acta*, 426, **1976**, 385-398.
(89) Macedo M.F., M.de Sousa *Inflamm Allergy Drug Targets*, 7 (1), **2008**, 41–52.
(90) Battin, E. E.; Lawhon, A.; Hamilton, D. H.; Brumaghim, J. L., *J. Chem. Ed*. 86, **2009**, 969-972.
(91) Chasteen N. D. *TIBS* 8, **1983**, 272-275.
(92) Aisen P. and Listowsky I., Ann. *Rev. Biochem.* 49, **1980**, 357-393.
(93) Chasteen N D, *Coord. Chem. Rev.* 22, **1977**, 1-36.
(94) Princiotto J. V., Zapolski, E J, *Nature* 255, **1975**, 87-88.
(95) Williams J. and Moreton K., *Biochem J* 185, **1980**, 483-488.
(96) S. Mehtab , G. Gonçalves, S. Roy, A. I. Tomaz, T. Santos-Silva, M. F.A. Santos, M. J. Romão, T. Jakusch, T. Kiss, J. C. Pessoa. *J. Inorg. Biochem.* 121, **2013**, 187–195.
(97) J. C. Pessoa, G. Gonçalves, S. Roy, I. Correia, S. Mehtab, M. F.A. Santos, T. Santos-Silva, *Inorg. Chim. Acta* 420, **2014**, 60–68.
(98) D. Sanna, G. Micera, E. Garribba, *Inorg. Chem*. 49, **2010**, 174–187.
(99) D. Sanna, L. Biró, P. Buglyó, G. Micera, E. Garribba, *Metallomics* 4, **2012,** 33–36.
(100) D. Sanna, P. Buglyó, G. Micera, E. Garribba, *J. Biol. Inorg. Chem.* 15, **2010**, 825–839.
(101) D. Sanna, L. Bíró, P. Buglyó, G. Micera, E. Garribba, *J. Inorg. Biochem.*115, **2012,** 87–99.
(102) D. Sanna, V. Ugone, G. Micera, E. Garribba, *Dalton Trans*. 41, **2012**, 7304-7318.
(103) D. Sanna, G. Micera, E. Garribba, *Inorg. Chem*. 52 , **2013,** (**1985**) 11975-11985.
(104) Smith T.S., LoBrutto R., Pecorarro V.L., *Coord. Chem Rev.*, **2002**, 228, 1-18.
(105) N. D. Chasteen, *Oxidovanadium (IV) EPR Spin Probes Inorganic and Biochemical Aspects;* Biological magnetic resonance, **1981**, Vol. 3, Chapter 2, 53-130.
(106) Kiss T., Jakusch T., Holler D., Dornyei A., Enyedy E. A., Pessoa J.C., Sakurai H., Sanz-Medel A. *Coord. Chem, Rev*., **2008**, 252, 1153-1162.
(107) Wallace B.A., Janes R.W. *Modern Techniques for Circular Dichroism and Synchrotron Radiation Circular Dichroism*; IOS Press: Amsterdam, **2009**.
(108) Pessoa J.C., Correia, I., Gonçalves G. , Tomaz, I. *J. Arg. Chem. Soc*.**2009**, 97, 151-165.
(109) Jakusch T., Hollender D., Enyedy E. A., Gonzalez C.S., Montes-Bayon M., Sanz-Medel A., Pessoa J.C., TomazI., Kiss T. *Dalton Trans*. **2009**, 2428-2437.
(110) Valeur B., *Molecular Fluorescence: Principles and Applications*; Wiley-VCH Verlag GmbH, **2001,** 381.
(111) H. Sun, H. Li, P.J. Sadler, *Chem. Rev*. 99, **1999**, 2817–2842.
(112) E. Cobbina, S. Mehtab, I. Correia, G. Gonçalves, I. Tomaz, I. Cavaco, T. Jakusch, E. Enyedi, T. Kiss, J. C. Pessoa, *J. Mex. Chem.Soc.* **2013**, 57(3), 194-205.
(113) E. Garribba, D. Sanna and G. Micera, *J. Inorg. Biochem*.,**2009**, 103,648–655.
(114) H. Sakurai, H. YasuiandY. Kunori, *Chem. Lett.*, **2003**, 32, 1032–1033.
(115) H. Sakurai, H. Yasui and K. Takechi, *J. Inorg.Biochem.*, **2000**, 78, 185–196.
(116) Rockenbauer A.; Korecz I. *Appl. Magn. Res*. **1996**, *10*, 29-43.

(117) M.F.A. Santos, I. Correia, A.R. Oliveira, E. Garriba, J. Costa Pessoa, T. Santos-Silva, *Eur. J. Inorg. Chem*., **2014**, 3293-3297.
(118) Marvin W. Makinen, M. Salehitazangi, *Coord. Chem. Rev*. **2014,** 279, 1–22.
(119) J.C. Cannon, N.D. Chasteen, *Biochemistry* **1975**, 14, 4573–4577.
(120) N.D. Chasteen, J.K. Grady, C.E. Holloway, *Inorg. Chem*. **1986**, 25, 2754–2760.
(121) D. Sanna, E. Garribba, G. Micera, *J. Inorg. Biochem*. **2009**, 103, 648–655.
(122) D.C. Harris, Biochemistry **1977**, 16, 560–564.
(123) D. Mustafi, E.V. Galtseva, J. Krzystek, L.C. Brunuel, M.W. Makinen, *J. Phys. Chem*. **1999**, 103, 11279–11286.
(124) T. Kiss, T. Jakusch, S. Bouhsina, H. Sakurai, E.A. Enyedy, *and Eur. J. Inorg. Chem.* **2006**, 18, 3607–3613.
(125) Sareh S., Jamshidkhan C.*J. Biol. Macromol.* **2010**, 47, 558–569.
(126) He Q.Y., Mason A.B., Lyons B.A, Tam B.M., Nguyen V., Macgillivray R. T. A, Woodworth R.C., *Biochem. J.* **2001** 354, 423–429.
(127) Liboiron, B.D.; Thompson, K.H.; Hanson, G.R.; Lam, E.; Aebischer, N.; Orvig, C. *J. Am. Chem. Soc.* **2005**, *127*, 5104-5115.
(128) Chasteen, N.D.; Francavilla, J. *J. Phys. Chem.* **1976**, *80*, 867-871.

Appendices

7.0. APPENDICES.

Appendix A. Preparation of solutions.

Tris buffer preparation (experiment 1.1.). To prepare 0.08 M solution 0.97 g of Tris powder was dissolved in 80 mL of Millipore water, then pH was adjusted to 7.4 using HCl and the solution was topped up to 100 mL mark.

Tris buffer preparation (experiment 5.1.).

To prepare 0.1 M solution 0.97 g of Tris powder was dissolved in 500 mL of Millipore water,. Then, 1.33 g of Na_2CO_3 was added to obtain $C(Na_2CO_3)= 2.5\times10^{-2}$ M . pH was adjusted to 7.4 using HCl and the solution was topped up to 500 mL mark.

$V^{IV}O(oda)(H_2O)_2$ solution preparation for stability studies.

Experiment 1.1. To prepare 3.6×10^{-3} M solution 2.54×10^{-3} g of $VO(oda)(H_2O)_2$ was dissolved in 300 µL of MeOH. 150 µL of this solution was added to 2850 µL of This buffer to make a total volume of 3 mL with the complex concentration of 1.8×10^{-3} M.

Appendix B. Infrared spectra of the $V^{IV}O(oda)(H_2O)_2$, $V^{IV}O(oda)(bipy)$, $V^{IV}O(oda)(phen)$ with the interpretation.

Appendix B 1. IR-spectrum of $V^{IV}O(oda)(H_2O)_2$

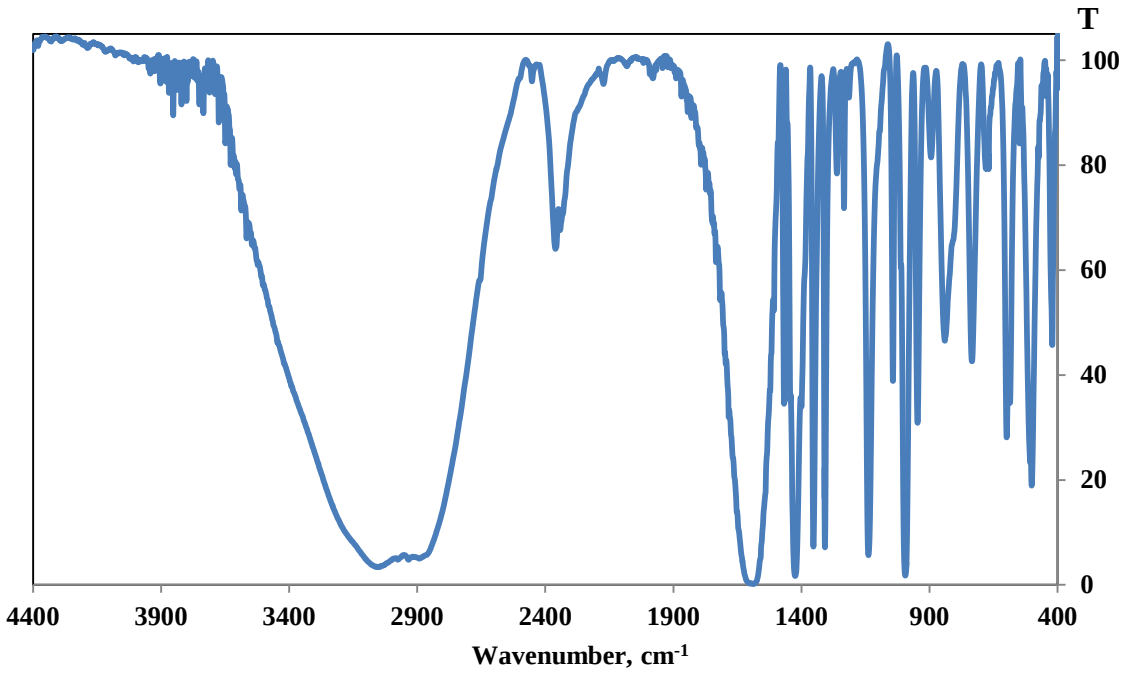

Appendix B 2. Interpretation of IR-spectrum of $V^{IV}O(oda)(H_2O)_2$

Wavenumber, cm^{-1} and intensity	**Assignments**
3052-2820 s vbr	ν(OH) (H_2O)
1615-1548 s br	ν(C=O)
995 s	ν(V=O)
1351 vs	$\nu_s(COO^-)$
1139-1134 vs	ν_{as}(C–O–C)
497 m	δ(C–O–C)
422-419 m, 404-402 w	ν(V–O) cm^{-1}

Appendix B 3. IR-spectrum of $V^{IV}O$(oda)(bipy)

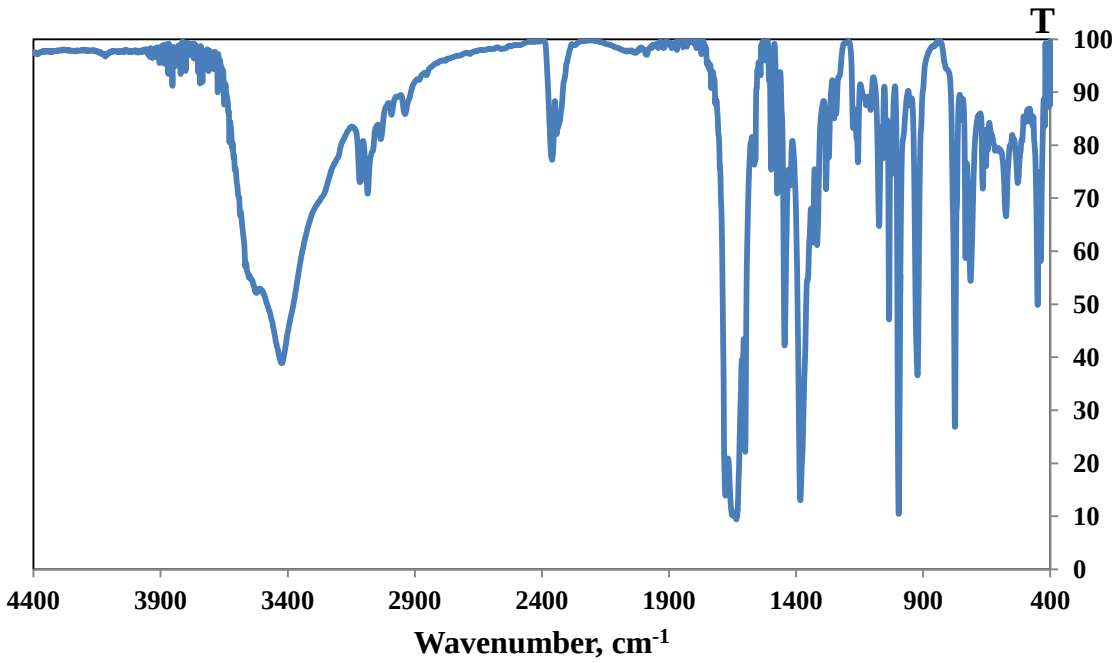

Appendix B 4. Interpretation of IR-spectrum of $V^{IV}O$(oda)(bipy)

Wavenumber, cm^{-1} and intensity	**Assignments**
3422.55 m vbr	ν(OH) (H_2O)
3116.4 w, 3085.55 w, 3030,58 vw	bipy ν(CH)
2989.12 vw, 2934.16 vw	$\nu(CH_2)$
1634.86 s br	$\nu_{as}(COO^-)$
1497.94 m, 1474,31 m	bipy - ν_{ring}
1444.9 m	bipy - ν_{ring} + δ_{ring}-H
1383.19 s	$\nu_s(COO^-)$
1317.63 m	ν_{ring} + inter ring stretch
1281.95 m, 1249.65 w	bipy - $\delta(CH)_{in\ plane}$
1156.6 m	bipy - ν_{ring} + $\delta(CH)_{in\ plane}$
1105,01 w	ν_{as}(C-O-C)
1073.67 m, 1034.14 m	bipy - $\delta(CH)_{in\ plane}$
996.53 vs	ν(V=O)
922.29 s	ν(C-C)
797.9 vw	ν_s(C-O-C)
775.24 s, 733.3 m, 713.53 m	bipy - $\delta(CH)_{out\ of\ plane}$
665.32 w, 652.78 w	$\rho(CH_2)$
612.77 w, 574.2 m	bipy - δ_{ring}
528.4 w	δ(C-O-C)
449.81 m, 437.28 m	ν(V-O)

Appendix B 5. IR-spectrum of $V^{IV}O$(oda)(phen)

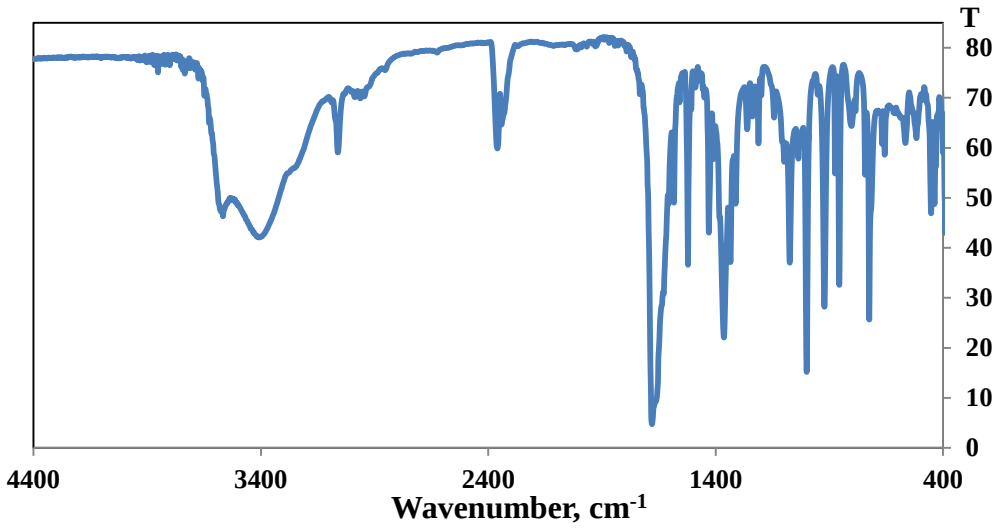

Appendix B 6. Interpretation of IR-spectrum of $V^{IV}O$(oda)(phen)

Wavenumber, cm^{-1} and intensity	**Assignments**
3566.7 m br, 3406.64 m vbr	ν(OH) (H_2O)
3061,44 w	ophen–ν(CH)
2941,39 vw	ν(CH_2)
1677,76 vs br	$\nu_{as}(COO^-)$
1521,56 m	*o*phen—$\delta(CH)_{in\ plane}$
1411,16 w	δ(CH_2)
1363.91s, 1334.98 m	$\nu_s(COO^-)$
1334.98 m, 1312.32 w	*o*phen—$\delta(CH)_{in\ plane}$
1238.56 w, 1221.68 w	*o*phen—ν_{ring}
1211.56 m, 1199.51 vw	*o*phen—ν_{ring}
1143.1 w	ν_{as}(C–O–C)
1112.72 w. 1098.74 w	*o*phen—$\delta(CH)_{in\ plane}$
1074.16 m	*o*phen—$\delta(CH)_{in\ plane}$
1036.07 w	ν(C–C)
999.91 vs	ν(V═O)
955.07 vw. 921.8 s	ν(C–C)
875.04 m	ν_s(C–O–C)
856.24 s	*o*phen—$\delta(CH)_{out\ of\ plane}$
784.4 w	*o*phen—$\delta(CH)_{out\ of\ plane}$
742.46 m	ν(C–C) + *o*phen—$\delta(CH)_{out\ plane}$
724.62 s	*o*phen—$\delta(CH)_{out\ of\ plane}$
656.64 w	ρ(CH_2)
565.52 w	*o*phen—$\delta(CH)_{in\ plane}$
516.83 w	δ(C–O–C)
452.71 m, 437.76 m	ν(V–O)

Appendix C. Concentrations of samples for CD and EPR analyses.

Appendix C 1. ***Experiment 2.1. CD of $V^{IV}O(oda)(H_2O)_2$ + hTF system.***

Sample	C(hTF)/M	C($V^{IV}O(oda)(H_2O)_2$)/M
hTF: $V^{IV}O(oda)(H_2O)_2$= 1:1	7.15×10^{-4}	7.16×10^{-4}
hTF: $V^{IV}O(oda)(H_2O)_2$= 1:2	7.08×10^{-4}	1.41×10^{-3}
hTF: $V^{IV}O(oda)(H_2O)_2$= 1:3	6.99×10^{-4}	2.1×10^{-3}
hTF: $V^{IV}O(oda)(H_2O)_2$= 1:4	6.91×10^{-4}	2.77×10^{-3}

Appendix C 2. ***Experiment 2.2. CD of $V^{IV}O(oda)(bipy)$ + hTF system.***

Sample	C(hTF)/M	C($V^{IV}O(oda)(bipy)$)/M
hTF: $V^{IV}O(oda)(bipy)$ = 1:0.36	4.23×10^{-4}	1.53×10^{-4}
hTF: $V^{IV}O(oda)(bipy)$ = 1:0.6	4.22×10^{-4}	2.54×10^{-4}
hTF: $V^{IV}O(oda)(bipy)$ = 1:0.84	4.20×10^{-4}	3.54×10^{-4}
hTF: $V^{IV}O(oda)(bipy)$ = 1:1.14	4.19×10^{-4}	4.79×10^{-4}
hTF: $V^{IV}O(oda)(bipy)$ = 1:1.75	4.16×10^{-4}	7.26×10^{-4}
hTF: $V^{IV}O(oda)(bipy)$ = 1:2.35	4.13×10^{-4}	9.7×10^{-4}
hTF: $V^{IV}O(oda)(bipy)$ = 1:2.95	4.10×10^{-4}	1.21×10^{-3}
hTF: $V^{IV}O(oda)(bipy)$ = 1:4.09	4.05×10^{-4}	1.66×10^{-3}
hTF: $V^{IV}O(oda)(bipy)$ = 1:4.7	4.02×10^{-4}	1.89×10^{-3}

Appendix C 3. ***Experiment 2.3. CD of $V^{IV}O(oda)(bipy)$ + HSA system.***

Sample	C(HSA)/M	C($V^{IV}O(oda)(bipy)$)/M
HSA: $V^{IV}O(oda)(bipy)$= 1:0.26	5.35×10^{-4}	1.37×10^{-4}
HSA: $V^{IV}O(oda)(bipy)$= 1:1.02	5.31×10^{-4}	5.43×10^{-4}
HSA: $V^{IV}O(oda)(bipy)$= 1:1.53	5.28×10^{-4}	8.1×10^{-4}
HSA: $V^{IV}O(oda)(bipy)$= 1:2.05	5.25×10^{-4}	1.07×10^{-3}
HSA: $V^{IV}O(oda)(bipy)$= 1:2.49	5.22×10^{-4}	1.30×10^{-3}
HSA: $V^{IV}O(oda)(bipy)$= 1:3.01	5.19×10^{-4}	1.56×10^{-3}
HSA: $V^{IV}O(oda)(bipy)$= 1:3.52	5.17×10^{-4}	1.82×10^{-3}

HSA: $V^{IV}O$(oda)(bipy)= 1:4.03	5.14×10^{-4}	2.07×10^{-3}
HSA: $V^{IV}O$(oda)(bipy)= 1:4.54	5.11×10^{-4}	2.32×10^{-3}
HSA: $V^{IV}O$(oda)(bipy)= 1:5.05	5.08×10^{-4}	2.57×10^{-3}

Appendix C 4. ***Experiment 2.4. $V^{IV}O$(oda)(phen) + hTF system.***

Sample	C(hTF)/M	C($V^{IV}O$(oda)(phen))/M
hTF: $V^{IV}O$(oda)(phen)= 1:1	5.32×10^{-4}	5.35×10^{-4}
hTF: $V^{IV}O$(oda)(phen)= 1:2.01	5.32×10^{-4}	1.07×10^{-3}
hTF: $V^{IV}O$(oda)(phen)= 1:3.09	5.32×10^{-4}	1.65×10^{-3}

Appendix C 5. ***Experiment 2.5. $V^{IV}O(acac)_2$ + hTF system.***

Sample	C(hTF)/M	C($V^{IV}O(acac)_2$)/M
hTF: $V^{IV}O(acac)_2$= 1:0.28	4.77×10^{-4}	1.34×10^{-4}
hTF: $V^{IV}O(acac)_2$= 1:0.51	4.76×10^{-4}	2.41×10^{-4}
hTF: $V^{IV}O(acac)_2$= 1:1.01	4.73×10^{-4}	4.79×10^{-4}
hTF: $V^{IV}O(acac)_2$= 1:1.52	4.7×10^{-4}	7.14×10^{-4}
hTF: $V^{IV}O(acac)_2$= 1:2.03	4.67×10^{-4}	9.46×10^{-4}
hTF: $V^{IV}O(acac)_2$= 1:2.48	4.64×10^{-4}	1.15×10^{-3}
hTF: $V^{IV}O(acac)_2$= 1:2.98	4.61×10^{-4}	1.38×10^{-3}
hTF: $V^{IV}O(acac)_2$= 1:3.49	4.59×10^{-4}	1.6×10^{-3}
hTF: $V^{IV}O(acac)_2$= 1:3.99	4.56×10^{-4}	1.82×10^{-3}
hTF: $V^{IV}O(acac)_2$= 1:4.5	4.53×10^{-4}	2.04×10^{-3}
hTF: $V^{IV}O(acac)_2$= 1:5.01	4.50×10^{-4}	2.25×10^{-3}

Appendix C 6. ***Experiment 2.6. CD of $V^{IV}O(acac)_2$ + HSA system***

Sample	C(HSA)/M	C($V^{IV}O(acac)_2$)/M
HSA: $V^{IV}O(acac)_2$= 1:0.51	5.97×10^{-4}	3.07×10^{-4}
HSA: $V^{IV}O(acac)_2$= 1:1.0	5.92×10^{-4}	5.91×10^{-4}
HSA: $V^{IV}O(acac)_2$= 1:1.51	5.87×10^{-4}	8.89×10^{-4}
HSA: $V^{IV}O(acac)_2$= 1:1.2	5.83×10^{-4}	1.16×10^{-3}

HSA: $V^{IV}O(acac)_2$= 1:1.3	5.92×10^{-4}	5.91×10^{-3}
HSA: $V^{IV}O(acac)_2$= 1:4.02	5.64×10^{-4}	2.27×10^{-3}
HSA: $V^{IV}O(acac)_2$= 1:5	5.56×10^{-4}	2.78×10^{-3}

Appendix C 7. ***Experiment 2.7. CD of hTF + $V^{IV}O^{2+}$ + phen system.***

Sample	C(hTF)/M	C($V^{IV}OSO_4$)/M	C(phen)/M
hTF: $V^{IV}OSO_4$: phen= 1:1:1	5.29×10^{-4}	5.32×10^{-4}	5.32×10^{-4}
hTF: $V^{IV}OSO_4$: phen= 1:2:2	5.26×10^{-4}	1.06×10^{-3}	1.05×10^{-3}
hTF: $V^{IV}OSO_4$: phen= 1:3:3	5.24×10^{-4}	1.57×10^{-3}	1.57×10^{-3}
hTF: $V^{IV}OSO_4$: phen= 1:3:5	5.19×10^{-4}	1.56×10^{-3}	2.59×10^{-3}

Appendix C 8. ***Experiment 3.1. EPR of $V^{IV}O(oda)(H_2O)_2$ + hTF system.***

Sample	C(hTF)/M	C($V^{IV}O(oda)(H_2O)_2$)/M
hTF: $V^{IV}O(oda)(H_2O)_2$= 1:0.73	4.899×10^{-4}	3.58×10^{-4}
hTF: $V^{IV}O(oda)(H_2O)_2$= 1:2.89	4.78×10^{-4}	1.38×10^{-3}
hTF: $V^{IV}O(oda)(H_2O)_2$= 1:4.28	4.71×10^{-4}	2.02×10^{-3}

Appendix C 9. ***Experiment 3.3. EPR of $V^{IV}O(oda)(bipy)$ + hTF system.***

Sample	C(hTF)/M	C($V^{IV}O(oda)(bipy)$)/M
hTF: $V^{IV}O(oda)(bipy)$= 1:0.49	4.89×10^{-4}	2.37×10^{-4}
hTF: $V^{IV}O(oda)(bipy)$= 1:0.97	4.86×10^{-4}	4.72×10^{-4}
hTF: $V^{IV}O(oda)(bipy)$= 1:2.08	4.81×10^{-4}	1.00×10^{-3}
hTF: $V^{IV}O(oda)(bipy)$= 1:4.02	4.72×10^{-4}	1.898×10^{-3}

Appendix C 10. ***Experiment 3.4. EPR of $V^{IV}O(oda)(phen)$ + hTF system.***

Sample	C(hTF)/M	C($V^{IV}O(oda)(phen)$/M
hTF: $V^{IV}O(oda)(phen)$= 1:2.01	5.32×10^{-4}	1.07×10^{-3}
hTF: $V^{IV}O(oda)(bipy)$= 1:3.09	5.32×10^{-4}	1.65×10^{-3}

Appendix C 11. ***Experiment 3.5. EPR of hTF + $V^{IV}O^{2+}$ + phen system.***

Sample	C(hTF)/M	C($V^{IV}OSO_4$)/M	C(phen)/M
hTF: $V^{IV}OSO_4$: phen= 1:2:2	5.26×10^{-4}	1.06×10^{-3}	1.05×10^{-3}
hTF: $V^{IV}OSO_4$: phen= 1:3:3	5.24×10^{-4}	1.57×10^{-3}	1.57×10^{-3}
hTF: $V^{IV}OSO_4$: phen= 1:3:5	5.19×10^{-4}	1.56×10^{-3}	2.59×10^{-5}

Appendix C 12. ***Experiment 3.6. EPR of $V^{IV}O(acac)_2$ + hTF system.***

Sample	C(hTF)/M	C($V^{IV}O(acac)_2$)/M
hTF: $V^{IV}O(acac)_2$= 1:5.01	4.50×10^{-4}	2.25×10^{-3}

Appendix C 13. ***Experiment 3.7. EPR of $V^{IV}O(acac)_2$ + HSA system.***

Sample	C(HSA)/M	C($V^{IV}O(acac)_2$)/M
HSA: $V^{IV}O(acac)_2$= 1:3	5.73×10^{-4}	1.72×10^{-3}
HSA: $V^{IV}O(acac)_2$= 1:5	5.56×10^{-4}	2.78×10^{-3}

Appendix D. CD of $V^{IV}O(oda)(H_2O)_2$ + hTF system.

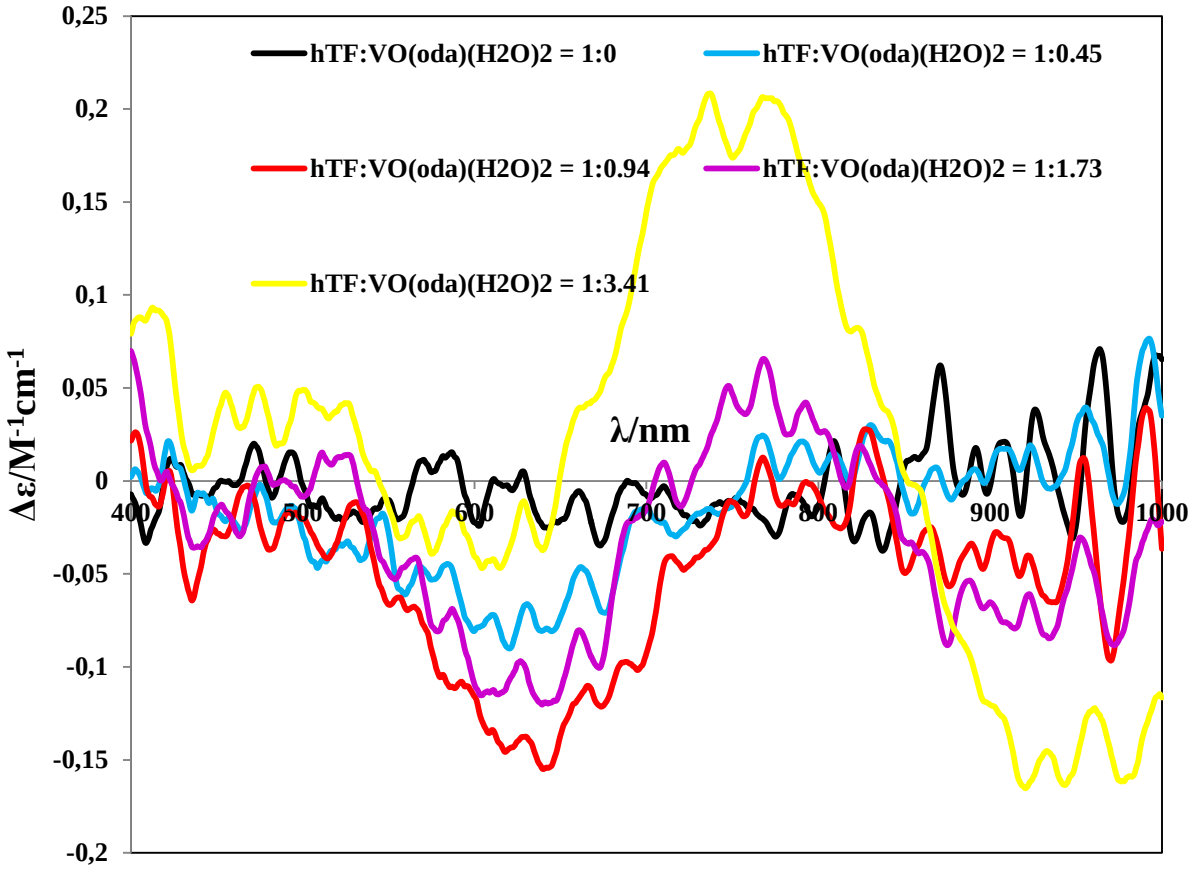

Appendix D 1. The CD spectra of solutions containing hTF (4.82×10^{-4} M) in PBS upon stepwise additions of adequate volumes of a solution of $V^{IV}O(oda)(H_2O)_2$ (4.63×10^{-2} M) in MeOH. Maximum % of MeOH added was 2.9; cell path length was 20 mm.